Supplementary Information (SI) for RSC Chemical Biology.
This journal is © The Royal Society of Chemistry

"MIDA masking" of boronic acid therapeutics for enhanced stability and economy

Forrest G. FitzGerald, Jasmin M. Frei, Erika Zhang, Oscar J. Molina, JoLynn B. Giancola, Malo Le Chevalier, Volga Kojasoy, and Ronald T. Raines*

Department of Chemistry, Massachusetts Institute of Technology, Cambridge, Massachusetts 02139, USA
Department of Biology, Massachusetts Institute of Technology, Cambridge, Massachusetts 02139, USA
Koch Institute for Integrative Cancer Research at MIT, Massachusetts Institute of Technology, Cambridge, Massachusetts 02139, USA

*Email: rtraines@mit.edu

Table of Contents

1. Abbreviations S2
2. Materials and Methods S4
3. Chemical Synthesis S7
4. LC-MS Assay Optimization S16
5. Boronate Ester Hydrolysis S18
6. H_2O_2-mediated Oxidation of BTZ, IXZ, and Boronate Esters S23
7. UV-induced Photodegradation of BTZ and Boronate Esters S25
8. Cytotoxicity Studies S33
9. In Vitro Proteasome Activity Assay S37
10. Esterase-mediated MIDA Ester Cleavage Studies S38
11. Computational Methods S40
12. NMR Spectra S45
13. Atomic Coordinates of DFT-Optimized Geometries S75
14. References S80

1. Abbreviations

ANOVA	analysis of variance
ATCC	American Type Culture Collection
ATP	adenosine 5′-triphosphate
BSA	bovine serum albumin
BTZ	bortezomib
BTZ–MIDA	MIDA-protected bortezomib
BTZ-ox-1	bortezomib oxidation product that elutes first from column
BTZ-ox-2	bortezomib oxidation product that elutes second from column
BTZ–pinanediol	pinanediol-protected bortezomib
Cat. No.	catalog number (or equivalent item identification number for vendor)
CES1	carboxylesterase 1
CES2	carboxylesterase 2
COSY	homonuclear correlation spectroscopy
DART	direct analysis in real time (ion source)
DCM	dichloromethane
DFT	density functional theory
DMC	dimethyl carbonate
DMEM	Dulbecco's Modified Eagle's Medium
DMSO	dimethyl sulfoxide
dr	diastereomeric ratio
DTT	dithiothreitol
EDTA	ethylenediaminetetraacetic acid
EGTA	ethylene glycol-bis(β-aminoethyl ether)-*N*,*N*,*N*′,*N*′-tetraacetic acid
ESIPT	excited-state intramolecular proton transfer
EtOAc	ethyl acetate
FBS	fetal bovine serum
h	hour
HBQ	10-hydroxybenzo[*h*]quinoline
HeLa	cervical cancer cell line derived from Henrietta Lacks
HEPES	4-(2-hydroxyethyl)-1-piperazineethanesulfonic acid
HMBC	heteronuclear multiple bond correlation
HRMS	high-resolution mass spectrometry
HSQC	heteronuclear single quantum coherence
IMDM	Iscove's modified Dulbecco's Medium
IXZ	ixazomib
IXZ–MIDA	MIDA-protected ixazomib
IXZ-ox	ixazomib oxidation product
IXZ–citrate	citrate-protected ixazomib
LC-MS	liquid chromatography-mass spectrometry
MeCN	acetonitrile
MeOH	methanol
MIDA	*N*-methyliminodiacetic acid
min	minute
MS	mass spectrometry

MTS	3-(4,5-dimethylthiazol-2-yl)-5-(3-carboxymethoxyphenyl)-2-(4-sulfophenyl)-2*H*-tetrazolium, inner salt
MWCO	molecular weight cut off
NMR	nuclear magnetic resonance
ox	oxidized
PBS	phosphate-buffered saline
P_i	inorganic phosphate
PON1	paraoxonase 1
RPMI	Roswell Park Memorial Institute
rt	room temperature
SAPT	symmetry-adapted perturbation theory
SE	standard error
THF	tetrahydrofuran
TLC	thin-layer chromatography
TOF	time of flight
UV	ultraviolet
vis	visible

2. Materials and Methods

Chemical Reagents. Commercial reagents were used without further purification. 10-Hydroxybenzo[*h*]quinoline (HBQ) was from Alfa Aesar (Haverhill, MA). All other reagents used in chemical synthesis were from Sigma–Aldrich (St. Louis, MO), Thermo Fisher Scientific (Waltham, MA), or AmBeed (Grove, IL). Normal saline was from Quality Biological (Gaithersburg, MD) and stored at 4 °C. Autosampler vials (Cat. No. 9509S-1WCP-RS) were from Microsolv Technology Corporation (Leland, NC). For small sample volumes (<500 μL), 150 μL glass inlets from Agilent (Santa Clara, CA) were used.

Solvent Removal. The phrase "concentrated under reduced pressure" refers to the removal of solvents and other volatile materials using a rotary evaporator at water aspirator pressure (<20 Torr) while maintaining the water-bath temperature of 30–40 °C. Residual solvent was removed from samples by the vacuum (<0.1 Torr) achieved by a mechanical belt-drive oil pump.

Conditions. All procedures were performed in air at ambient temperature (~23 °C) and pressure (1.0 atm) unless indicated otherwise. Reactions requiring heat were heated with a silicone oil bath.

Instrumentation. NMR spectra were obtained with an Avance Neo 400.17 MHz or an Avance Neo 500.34 MHz spectrometer from Bruker (Billerica, MA). High-resolution mass spectra were obtained with an AccuTOF-DART 4G from JEOL (Peabody, MA) by helium DART ionization. Column chromatography was performed on a Selekt flash chromatography system from Biotage (Uppsala, Sweden) using prepacked Sfar Duo silica gel columns for normal-phase purification or Sfar Duo C18 columns for reversed-phase purification. UV–vis measurements were obtained using a Cary 60 UV–vis spectrophotometer from Agilent Technologies (Santa Clara, CA). LC-MS measurements were performed on an Agilent InfinityLab LC/MSD and Agilent 1260 Infinity II LC unit. Absorbance, MTS assay, and proteasome assay readouts were measured on a Spark Multimode Microplate Reader from Tecan (Männedorf, Switzerland). A UV lamp UVP UVGL-25, 95-0021-12 from AnalytikJena 4 Watt, 254/365 nm was used for photodegradation experiments. Data analyses were performed using Microsoft Excel and GraphPad Prism.

pH Measurements. pH measurements were performed using a Thermo Fisher Scientific accumet LX500 Dual Channel pH/mV/Ion/Conductivity Meter. The instrument was standardized before every measurement using Buffer Reference Standard solutions of pH 4.00, 7.00, and 10.00 from VWR Chemicals.

^{11}B NMR Spectroscopy. Variability in boron NMR shifts may be induced by solvent type and the chemical identity of the boron species. A standard proton-decoupled boron NMR spectrum, with or without background suppression, was acquired. Samples were prepared in borosilicate NMR tubes. Background signal from NMR tubes can often be observed even with a background-suppression NMR method. Common ppm ranges for trigonal (sp^2) alkyl and aryl boronic acids were typically observed at ~30 ± 5 ppm. Boric acid, if present, is typically observed with a shift of ~19–20 ppm. The tetrahedral (sp^3) boron of MIDA-protected boronates is typically observed with a shift of 10–15 ppm. The carbon bonded directly to the boron might also go undetected due to quadrupolar broadening.

TLC Staining for Boronic Acid-containing Molecules. A 4 mM solution of HBQ was prepared in methanol and used as a boronic acid stain for thin-layer chromatography (TLC). In brief, the silica TLC plate was dipped in an HBQ solution, air-dried, and then heated until the silica turned pale yellow. Upon exposure to long-wavelength (365 nm) UV light, spots containing boronic acids that can complex with HBQ appear cyan (495 nm) due to the interruption of the excited-state intramolecular proton transfer (ESIPT) of HBQ, as reported previously.[1]

Biological Reagents. Sucrose was from MP Biomedicals (Cat. No. 821713), DTT was from Life Technologies (Cat. No. 15508013), the proteasome substrate for in vitro activity assays was from Sigma–Aldrich (Suc-LLVY-AMC; Cat. No. S6510), and the MycoAlert PLUS assay kit was from Lonza Biosciences (Cat. No. LT07-710). Fetal bovine serum (FBS) was from Corning (Cat. No. 45001-108). These reagents were obtained from Sigma–Aldrich: DMSO (Cat. No. D8418), PBS without Ca^{2+} and Mg^{2+} (Cat. No. P802), EGTA (Cat. No. E4378), EDTA (Cat. No. E5134), ATP (Cat. No. A3377), $MgCl_2$ (Cat. No. M2670), and HEPES (Cat. No. H3375). These reagents were obtained from Thermo Fisher Scientific: Coomassie Protein Assay Reagent (Cat. No. 1856209), BSA Protein Standard (Cat. No. 23209), DMEM with high glucose and pyruvate (Cat. No. 11995065), penicillin–streptomycin (10,000 U/mL) (Cat. No. 15140122) and trypsin–EDTA (0.25% w/v) with phenol red (Cat. No. 25200056), TrypLE Express (Cat. No. 12605010), SYTOX Blue dead-cell indicator (Cat. No. S34857), RPMI 1640 culture media (Cat. No. 11875075), high glucose DMEM (Cat. No. 12100046), and IMDM media (Cat. No. 12330053).

Recombinant human serum paraoxonase/arylesterase 1 (PON1) (Cat. No. CSB-EP018369HU) was from Cusabio. Pig liver esterase (Cat. No. E3019) was from Sigma–Aldrich. Recombinant human carboxylesterase 1 (CES1) (Cat. No. 30105-H08H) was from Sino Biological. Recombinant human carboxylesterase 2 (CES2) (Cat. No. HY-P76192) was from MedChemExpress.

Mammalian Cell Culture. All cell lines were grown in sterile culture flasks in a cell culture incubator at 37 °C under CO_2(g) (5% v/v). Cells were counted to determine seeding density using a Countess II FL Automated Cell Counter (Cat. No. AMQAF1000) and Countess Cell Counting Chamber Slides (Cat. No. C10283) from Thermo Fisher Scientific. To minimize genetic drift, thawed vials were used for fewer than twenty passages. The cells were passaged upon reaching 80% confluency with trypsin–EDTA (0.05% w/v).

- **HeLa.** HeLa cells (ATCC Cat. No. CCL-2) were cultured according to ATCC guidelines. Cells were cultured in high-glucose DMEM supplemented with FBS (10% v/v), penicillin (100 units/mL), and streptomycin (100 μg/mL) and grown in an incubator at 37 °C and humidified with CO_2(g) (5% v/v). Cells tested negative for mycoplasma using a Lonza MycoAlert Plus kit.

- **M21.** The human melanoma M21 cell line was a gift from Dr. Oscar Ortiz (Merck KGaA, Darmstadt, Germany). M21 cells were grown in high-glucose DMEM supplemented with sodium bicarbonate (1.5 g/L), FBS (10% v/v), penicillin (100 units/mL), and streptomycin (100 μg/mL). Cells tested negative for mycoplasma using a Lonza MycoAlert Plus kit.

- **KMS11.** The human multiple myeloma KMS11 cell line was a gift from Professor Jeremiah A. Johnson (Massachusetts Institute of Technology, Cambridge, MA, USA). Cells were cultured in RPMI 1640 supplemented with FBS (10% v/v), penicillin (100 units/mL), and streptomycin (100 μg/mL) in an incubator at 37 °C and humidified with CO_2(g) (5% v/v). Cells tested negative for mycoplasma using a Lonza MycoAlert Plus kit.

- **HAP1.** The human near-haploid 1 (human leukemia) cell line was obtained from Horizon Discovery. Cells were grown in IMDM supplemented with FBS (10% v/v), penicillin (100 units/mL), and streptomycin (100 μg/mL) in an incubator at 37 °C, humidified with CO_2(g) (5% v/v). Cells tested negative for mycoplasma using a Lonza MycoAlert Plus kit.

MTS Cytotoxicity Assay. The cytotoxicity of compounds used herein was determined using the CellTiter 96 AQueous One Solution Cell Proliferation assay kit from Promega (Madison, WI; Cat. No. G3580). This colorimetric assay leverages the metabolic activity of viable cells to convert a tetrazolium salt [3-(4,5-dimethylthiazol-2-yl)-5-(3-carboxymethoxyphenyl)-2-(4-sulfophenyl)-2*H*-tetrazolium, inner salt; MTS] into a colored, soluble formazan compound with absorbance in the visible light range.[2] The absorbance of formazan produced is directly proportional to the living cell count.

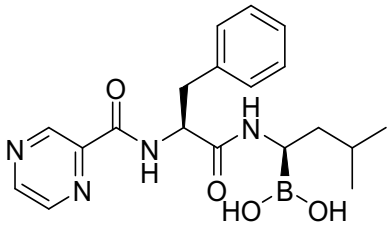
Cells were seeded in a tissue culture-treated, clear-bottom 96-well plate (Greiner-Bio CELLSTAR Cat. No. 655180). HeLa, M21, and KMS11 cells were seeded at 5,000 cells/well. Cells were grown for 24 h prior to treatment with compounds. The confluency at the time of the experiment was 10%, in line with assay requirements for proliferating cells. Each compound was prepared as a 100 mM stock solution in DMSO. A dilution series, tailored to the potency of each compound, was prepared. To prevent membrane permeabilization, cells were treated with up to 1% v/v DMSO as a vehicle. The working volume of each treatment condition was 100 μL. After treatment, cells were incubated for 48 h. Cells were then treated with 20 μL of the MTS reagent and incubated for 1.5 h at 37 °C in a humidified 5% v/v CO_2(g) atmosphere. Absorbance readings were collected at 490 nm on a Tecan Spark plate reader. Values represent data collected with three technical replicates and are normalized to the average background absorbance signal from formazan in media alone and from untreated cells. Data are plotted as a mean ± SE using GraphPad Prism software.

In vitro Proteasome Assay. HAP1 cells were grown to confluence and washed 2 × with ice-cold PBS without Ca^{2+}/Mg^{2+} before collection. The cells were collected using TrypLE Express, and the cell pellet was resuspended in 100 μL of lysis buffer per 1×10^6 cells. The lysis buffer was 50 mM HEPES–NaOH buffer, pH 7.8, containing NaCl (10 mM), $MgCl_2$ (1.5 mM), EDTA (1 mM), EGTA (1 mM), sucrose (250 mM), and DTT (5 mM). Cells were lysed using 3 freeze-thaw cycles, with freezing at −80 °C and thawing on ice. The lysate was clarified at 15,000*g* for 15 min at 4 °C. The supernatant was transferred to a fresh 1.7 mL microcentrifuge tube and stored at −70 °C until used in the assay. Assay buffer was 50 mM HEPES–NaOH buffer, pH 7.8, containing NaCl (10 mM), $MgCl_2$ (1.5 mM), EDTA (1 mM), EGTA (1 mM), and sucrose (250 mM), and was stored at 4 °C. Before assays, DTT was added to a final concentration of 5 mM, and ATP was added to a final concentration of 2 mM.

Proteasome substrate (Suc-LLVY-AMC) was dissolved in DMSO to a concentration of 10 mM and stored at −20 °C. A 50-µL aliquot of cellular lysate was added to each well of a 96-well black flat-bottom plate (Corning, Cat. No. 3991). A final concentration of 50 µM BTZ, BTZ–MIDA, or MIDA in assay buffer was added to the lysate under the tested conditions. For the positive control, no BTZ or BTZ–MIDA was added to the lysate. Negative control wells contained 100 µL of lysis buffer with 100 µM Suc-LLVY-AMC. The samples were incubated for 30 min at 37 °C. Afterward, 50 µL of assay buffer containing 200 µM (2×) Suc-LLVY-AMC was added to all wells containing lysate with either compound or no compound. The plate was incubated for 90 min at 37 °C. Fluorescence was monitored continuously for 90 min at $\lambda_{ex} = 360 \pm 5$ nm and $\lambda_{em} = 460 \pm 5$ nm using a Tecan Spark plate reader. Readout was normalized to protein concentrations determined using a Coomassie (Bradford) Protein Assay kit following the manufacturer's protocol, with a microplate reader and 5 µL of lysate.

Safety Statement. Bortezomib and ixazomib are hazardous, cytotoxic chemotherapeutic agents and should be handled with care. H_2O_2 (30% w/w or 9.79 M in water) is a strong oxidizer and should not be combined with other organic waste streams. Stock solutions of H_2O_2 were stored at 4 °C in a secondary container and protected from light. All solutions containing H_2O_2 were quenched with MnO_2 in a fume hood, which catalyzes the decomposition of H_2O_2 into O_2(g) and water. Once the reaction had finished (*i.e.*, no more effervescence was observed), the solutions were disposed of in a separate waste container. No other unexpected or unusually high safety hazards were encountered in this work.

3. Chemical Synthesis



Compound: Bortezomib (BTZ) — Purchased from AmBeed
NMR spectra were obtained for reference.
NMR in 5:1 d_3-MeCN:D_2O. ^{1}H NMR (500 MHz, CD_3CN/D_2O, δ): 9.16–9.09 (m, 1H), 8.76 (t, J = 2.6 Hz, 1H), 8.63 (dq, J = 3.1, 1.5 Hz, 1H), 7.27 (s, 1H), 7.26 (d, J = 4.4 Hz, 3H), 7.21 (ddd, J = 8.8, 5.2, 3.9 Hz, 1H), 4.81 (dd, J = 8.2, 5.8 Hz, 1H), 3.23 (dd, J = 13.9, 5.8 Hz, 1H), 3.10 (dd, J = 13.9, 8.2 Hz, 1H), 3.01–2.95 (m, 1H), 1.45 (d, J = 24.0 Hz, 2H), 1.27 (ddd, J = 13.9, 8.6, 5.3 Hz, 1H), 0.82 (dd, J = 8.1, 6.4 Hz, 6H). **^{13}C{^{1}H} NMR** (126 MHz, CD_3CN/D_2O, δ): 171.75, 163.86, 148.11, 144.44, 144.04, 143.84, 137.13, 129.84, 129.76, 128.86, 127.22, 54.27, 39.62, 37.94, 25.34, 22.97, 21.37. **^{11}B{^{1}H} NMR** (160 MHz, CD_3CN/D_2O, δ): 28.24.

HRMS (DART-TOF) m/z: $[M + H]^+$ calculated for $C_{19}H_{26}BN_4O_4^+$, 385.2042; found, 385.2038

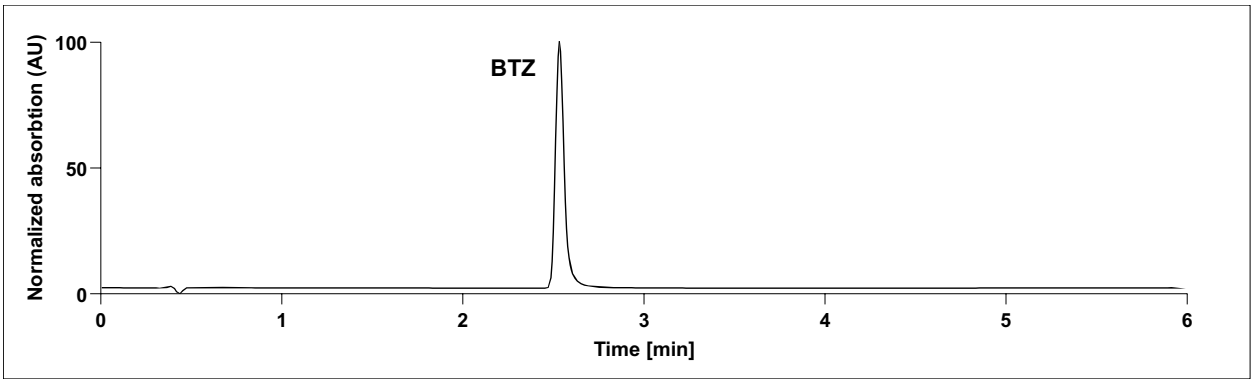


Fig. S1 LC chromatogram of BTZ at 280.4 nm using a 20–80% v/v MeCN gradient (Table S1).

Note: the most frequently observed ionized fragments of bortezomib are shown below.

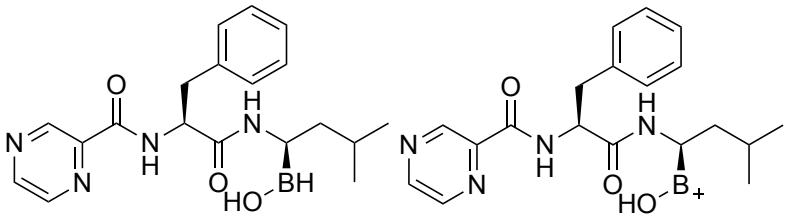
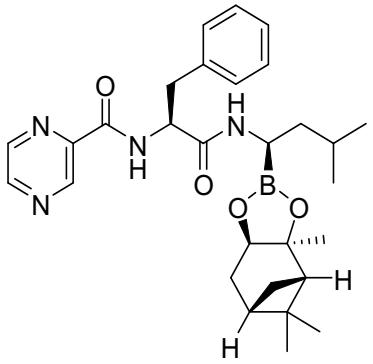


Fig. S2 Frequently observed fragments of BTZ in MS.



Compound: Pinanediol-protected bortezomib (BTZ–pinanediol) — Purchased from AmBeed

HRMS (DART-TOF) *m*/*z*: $[M + H]^+$ calculated for $C_{29}H_{40}BN_4O_4^+$, 519.3137; found, 519.3186.

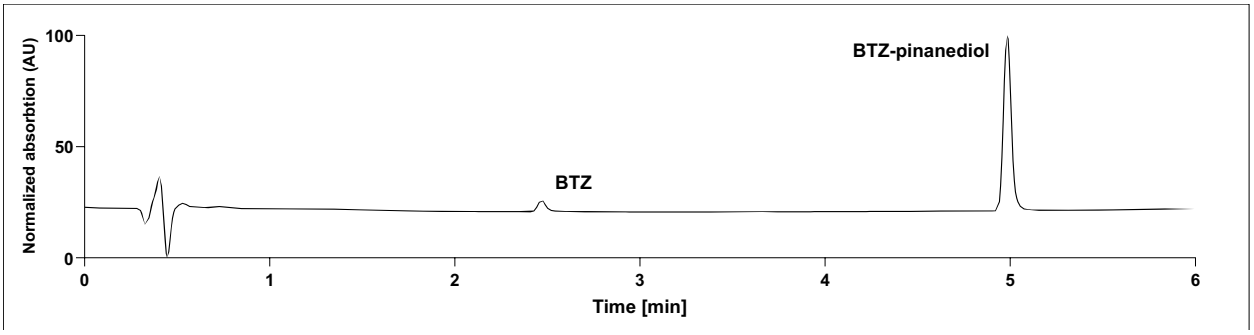
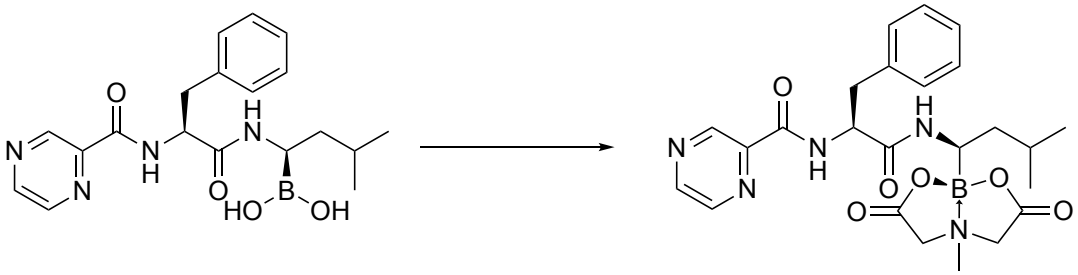


Fig. S3 LC chromatogram of BTZ–pinanediol at λ = 280.4 nm using a 20–100% v/v MeCN gradient (Table S1). Note: The presence of unprotected BTZ is due to rapid hydrolysis of the pinanediol in the aqueous conditions, further enhanced by the acidic pH of mobile phase (containing 0.1% formic acid).



Compound: Bortezomib MIDA ester (BTZ–MIDA)

Procedure: Adapted from Kelly et al. (2020).[3] Bortezomib (0.0999 g, 0.26 mmol) and 4-methylmorpholine-2,6-dione (MIDA anhydride) (0.1343 g, 1.04 mmol, 4 equiv) were dissolved in 4 mL of anhydrous DMSO. The reaction mixture was heated to 70 °C, stirred overnight, and monitored by TLC and staining with HBQ for the boronic acid until the reaction was complete. The reaction mixture was then diluted in ethyl acetate, washed twice with water and once with brine, dried over Na_2SO_4(s), and purified by flash chromatography on silica using dichloromethane and methanol. The product was isolated as a white solid (0.1275 g, 0.258 mmol, 99%).

Note: Prior attempts to perform this reaction in 1,4-dioxane, tetrahydrofuran, acetonitrile, or acetone were low-yielding due to starting material insolubility.

^{1}H NMR (500 MHz, DMSO-d_6, δ): 9.08 (d, J = 1.4 Hz, 1H), 8.91 (d, J = 8.4 Hz, 1H), 8.86 (d, J = 2.5 Hz, 1H), 8.73 (t, J = 1.9 Hz, 1H), 7.35–7.20 (m, 5H), 7.16 (t, J = 7.2 Hz, 1H), 4.68 (td, J = 8.5, 6.2 Hz, 1H), 4.22 (d, J = 17.3 Hz, 1H), 4.07 (d, J = 16.8 Hz, 1H), 3.98 (d, J = 17.3 Hz, 1H), 3.55 (ddd, J = 12.5, 9.7, 3.1 Hz, 1H), 3.42 (d, J = 16.8 Hz, 1H), 3.13–3.03 (m, 2H), 2.82 (s, 3H), 1.57 (dpd, J = 10.3, 6.6, 3.1 Hz, 1H), 1.40 (ddd, J = 15.2, 12.1, 3.5 Hz, 1H), 1.20 (ddd, J = 13.7, 10.4, 3.2 Hz, 1H), 0.83 (dd, J = 12.8, 6.6 Hz, 6H). **^{13}C{^{1}H} NMR** (126 MHz, DMSO-d_6, δ): 170.5, 168.9, 168.0, 162.9, 147.8, 143.9, 143.6, 143.3, 137.8, 129.0, 128.3, 126.4, 62.4, 61.9, 55.5, 45.6, 40.3, 37.1, 23.9, 23.8, 21.2. **^{11}B{^{1}H} NMR** (160 MHz, DMSO-d_6, δ): 11.99.

HRMS (DART-TOF) m/z: $[M - H]^-$ calculated for $C_{24}H_{29}BN_5O_6^-$, 494.2211; found, 494.2240.

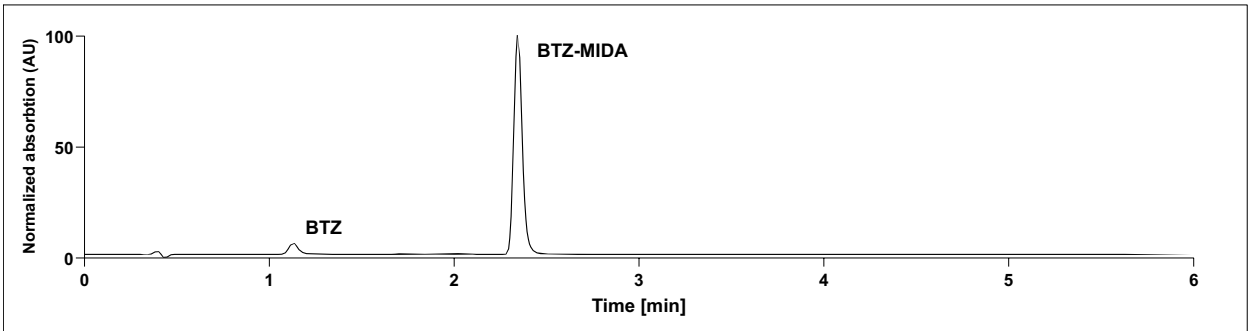


Fig. S4 LC chromatogram of BTZ–MIDA at λ = 280.4 nm using a 30–80% v/v MeCN gradient (Table S1).
Note: the small peak at 1.13 min corresponds to a small amount (<5%) of hydrolyzed BTZ–MIDA, which occurs during dissolution for injection into the LC-MS. No traces of unprotected BTZ were observed in the ^{1}H NMR of the sample in organic solvent.

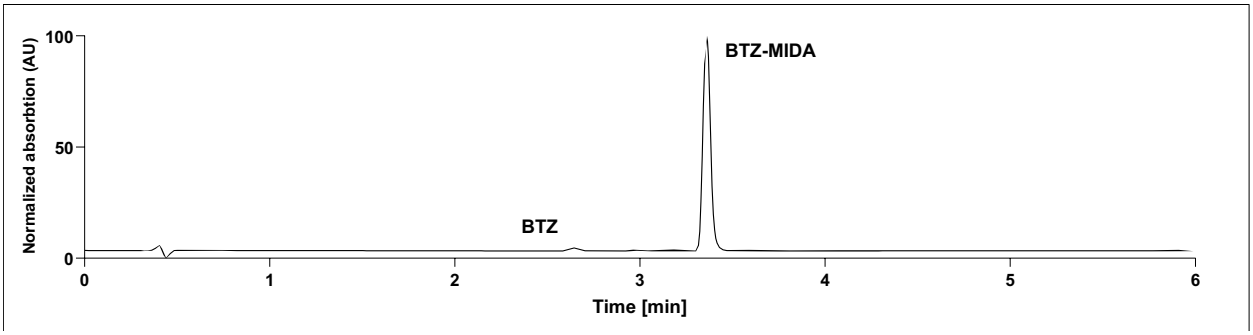
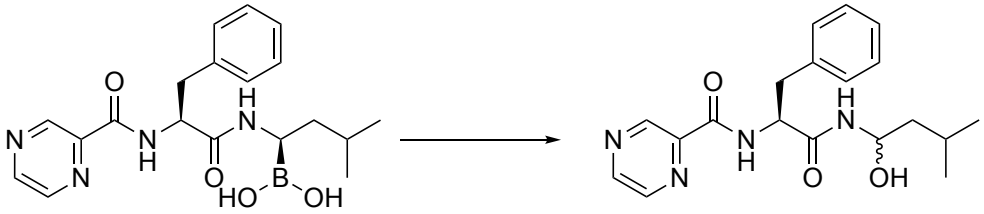


Fig. S5 LC chromatogram of BTZ–MIDA at λ = 280.4 nm using a 20–80% v/v MeCN gradient (Table S1).
Note: the small peak at 2.53 min corresponds to a small amount (<5%) of hydrolyzed BTZ–MIDA, which occurs during dissolution for injection into the LC-MS. No traces of unprotected BTZ were observed in the ^{1}H NMR of the sample in organic solvent.



Compound: Oxidized Bortezomib (BTZ-ox-1/BTZ-ox-2). BTZ-ox-1 elutes first from LC column. BTZ-ox-2 elutes second from LC column.

Procedure: Adapted from Wagh and Nagarkar (2017).[4] Bortezomib (0.0499 g, 0.13 mmol) was suspended in 2 mL of DMC. Hydrogen peroxide (0.26 mmol, 2 equiv of a 30% w/w aqueous solution) was added to the mixture, which resulted in a clear solution within a few seconds. The reaction mixture was stirred for 1 h and continuously monitored by TLC (5% v/v methanol in dichloromethane) and staining for the boronic acid with HBQ until the reaction was complete. The

reaction mixture was diluted with deionized water. The aqueous phase was extracted four times with ethyl acetate. The combined organic layers were washed once with deionized water, once with brine, dried over Na_2SO_4(s), and concentrated under reduced pressure. The product was purified on silica with flash chromatography using dichloromethane and methanol. The product was isolated as a white solid (0.0426 g, 0.12 mmol, 92%) with a diastereomeric ratio (dr) > 10:1, with "BTZ-ox-1" being the major diastereomer. The two diastereomers were separated via preparative TLC (95:5, dichloromethane:methanol) and characterized separately.

BTZ-ox-1: ^{1}H NMR (500 MHz, DMSO-d_6, δ): 9.11 (d, J = 1.5 Hz, 1H), 8.87 (d, J = 2.5 Hz, 1H), 8.73 (dd, J = 2.5, 1.5 Hz, 1H), 8.67 (d, J = 8.8 Hz, 1H), 8.49 (d, J = 8.5 Hz, 1H), 7.28–7.19 (m, 4H), 7.18–7.12 (m, 1H), 5.67 (d, J = 5.4 Hz, 1H), 5.26 (dq, J = 8.6, 6.5 Hz, 1H), 4.75 (td, J = 8.8, 4.4 Hz, 1H), 3.13 (dd, J = 13.9, 4.5 Hz, 1H), 3.05 (dd, J = 13.8, 8.9 Hz, 1H), 1.65 (dh, J = 13.5, 6.7 Hz, 1H), 1.47 (dt, J = 13.8, 7.0 Hz, 1H), 1.36 (dt, J = 13.4, 6.7 Hz, 1H), 0.86 (dd, J = 9.5, 6.6 Hz, 6H). **^{13}C{^{1}H} NMR** (126 MHz, DMSO-d_6, δ): 169.6, 162.2, 147.8, 144.1, 143.4 (two signals coincident), 137.4, 129.3, 128.1, 126.4, 71.3, 54.0, 45.3, 37.6, 24.1, 22.6, 22.3.

HRMS (DART-TOF**)** m/z: $[M - H]^-$ calculated for $C_{19}H_{23}N_4O_3^-$, 355.1770; found, 355.1769.

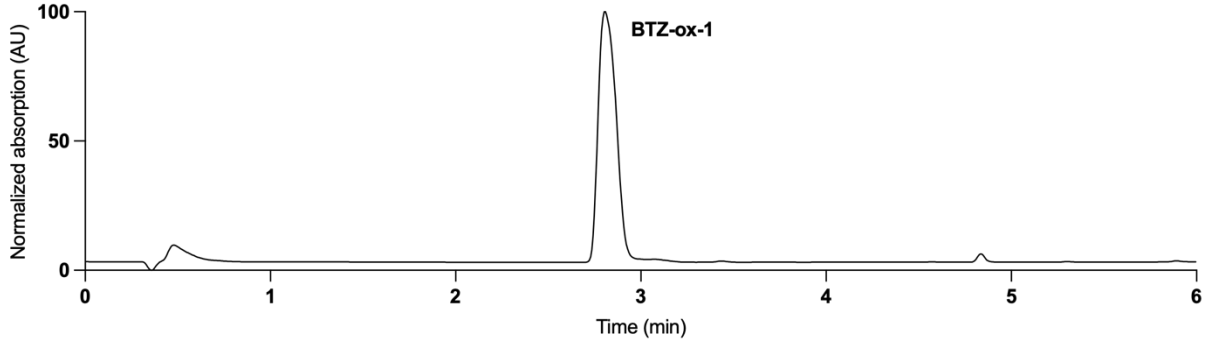


Fig. S6 LC chromatogram of BTZ-ox-1 at λ = 280.4 nm using a 20–80% v/v MeCN gradient (Table S1).

BTZ-ox-2: ^{1}H NMR (500 MHz, DMSO-d_6, δ): 9.12 (d, J = 1.4 Hz, 1H), 8.88 (d, J = 2.5 Hz, 1H), 8.74 (t, J = 2.0 Hz, 1H), 8.60 (d, J = 8.7 Hz, 1H), 8.54 (d, J = 8.6 Hz, 1H), 7.22 (d, J = 4.3 Hz, 4H), 7.16 (h, J = 4.1 Hz, 1H), 5.63 (d, J = 5.0 Hz, 1H), 5.21 (dtd, J = 8.6, 6.7, 4.9 Hz, 1H), 4.80 (td, J = 8.2, 5.8 Hz, 1H), 3.12–3.01 (m, 2H), 1.50 (dq, J = 13.4, 6.7 Hz, 1H), 1.39 (dt, J = 13.8, 7.0 Hz, 1H), 1.32–1.27 (m, 1H), 0.83 (t, J = 6.2 Hz, 6H). **^{13}C{^{1}H} NMR** (126 MHz, DMSO-d_6, δ): 169.6, 162.0, 147.8, 144.0, 143.5, 143.4, 137.2, 129.2, 128.0, 126.4, 71.2, 53.8, 45.0, 38.0, 24.0, 22.5, 22.4.

HRMS (DART-TOF) m/z: $[M - H]^-$ calculated for $C_{19}H_{23}N_4O_3^-$, 355.1770; found, 355.1776.

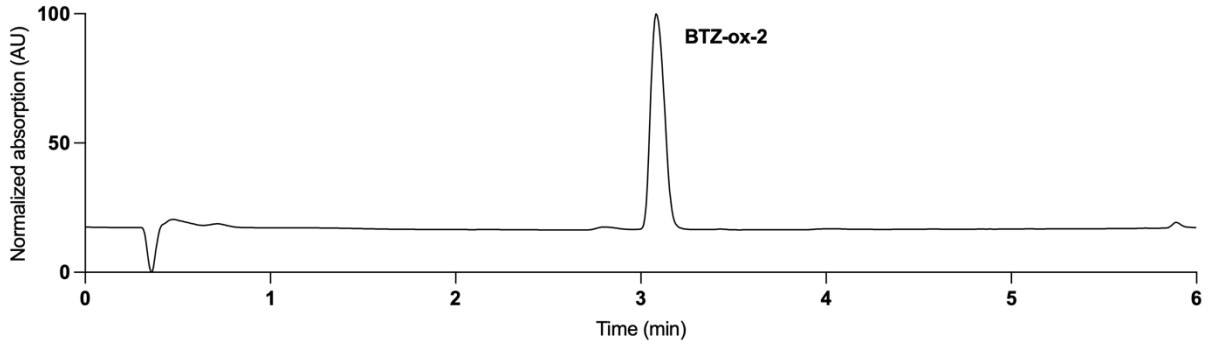
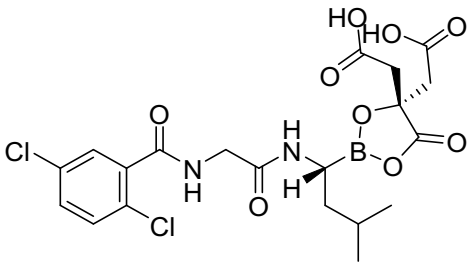


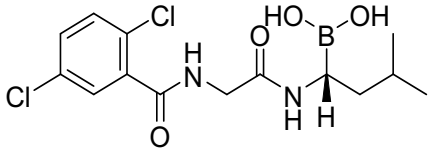
Fig. S7 LC chromatogram of BTZ-ox-2 at λ = 280.4 nm using a 20–80% v/v MeCN gradient (Table S1).



Compound: Ixazomib–citrate (IXZ–citrate) — Purchased from AmBeed

HRMS (DART-TOF**)** *m*/*z*: $[M + H]^+$ calculated for $C_{20}H_{24}BN_2O_9Cl_2^+$, 517.0946; found, 517.0918.

Note: the citric acid moiety is rapidly hydrolyzed from the boronic acid upon exposure to aqueous conditions.



Compound: Ixazomib (IXZ) — Purchased from AmBeed

HRMS (DART-TOF**)** *m*/*z*: $[M]^+$ calculated for $C_{14}H_{19}BN_2O_4Cl_2^+$, 360.0809; found, 360.0836.

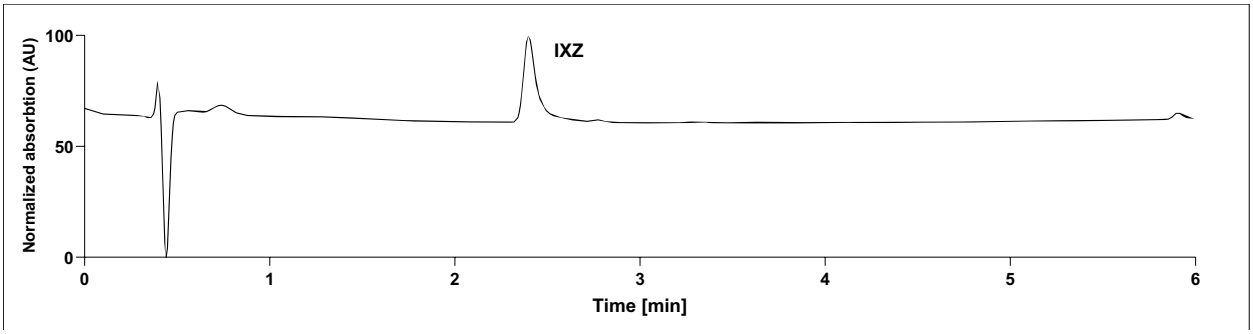


Fig. S8 LC trace of IXZ at 280.4 nm using a 20–80% v/v MeCN gradient (Table S1).
Note: the most frequently observed fragments of Ixazomib are shown below (Fig. S9).

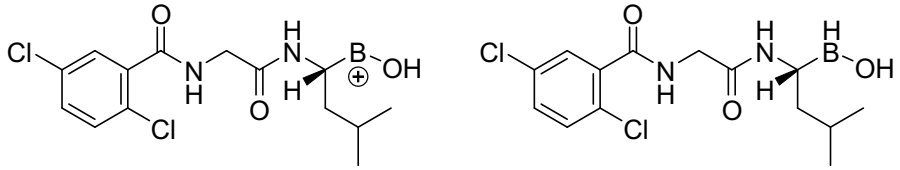
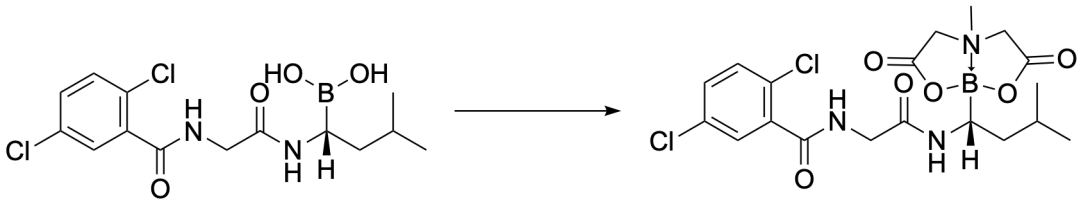


Fig. S9 Frequently observed fragments of IXZ in MS.



Compound: Ixazomib MIDA Ester (IXZ–MIDA)

Procedure: Adapted from Kelly et al. (2020).[3] Ixazomib (0.0332 g, 0.092 mmol) and 4-methylmorpholine-2,6-dione (0.0356 g, 0.276 mmol, 3 equiv) were dissolved in 1 mL of anhydrous DMSO under N_2(g). The solution was heated to 70 °C and stirred for 16 h. Reaction progress was monitored by TLC and by staining for boronic acid with HBQ until the reaction was complete. The reaction mixture was then poured into water, and the aqueous phase was extracted four times with EtOAc. The combined organic layers were washed twice with brine, dried over Na_2SO_4(s), and separated on silica with flash chromatography using DCM and MeOH. The product was obtained as a white solid (0.0430 g, 0.091 mmol, 99%).

^{1}H NMR (500 MHz, DMSO-d_6, δ): 8.82 (td, J = 5.9, 2.1 Hz, 1H), 7.54 (d, J = 1.5 Hz, 2H), 7.51 (d, J = 1.6 Hz, 1H), 7.31 (d, J = 10.0 Hz, 1H), 4.25 (d, J = 17.3 Hz, 1H), 4.15 (d, J = 16.7 Hz, 1H), 4.03–3.93 (m, 2H), 3.88 (dd, J = 15.9, 5.7 Hz, 1H), 3.68 (dd, J = 15.9, 6.0 Hz, 1H), 3.58 (ddd, J = 12.5, 9.9, 3.0 Hz, 1H), 2.87 (s, 3H), 1.54 (dpd, J = 10.1, 6.5, 4.1 Hz, 1H), 1.38 (ddd, J = 13.5, 12.0, 3.4 Hz, 1H), 1.27–1.18 (m, 1H), 0.85 (dd, J = 11.9, 6.6 Hz, 6H). **^{13}C{^{1}H} NMR** (126 MHz, DMSO-d_6, δ): 168.9, 168.5, 168.1, 165.5, 137.7, 131.6, 131.5, 130.8, 128.9, 128.8, 62.4, 61.9, 45.5, 40.4, 23.9 (2C), 21.3. **^{11}B{^{1}H} NMR** (160 MHz, DMSO-d_6, δ): 11.5.

HRMS (DART-TOF**)** *m*/*z*: $[M + H]^+$ calculated for $C_{19}H_{25}BN_3O_6Cl_2^+$, 472.1208; found, 472.1211.

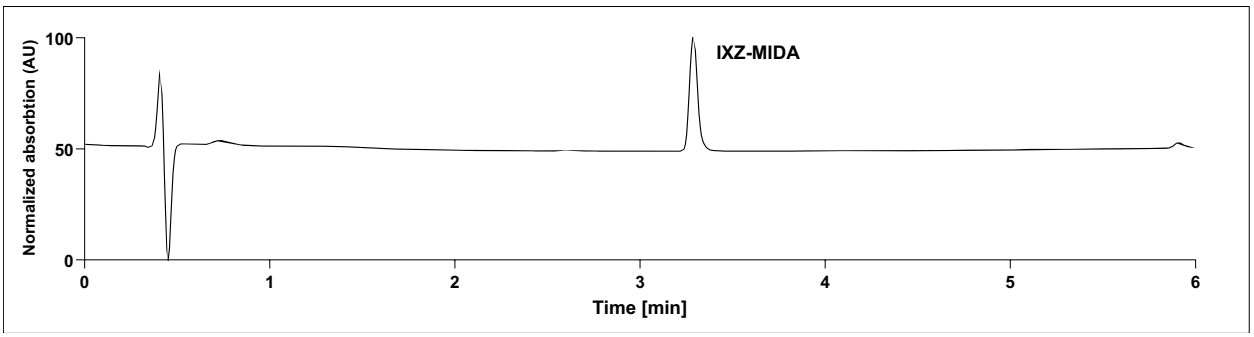
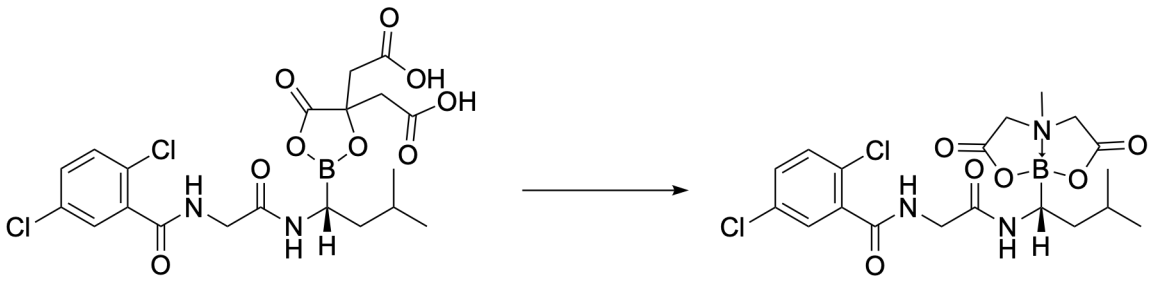


Fig. S10 LC trace of IXZ–MIDA at 280.4 nm using a 20–80% v/v MeCN gradient (Table S1).



Compound: Ixazomib MIDA Ester (IXZ–MIDA)

Procedure: Adapted from Kelly et al. (2020).[3] IXZ–citrate (0.1028 g, 0.200 mmol) and potassium carbonate (0.0829 g, 0.600 mmol, 3 equiv) were dissolved in 4 mL of 1:1 MeOH/H_2O, which was previously degassed for 30 min by bubbling N_2(g) through the solution. The reaction mixture was stirred for 1 h under N_2(g). The reaction mixture was diluted with water and extracted four times with EtOAc. The combined organic layers were washed once with brine, dried over Na_2SO_4(s), and concentrated in vacuo. The obtained white solid was used without further purification. To the white solid, 4-methylmorpholine-2,6-dione (0.0775 g, 0.600 mmol, 3 equiv) was added. Under N_2(g), the solids were dissolved in 2 mL of anhydrous DMSO. The solution was heated to 70 °C and stirred for 20 h. Reaction progress was monitored by TLC, staining for the boronic acid with HBQ, until the reaction was complete. The reaction mixture was then poured into water, and the aqueous phase was extracted four times with EtOAc. The combined organic layers were washed twice with brine, dried over Na_2SO_4(s), and separated on silica with flash chromatography using DCM and MeOH. The product was obtained as a white solid (0.0803 g, 0.170 mmol, 85%).

^{1}H NMR (500 MHz, DMSO-d_6, δ): 8.82 (td, J = 5.9, 2.1 Hz, 1H), 7.54 (d, J = 1.5 Hz, 2H), 7.51 (d, J = 1.6 Hz, 1H), 7.31 (d, J = 10.0 Hz, 1H), 4.25 (d, J = 17.3 Hz, 1H), 4.15 (d, J = 16.7 Hz, 1H), 4.03–3.93 (m, 2H), 3.88 (dd, J = 15.9, 5.7 Hz, 1H), 3.68 (dd, J = 15.9, 6.0 Hz, 1H), 3.58 (ddd, J = 12.5, 9.9, 3.0 Hz, 1H), 2.87 (s, 3H), 1.54 (dpd, J = 10.1, 6.5, 4.1 Hz, 1H), 1.38 (ddd, J = 13.5, 12.0, 3.4 Hz, 1H), 1.27–1.18 (m, 1H), 0.85 (dd, J = 11.9, 6.6 Hz, 6H). **^{13}C{^{1}H} NMR** (126 MHz, DMSO-d_6, δ): 168.9, 168.5, 168.1, 165.5, 137.7, 131.6, 131.5, 130.8, 128.9, 128.8, 62.4, 61.9, 45.5, 40.4, 23.9, 23.9, 21.3. **^{11}B{^{1}H} NMR** (160 MHz, DMSO-d_6, δ): 11.5.

HRMS (DART-TOF**)** *m*/*z*: $[M + H]^+$ calculated for $C_{19}H_{25}BN_3O_6Cl_2^+$, 472.1208; found, 472.1211.

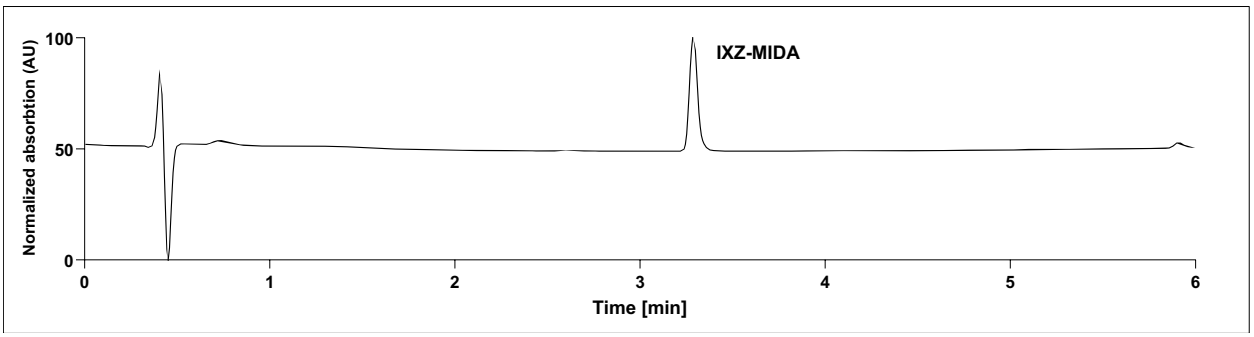
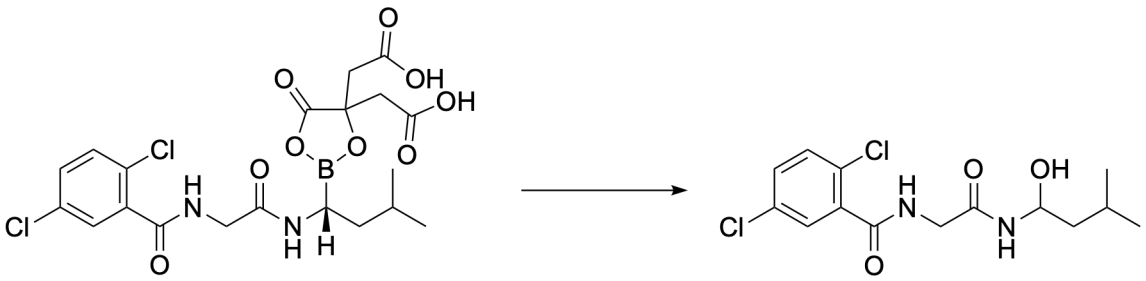


Fig. S11 LC trace of IXZ–MIDA at 280.4 nm using a 20–80% v/v MeCN gradient (Table S1).



Compound: Oxidized Ixazomib (IXZ-ox)

Procedure: Adapted from Wagh and Nagarkar (2017).[4] IXZ (0.0350 g, 0.097 mmol) was suspended in 2 mL of 2:1:1 DMC/H_2O/acetone. Hydrogen peroxide (2 equiv of a 30% w/w aqueous solution) was added to the mixture. The reaction mixture was stirred for 2.5 h and continuously monitored with TLC and staining for the boronic acid with HBQ, until the reaction was complete. The reaction mixture was diluted with water. The aqueous phase was extracted four times with EtOAc. The combined organic layers were washed once with water, once with brine, dried over Na_2SO_4(s), and concentrated under reduced pressure. The product was purified on silica with flash chromatography using DCM and MeOH. The product was obtained as a white solid (0.0149 g, 0.044 mmol, 46%) as a single diastereomer. A small sample was prepared for analytical purposes via preparative TLC (9:1 DCM/MeOH).

^{1}H NMR (500 MHz, DMSO-d_6, δ): 8.72 (t, J = 5.9 Hz, 1H), 8.14 (d, J = 8.6 Hz, 1H), 7.55 (dd, J = 4.4, 1.3 Hz, 3H), 5.61 (d, J = 5.1 Hz, 1H), 5.26 (dtd, J = 8.8, 6.7, 5.1 Hz, 1H), 3.90–3.75 (m, 2H), 1.73–1.57 (m, J = 6.7 Hz, 1H), 1.44 (dt, J = 13.8, 6.9 Hz, 1H), 1.33 (dt, J = 13.5, 6.8 Hz, 1H), 0.86 (t, J = 6.4 Hz, 6H). **^{13}C{^{1}H} NMR** (126 MHz, DMSO-d_6, δ): 167.5, 165.2, 137.8, 131.5 (2C), 130.7, 128.9, 128.8, 71.1, 45.3, 42.2, 24.1, 22.6, 22.3.

HRMS (DART-TOF**)** *m*/*z*: $[M + 2H]^{2+}$ calculated for $C_{14}H_{20}N_2O_3Cl_2^{2+}$, 334.0846; found, 334.0885.

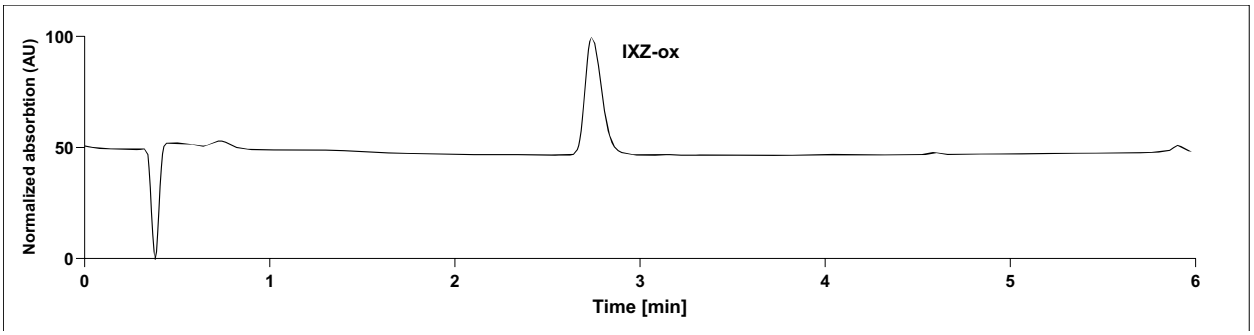


Fig. S12 LC trace of IXZ-ox at 280.4 nm using a 20–80% v/v MeCN gradient (Table S1).

4. LC-MS Assay Optimization

LC-MS Measurements. The column used was an Agilent Poroshell 120 for InfinityLab HPLC systems, EC-C18 with a particle size of 2.7 μm and dimensions of 3.0 × 50 mm. The flow rate on the column was kept at 0.8 mL/min for all measurements. The mobile phase was composed of HPLC-grade water and acetonitrile, each containing 0.1% v/v formic acid. The column was equilibrated to the respective starting gradient for 2 min before any sample sequence and then equilibrated with 9:1 water/acetonitrile after each sample sequence. Aqueous blanks were measured at the start and end of any sample sequence. The different gradients used for the LC-MS studies are described in Table S1. Integration of the LC-MS data was performed using the Agilent OpenLab Data Analysis Software. Integration was performed on the 280.4 nm channel with a Straight skim peak separation mode and a skim ratio of 50.0.

Table S1. Gradients used in LC-MS analysis of all compounds

Time (min)	30–80% v/v MeCN	20–80% v/v MeCN	20–100% v/v MeCN
0.00	30	20	20
5.00	80	80	100
5.30	30	20	20
6.00	30	20	20

Determination of Molar Extinction Coefficients at 280 nm
Absorbances were measured on a Spark Multimode Microplate Reader from Tecan in a 96-well plate (Clear, PS, Flat Bottom 96-well plate, Cat. No. 12565501 from Thermo Fisher Scientific). Data were evaluated with SparkControl V3.1 SP1. All molar extinction coefficients were obtained at 280 nm from a concentration range of 50 to 500 μM and are summarized in Table S3. The absorbance for each compound was measured in the respective LC-MS solvent compositions where the compounds elute. The respective solvent compositions are described in Table S2.

Table S2. Percent of solvent B (MeCN) required to elute each compound.

Compound	% v/v MeCN
BTZ	51
BTZ–MIDA	60.5
BTZ–pinanediol	100
BTZ-ox-1	55.5
BTZ-ox-2	58.5
IXZ	49
IXZ–MIDA	59.5
IXZ-ox	53

Procedure: The samples were mixed directly in the 96-well plate, with a final volume of 200 µL per well. To achieve the desired concentrations, BTZ, BTZ–MIDA, BTZ–pinanediol, IXZ, and IXZ–MIDA were added to the wells from 10 and 50 mM stock solutions in anhydrous DMSO, resulting in DMSO concentrations of 0.5–2.0% v/v. The molar extinction coefficients of all compounds were calculated from the slopes of absorbance versus concentration plots using Eq S1. The data from three measurements across six replicates are listed in Table S3, along with their 95% confidence intervals. Example simple linear regression plots for BTZ and BTZ–MIDA are shown in Fig. S13 and S14, respectively.

$$\varepsilon = \frac{\text{slope}}{l}, \text{ where } l = 0.52 \text{ cm} \quad \text{(S1)}$$

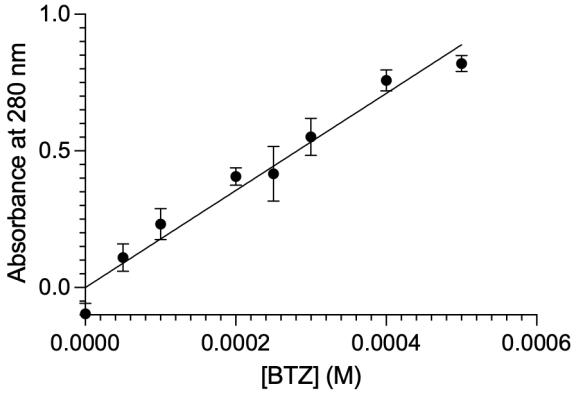


Fig. S13. Simple linear regression analysis for determining the extinction coefficient of BTZ in 51% v/v MeCN in water (0.1% v/v formic acid). $\varepsilon = 3416.35 \pm 150.96$ M^{-1} cm^{-1}.

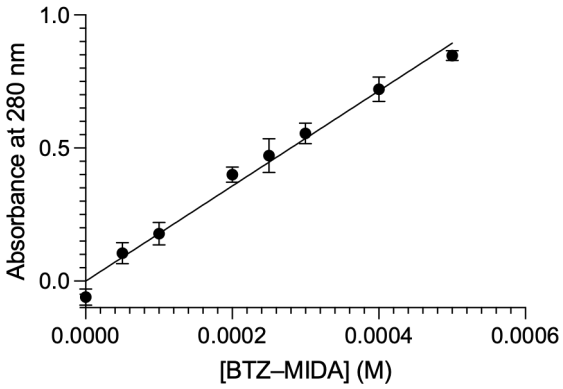


Fig. S14 Simple linear regression analysis for determining the extinction coefficient of BTZ–MIDA in 60.5% v/v MeCN (0.1% v/v formic acid). ε = 3437.5 ± 101.0 M^{-1} cm^{-1}.

Table S3. Mean molar extinction coefficients with 95% confidence intervals.

Compound	ε (M^{-1} cm^{-1}) at 280 nm
BTZ	3416.4 ± 151.0
BTZ–MIDA	3437.5 ± 101.0
BTZ–pinanediol	2779.8 ± 116.4
BTZ-ox-1	3264.4 ± 106.7
BTZ-ox-2	2930.8 ± 111.5
IXZ	596.15 ± 122.12
IXZ–MIDA	325.29 ± 83.36
IXZ-ox	895.10 ± 195.58

5. Boronate Ester Hydrolysis

Hydrolysis of BTZ–MIDA in Phosphate Buffer (pH 7.0 or 8.0)
Procedure. Hydrolysis of BTZ–MIDA was performed in 100 mM sodium phosphate buffer. The solutions were prepared in 20 mL disposable scintillation glass vials. To 5 mL of buffer, 50 µL of a stock solution of BTZ–MIDA (81 mM) in anhydrous DMSO was added, yielding an overall concentration of 0.4 mg/mL of BTZ–MIDA in 1% v/v DMSO. For LC-MS measurements, 50 µL of sample was diluted with 150 µL of Milli-Q water. 20 µL of this diluted sample was injected into the LC-MS and separated using a 30–80% v/v MeCN gradient (Table S1). The samples were protected from light during hydrolysis monitoring.

Hydrolysis of BTZ–MIDA in Phosphate Buffer (pH 7.2) at 4 °C
Procedure. The hydrolysis of BTZ–MIDA at pH 7.2 and 4 °C was performed in 100 mM sodium phosphate buffer. 2970 µL of buffer was added to 20 mL disposable scintillation glass vials, and the solutions were chilled to 4 °C for 30 min. 30 µL of an 81 mM stock solution of BTZ–MIDA in anhydrous DMSO was added, resulting in an overall concentration of 0.4 mg/mL of BTZ–MIDA with 1% v/v DMSO. For LC-MS measurements, 50 µL of sample was diluted with 150 µL of Milli-Q water. 20 µL of this diluted sample was injected into the LC-MS and separated using a

20–80% v/v MeCN gradient (Table S1). During hydrolysis monitoring, the samples were kept at 4 °C and protected from light.

Hydrolysis of BTZ–MIDA in Normal Saline (pH 4.0–6.5)

Procedure. Hydrolysis of BTZ–MIDA in normal saline was performed by dissolving 30 µL of BTZ–MIDA stock solution in anhydrous DMSO in 2970 µL of normal saline in 20 mL disposable scintillation glass vials. To arrive at a final concentration of 0.4 mg/mL or 1.0 mg/mL BTZ–MIDA, a stock solution of 81 mM BTZ–MIDA or 203 mM BTZ–MIDA, respectively, was used, both resulting in a concentration of 1% v/v DMSO. In cases where a tenfold mass excess of D-mannitol was added, 12 mg of D-mannitol (in the case of a 0.4 mg/mL BTZ–MIDA sample) was first added to the vial, then dissolved in normal saline, and finally the BTZ–MIDA stock solution was added. For LC-MS measurements of 0.4 mg/mL BTZ–MIDA samples, 50 µL of the sample was diluted with 150 µL of Milli-Q water. For LC-MS measurements of 1 mg/mL BTZ–MIDA samples, 20 µL of the sample was diluted with 180 µL of Milli-Q water. 20 µL of this diluted sample was injected into the LC-MS and separated using a 20–80% v/v MeCN gradient (Table S1). During hydrolysis monitoring, the samples were kept protected from light.

Note: Without buffering capacity, normal saline becomes acidic upon exposure to air due to the generation of carbonic acid from dissolved CO_2. Additionally, the hydrolysis of MIDA group leads to the release of acidic protons from water through the hydration of the boron (R–B(MIDA) + 2 H_2O ⟶ R–B$(OH)_2$ + 2 H^+ + $MIDA^{2-}$). The pH of the solution, measured throughout our experiments, decreased from about 6.5 to 4.0 in some cases. We did not attempt to control the pH of the solution via buffering or degassing, as these methods are not used in pharmaceutical preparations for in vivo administration. The % hydrolysis of BTZ–MIDA was calculated with Eq S2.

$$\%\ \text{hydrolysis} = \frac{A_{\text{BTZ}}^{280.4} + A_{\text{BTZ-ox-1}}^{280.4}}{A_{\text{BTZ}}^{280.4} + A_{\text{BTZ-ox-1}}^{280.4} + A_{\text{BTZ-MIDA}}^{280.4}} \times 100\% \tag{S2}$$

Note: *A* is the area of the peak of the specified compound in the 280.4 nm UV trace of the LC experiment.

Hydrolysis of BTZ–MIDA and IXZ–MIDA in Phosphate Buffer (pH 7.0)

Procedure. Hydrolysis experiments of BTZ–MIDA and IXZ–MIDA in 10 mM sodium phosphate buffer, pH 7.0, were performed by dissolving 40 µL of a 50 mM stock solution of the respective compound in 3960 µL of 10 mM sodium phosphate buffer, pH 7.0, resulting in an overall concentration of 0.5 mM of the respective compound with 1% v/v DMSO. For LC-MS measurements, 100 µL of sample was diluted with 30 µL of Milli-Q water. A 10-µL aliquot of this diluted sample was injected into the LC-MS and separated using a 20–80% v/v MeCN gradient (Table S1). % hydrolysis of BTZ–MIDA was calculated with Eq S2.

The % hydrolysis of IXZ–MIDA was calculated according to the ratiometric change in IXZ–MIDA and IXZ in the presence of an internal standard (caffeine). The use of the internal standard for the IXZ–MIDA hydrolysis assay proved more reliable than applying a correction value from the difference in extinction coefficients due to the low absorbance of IXZ and IXZ–MIDA at λ = 280

nm. An internal standard was not necessary for any other experiments, as the ratiometric data for BTZ–MIDA were the same in the presence or absence of an internal standard.

Hydrolysis of BTZ–pinanediol in Normal Saline (pH 4.0–6.5)

Procedure. Hydrolysis experiments of BTZ–pinanediol were performed directly in LC-MS autosampler vials. To 1500 µL of normal saline, 1 µL of 39 mM BTZ–pinanediol stock solution in anhydrous DMSO was added. The sample was quickly vortexed. The result was a solution of 25.7 µM BTZ–pinanediol in normal saline with 0.07% v/v DMSO. For LC-MS measurements, 20 µL from the vial was injected into the LC-MS and separated using a 20–100% v/v MeCN gradient (Table S1). During hydrolysis monitoring, the samples were kept directly in the LC-MS autosampler, protected from light, and frequently checked for signs of solution changes. % Hydrolysis of BTZ–pinanediol was calculated with Eq S3. The absorption of BTZ–pinanediol is corrected by a factor of 1.23, which corresponds to the relative difference in molar extinction coefficients of BTZ and BTZ–pinanediol in their respective LC-MS solvent composition of elution, see Table S3.

$$\%\ \text{hydrolysis} = \frac{A_{\text{BTZ}}^{280.4} + A_{\text{BTZ-ox-1}}^{280.4}}{A_{\text{BTZ}}^{280.4} + A_{\text{BTZ-ox-1}}^{280.4} + 1.23 \times A_{\text{BTZ-pinanediol}}^{280.4}} \times 100\% \quad \text{(S3)}$$

Note: *A* is the area of the peak of the specified compound in the 280.4 nm UV trace of the LC experiment.

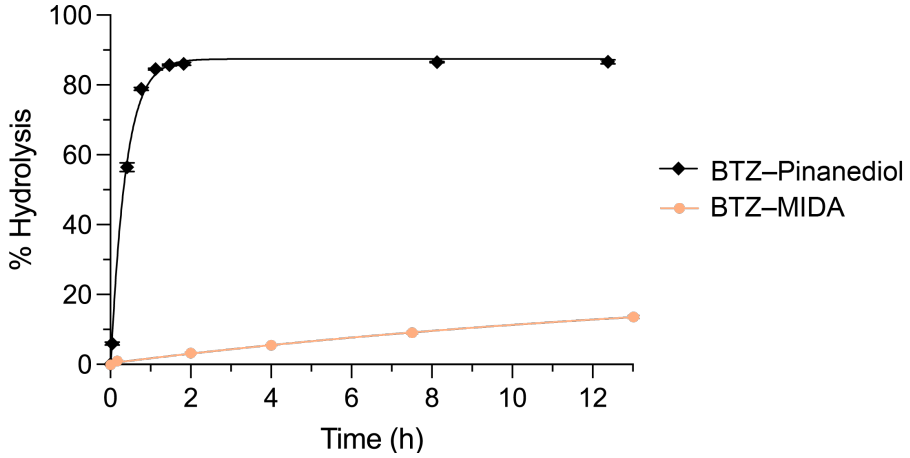


Fig. S15 Hydrolysis of BTZ–MIDA versus BTZ–pinanediol in normal saline (pH 4.0–6.5), determined by LC-MS from the ratiometric change in starting material and hydrolysis products. Values are the mean ± SE for three replicates.

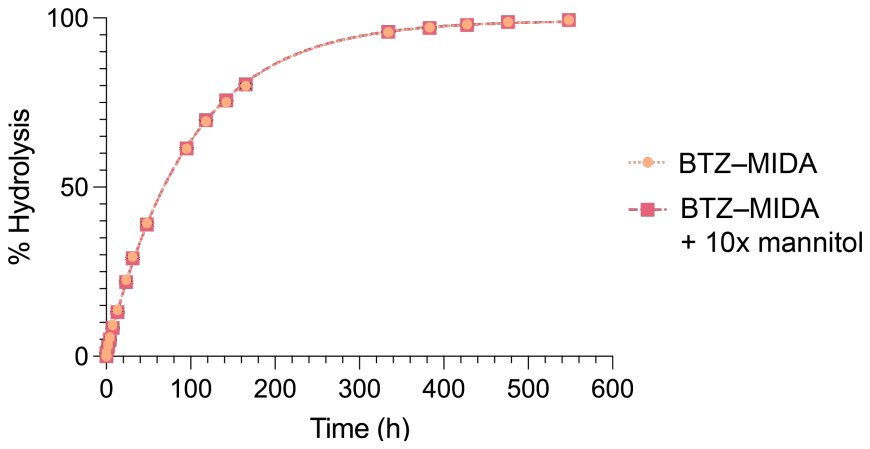


Fig. S16 Hydrolysis of BTZ–MIDA in normal saline (pH 4.0–6.5) in the presence or absence of 10× (w/w) D-mannitol (according to clinical-use formulation for single use) determined by LC-MS as the ratiometric change in starting material and hydrolysis products. Values are the mean ± SE for three replicates.

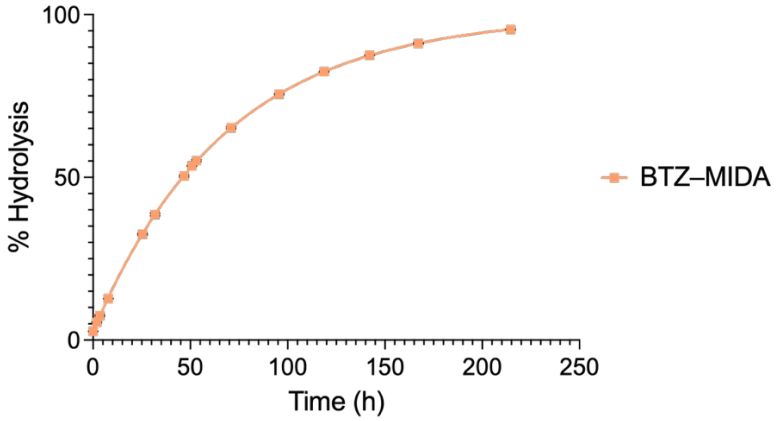


Fig. S17 Hydrolysis of BTZ–MIDA in 100 mM sodium phosphate buffer, pH 7.0, determined by LC-MS as the ratiometric change in starting material and hydrolysis products. Values are the mean ± SE for three replicates.

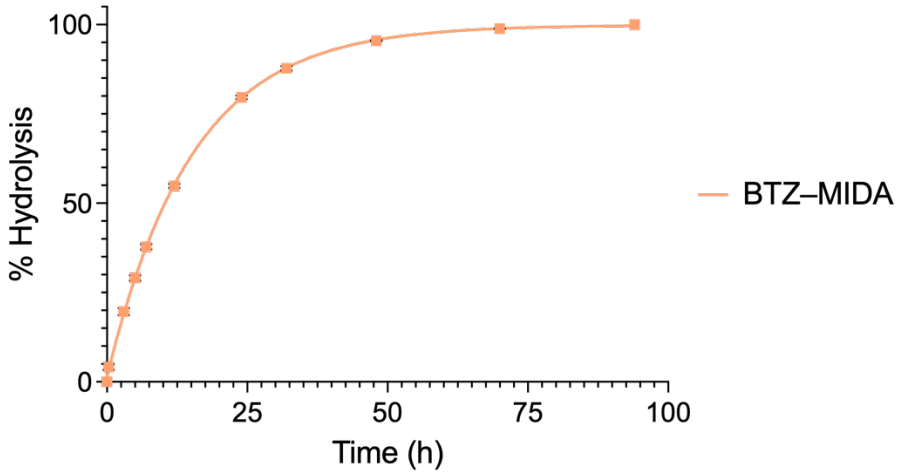


Fig. S18 Hydrolysis of BTZ–MIDA in 100 mM sodium phosphate buffer, pH 8.0, determined by LC-MS as ratiometric change in starting material and hydrolysis products. Values are the mean ± SE for three replicates.

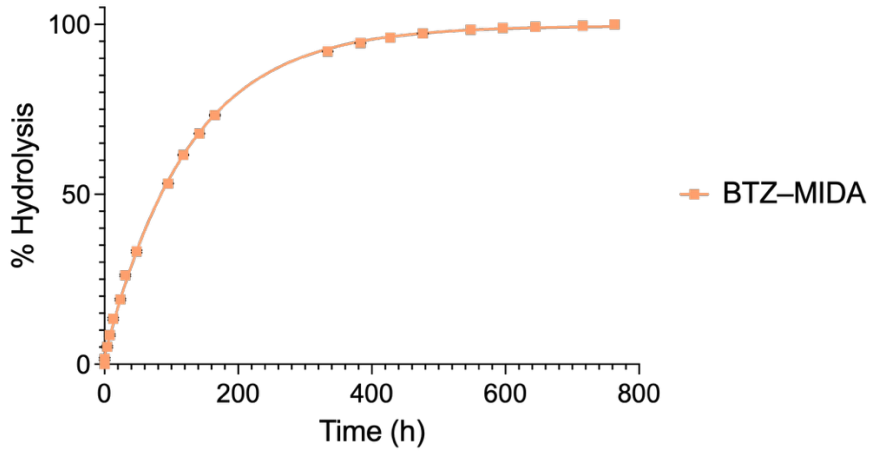


Fig. S19 Hydrolysis of BTZ–MIDA in 100 mM sodium phosphate buffer, pH 7.2, at 4 °C, determined by LC-MS as the ratiometric change in starting material and hydrolysis products. Values are the mean ± SE for three replicates.

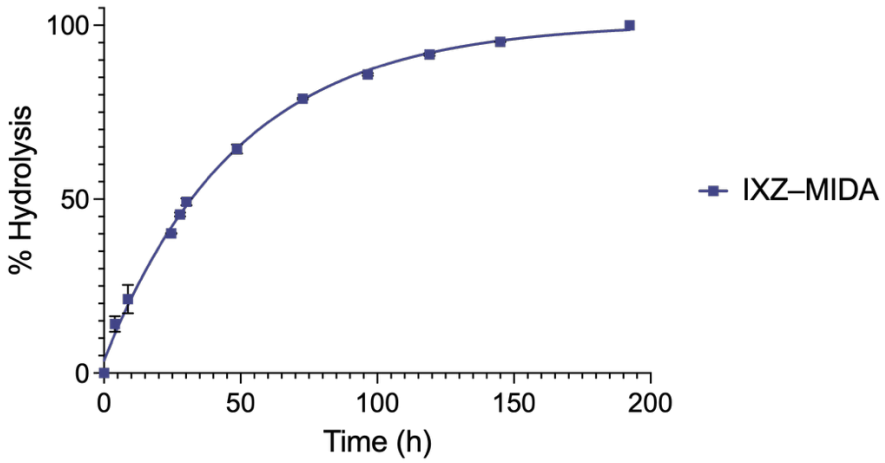


Fig. S20 Hydrolysis of IXZ–MIDA in 10 mM sodium phosphate buffer, pH 7.0, determined by LC-MS as the ratiometric change in starting material and hydrolysis products. Values are the mean ± SE for three replicates.

6. H_2O_2-mediated Oxidation of BTZ, IXZ, and Boronate Esters

Solutions for LC-MS measurements of compound oxidation were directly prepared in autosampler vials. Stock solutions of the compounds were prepared in anhydrous DMSO and only added to the aqueous hydrogen peroxide solution 2 min before the first injection. Hydrogen peroxide solutions were freshly prepared each day from a 30% w/w aqueous solution and were stored on ice and protected from light. A 20–80% v/v MeCN gradient (Table S1) was used for BTZ, BTZ–MIDA, IXZ, IXZ–MIDA. A 20–100% v/v MeCN gradient (Table S1) was used for BTZ–pinanediol. Oxidation of BTZ and BTZ–MIDA was calculated with Eq S4, and oxidation of IXZ and IXZ–MIDA was calculated with Eq S5. Oxidation of BTZ–pinanediol was calculated with Eq S6.

$$\%\ \text{oxidation} = \frac{A^{280.4}_{\text{BTZ-ox-1}}}{A^{280.4}_{\text{BTZ}} + A^{280.4}_{\text{BTZ-ox-1}} + A^{280.4}_{\text{BTZ-MIDA}}} \times 100\% \tag{S4}$$

Note: *A* is the area of the peak of the specified compound in the 280.4 nm UV trace of the LC experiment.

$$\%\ \text{oxidation} = \frac{A^{280.4}_{\text{IXZ-ox}}}{A^{280.4}_{\text{IXZ}} + A^{280.4}_{\text{IXZ-ox}} + 1.83 \times A^{280.4}_{\text{IXZ-MIDA}}} \times 100\% \tag{S5}$$

Note: *A* is the area of the peak of the specified compound in the 280.4 nm UV trace of the LC experiment. The absorption of IXZ–MIDA is corrected by a factor of 1.83, which corresponds to the relative difference in molar extinction coefficients of IXZ and IXZ–MIDA in their respective LC-MS solvent compositions of elution (Tables S2 and S3). Any error propagation from extinction

coefficient measurements of IXZ/IXZ–MIDA into the correction value for IXZ–MIDA had little impact on the oxidation rates because they were so slow.

$$\%\ \text{oxidation} = \frac{A^{280.4}_{\text{BTZ-ox-1}}}{A^{280.4}_{\text{BTZ}} + A^{280.4}_{\text{BTZ-ox-1}} + 1.23 \times A^{280.4}_{\text{BTZ-pinanediol}}} \times 100\% \quad \text{(S6)}$$

Note: *A* is the area of the peak of the specified compound in the 280.4 nm UV trace of the LC experiment. The absorption of BTZ–pinanediol is corrected by a factor of 1.23, which corresponds to the relative difference in molar extinction coefficients of BTZ and BTZ–pinanediol in their respective LC-MS solvent composition of elution (Tables S2 and S3).

Oxidation in Normal Saline (pH 4.0–6.5)

Procedure. For oxidation assays of all compounds (BTZ, BTZ–MIDA, and BTZ–pinanediol), 1500 µL of normal saline and 1 µL of 30% w/w aqueous hydrogen peroxide were pre-mixed in the autosampler vial. 1 µL of the respective stock solution in DMSO was added to the vial, followed by quick vortexing before placing it in the autosampler of the LC-MS instrument. The result was a final concentration of 6.4 mM H_2O_2 and 0.07% v/v DMSO. Measurements were performed every 14 min for 1.2 h. For BTZ–pinanediol, a 77.2 mM stock solution in DMSO was used, yielding a final concentration of 51.4 µM. For BTZ–pinanediol, a 20–100% v/v MeCN gradient (Table S1) was used. For BTZ–MIDA, an 81.1 mM stock solution in DMSO was used, resulting in a final concentration of 54.0 µM. For BTZ, a 104 mM stock solution in DMSO was used, resulting in a final concentration of 69.3 µM. The normal-saline oxidation data are shown in Fig. S21.

Oxidation in Phosphate Buffer (pH 7.0)

Procedure. Oxidation series in 50 mM sodium phosphate buffer, pH 7.0: 1500 µL of 50 mM sodium phosphate buffer, pH 7.0, and 0.5 µL of 3% v/v aqueous hydrogen peroxide were pre-mixed in the autosampler vial. 0.5 µL of a 70 mM stock solution in DMSO was added to the vial, followed by quick vortexing before placing it in the autosampler of the LC-MS instrument. The result was final concentrations of 23 µM of the respective compound, 330 µM H_2O_2, and 0.03% v/v DMSO. Measurements were performed every 7 min for 44 min. Data are presented in Fig. 2.

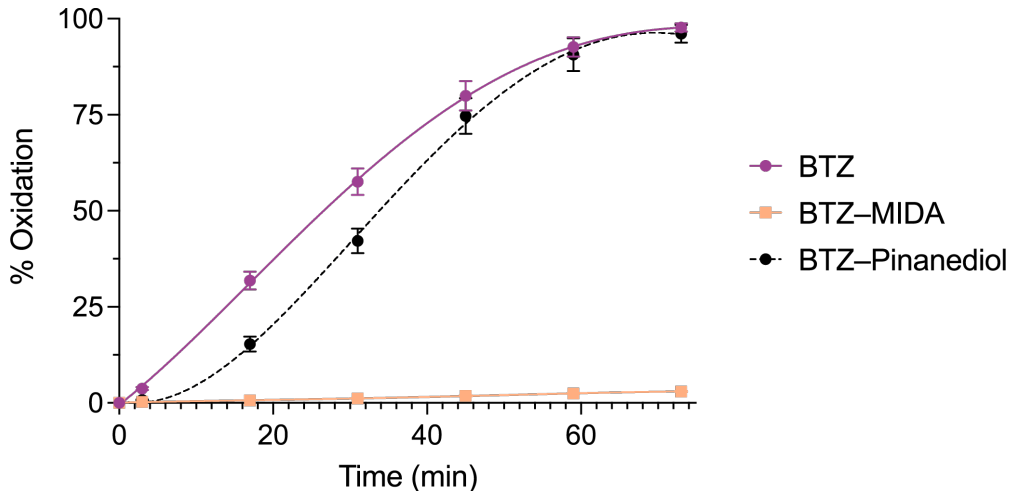


Fig. S21 Oxidation studies in normal saline, pH 4.0–6.5, as determined by LC-MS as the ratiometric change in starting material and oxidation products. Values are the mean ± SE for three replicates.

7. UV-induced Photodegradation of BTZ and Boronate Esters

LC-MS Analysis of Photodegradation in Borosilicate Glass with λ = 254 nm UV Light
Procedure. Compounds were prepared in 5 mL borosilicate glass vials. 990 µL of normal saline and a 10 µL stock solution (40 mg/mL) of BTZ or BTZ–MIDA in DMSO were mixed in the glass vial. The result was a final concentration of 0.4 mg/mL of the respective compound and 1% v/v DMSO. Three replicates were performed for each compound. The six vials were placed in front of the UV lamp, as shown in Fig. S22, and irradiated with λ = 254 nm light. The vial positions were scrambled regularly to ensure uniform exposure to UV light. For LC-MS measurements, 50 µL of each sample was diluted with 150 µL of Milli-Q water. 20 µL of this diluted sample was injected into the LC-MS and separated using a 20–80% v/v MeCN gradient (Table S1).

LC-MS Analysis of Photodegradation in Quartz Glass with λ = 254 nm or 365 nm UV Light
Procedure. Compounds were prepared in 1 mL quartz glass cuvettes. The cuvettes were sealed tightly with parafilm to prevent evaporation. 990 µL of normal saline and a 10 µL stock solution (40 mg/mL) of BTZ or BTZ–MIDA in DMSO were mixed in the cuvette. The result was a final concentration of 0.4 mg/mL of the respective compound and 1% v/v DMSO. Three replicates were performed for each compound. The six cuvettes were placed in front of the UV lamp, as shown in Fig. S22, and irradiated with λ = 254 nm light. The cuvette positions were scrambled regularly to ensure uniform exposure to UV light. For LC-MS measurements, 50 µL of each sample was diluted with 150 µL of Milli-Q water. 20 µL of this diluted sample was injected into the LC-MS and separated using a 20–80% v/v MeCN gradient (Table S1).



Fig. S22 Set-up for photodegradation assay using a UV lamp emitting λ = 254 nm or 365 nm light. Vials/cuvettes were scrambled regularly to ensure that each received the same exposure.

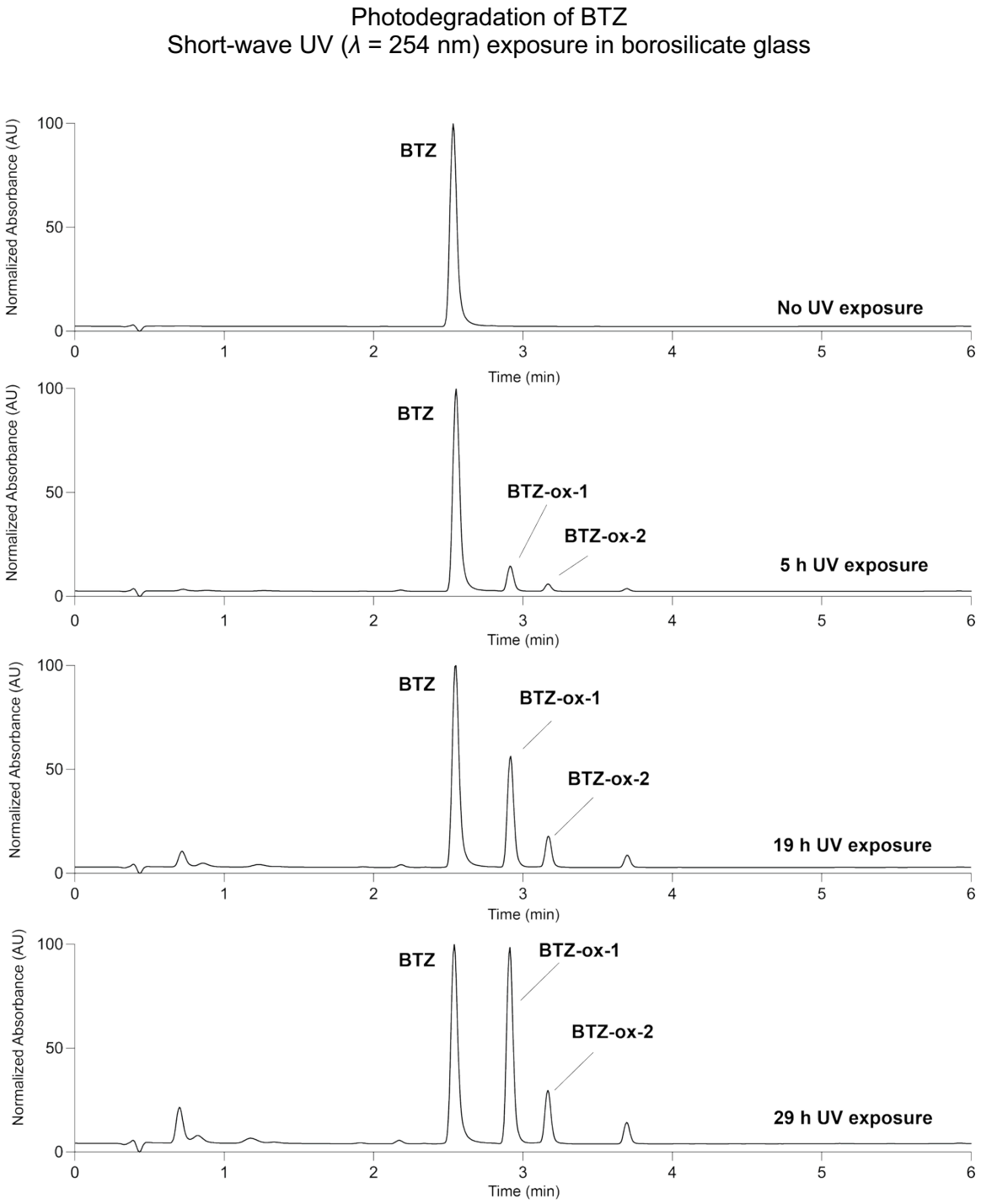


Fig. S23 Representative LC-MS traces from photodegradation (λ = 254 nm) of BTZ performed in triplicate in normal saline pH 4.0–6.5 and in borosilicate glass vials.

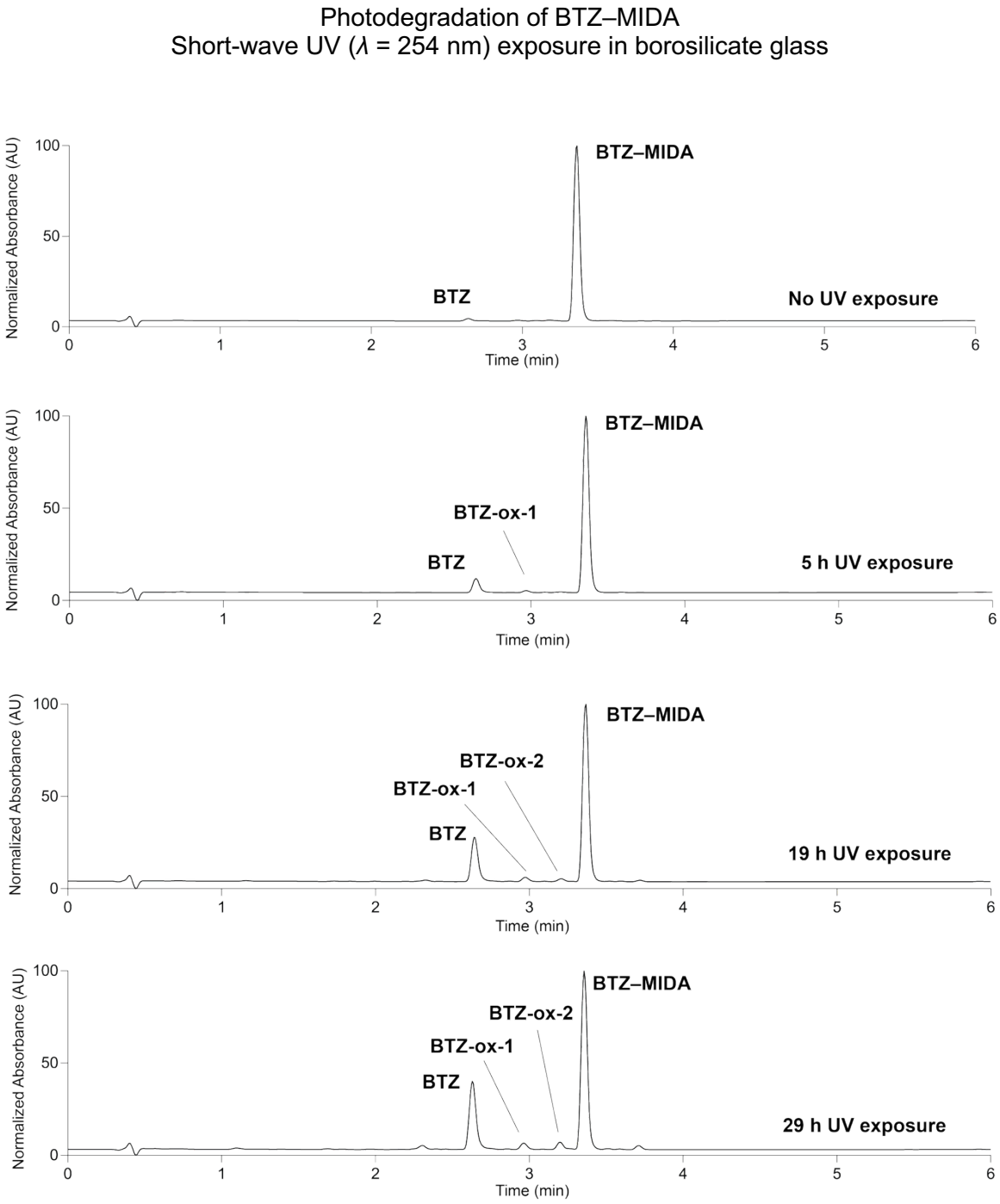


Fig. S24 Representative LC-MS traces from photodegradation of BTZ–MIDA (λ = 254 nm) performed in triplicate in normal saline pH 4.0–6.5 and in borosilicate glass vials.

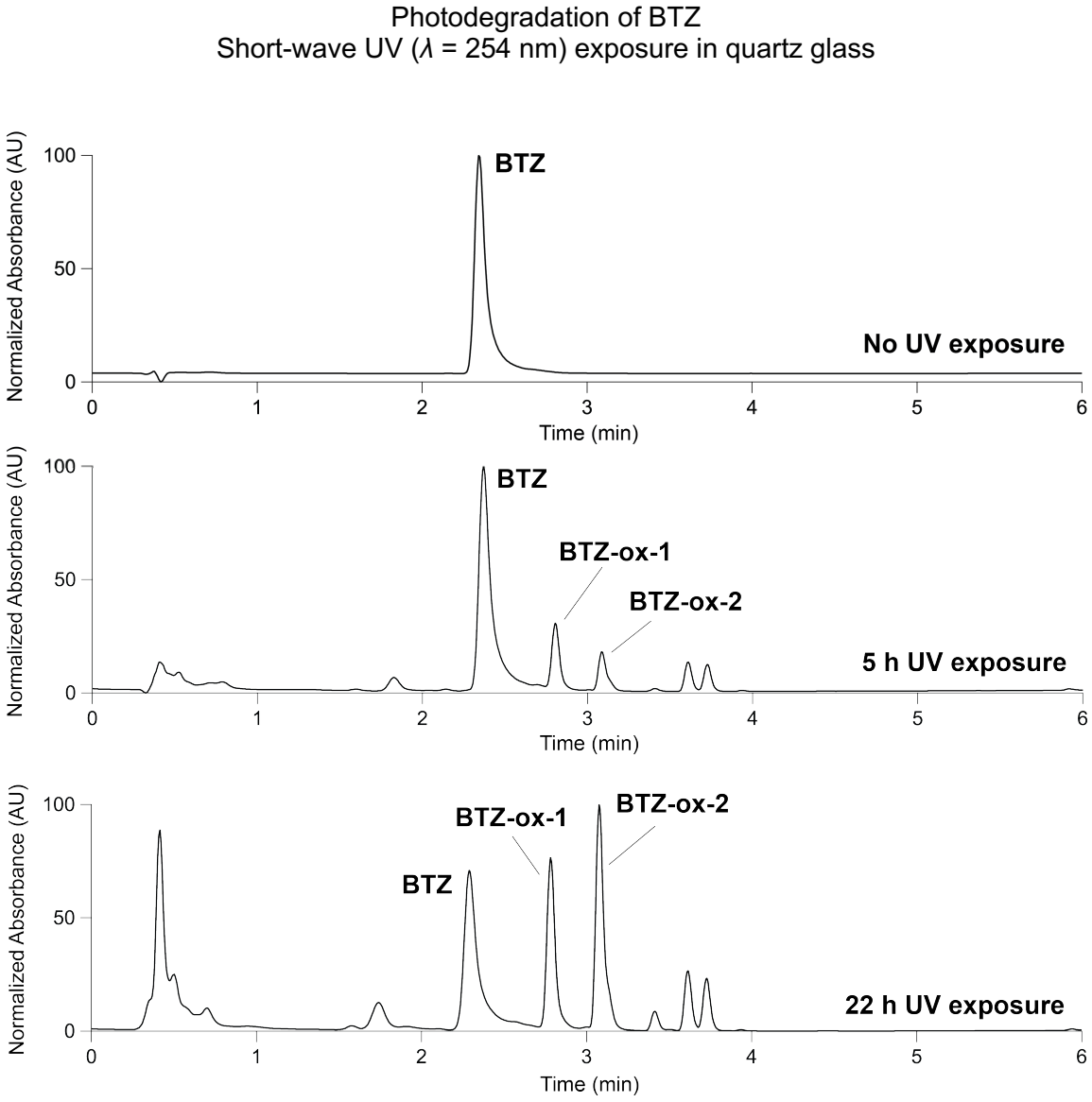


Fig. S25 Representative LC-MS traces from photodegradation of BTZ (λ = 254 nm) performed in triplicate in normal saline pH 4.0–6.5 and in quartz glass cuvettes.

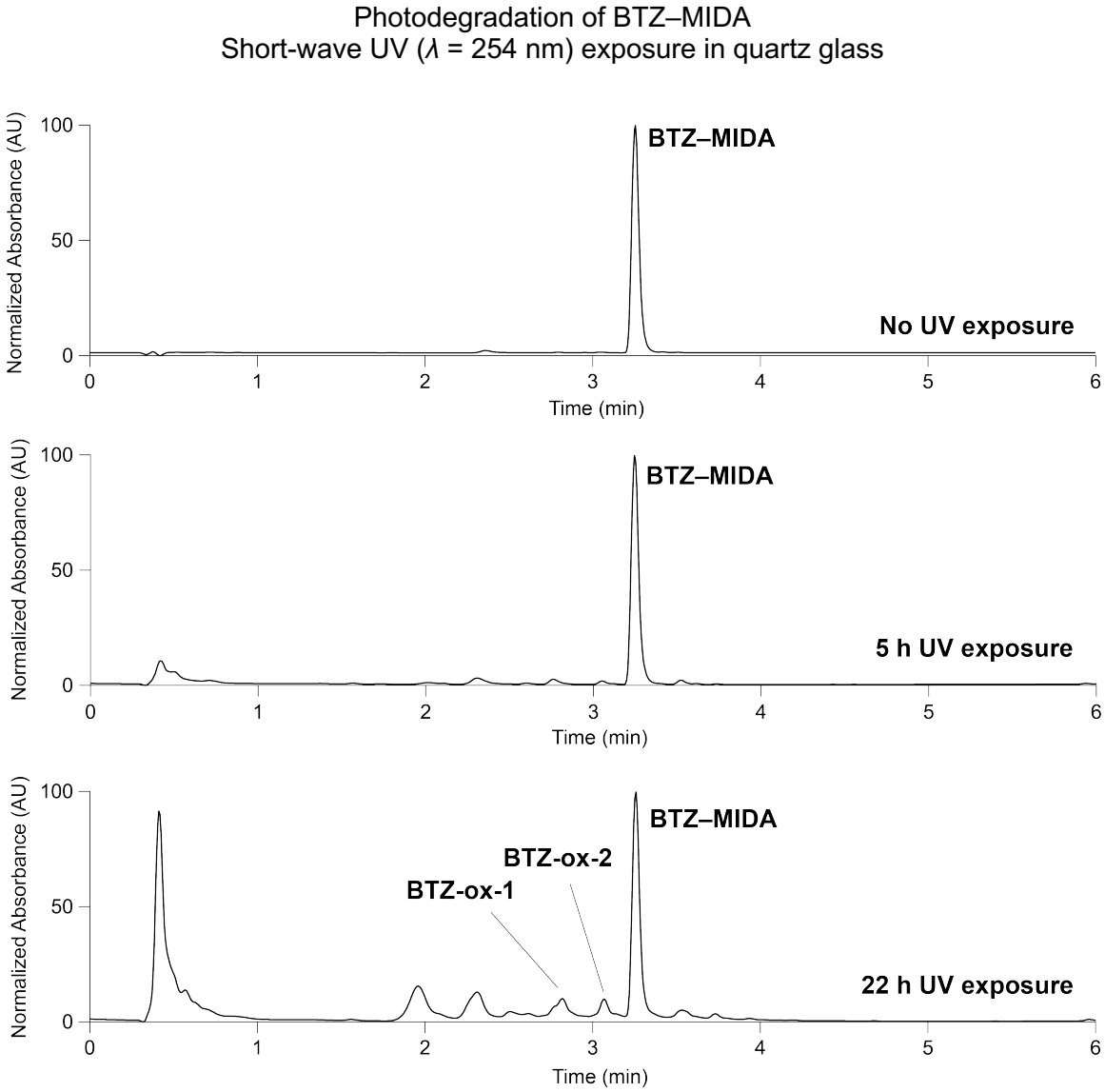


Fig. S26 Representative LC-MS traces from photodegradation of BTZ–MIDA (λ = 254 nm) performed in triplicate in normal saline pH 4.0–6.5 and in quartz glass cuvettes.

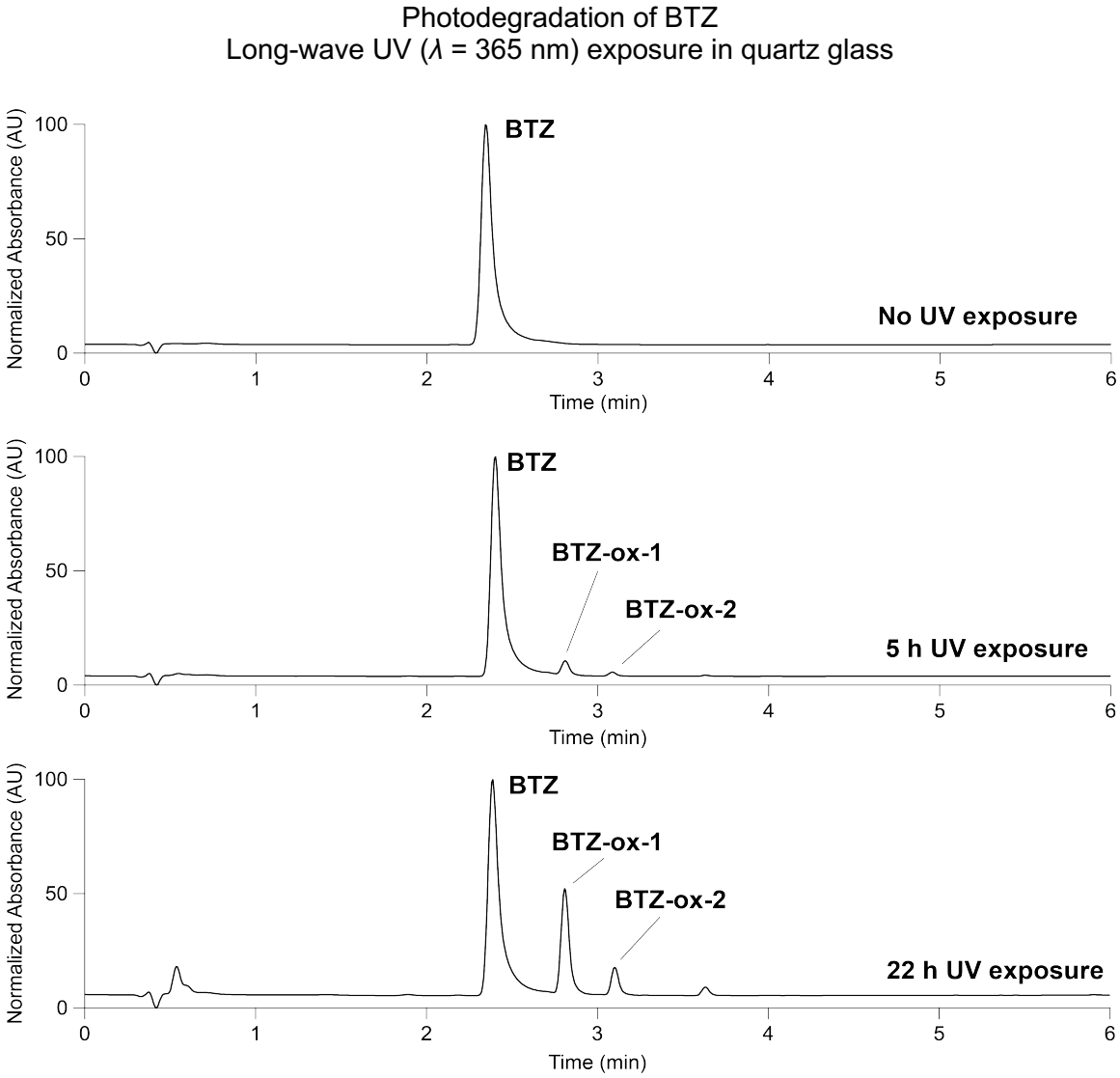


Fig. S27 Representative LC-MS traces from photodegradation of BTZ (λ = 365 nm) performed in triplicate in normal saline pH 4.0–6.5 and in quartz glass cuvettes.

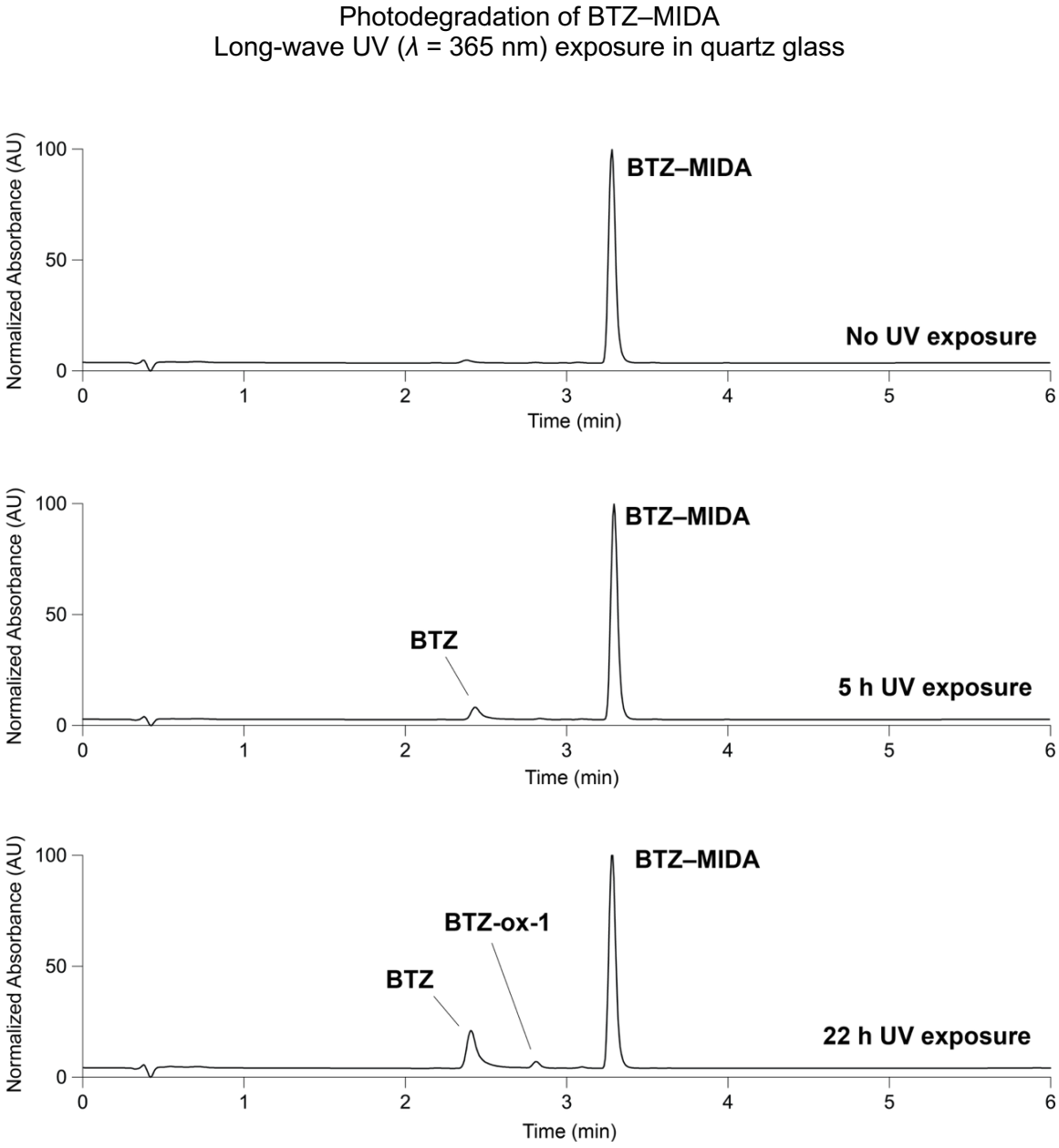


Fig. S28 Representative LC-MS traces from photodegradation of BTZ–MIDA (λ = 365 nm) performed in triplicate in normal saline pH 4.0–6.5 and in quartz glass cuvettes.

8. Cytotoxicity Studies

Procedures are reported in the Materials and Methods section.

KMS11 Cell Culture (Multiple Myeloma)

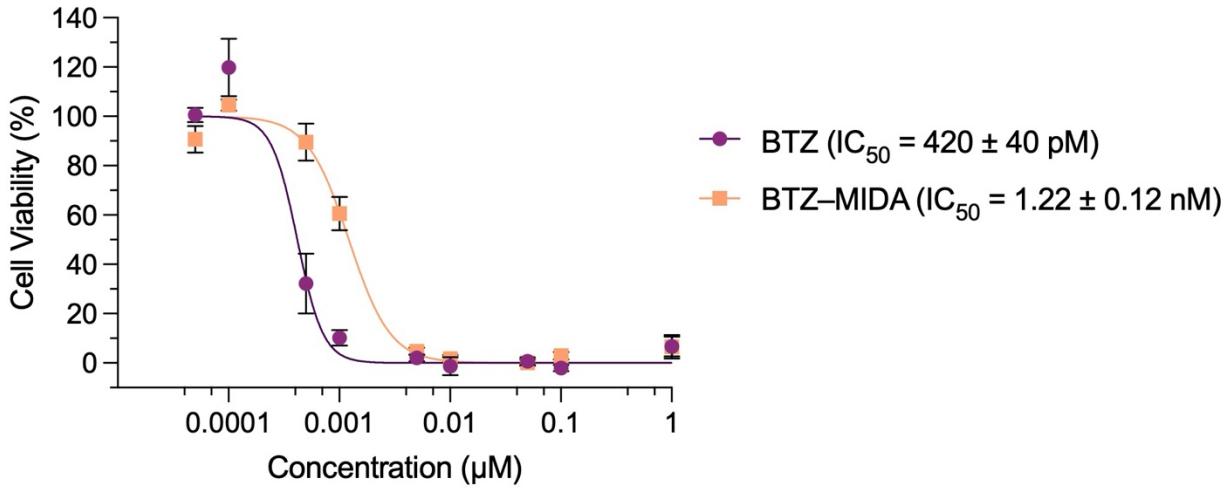


Fig. S29 48 h MTS cytotoxicity assay performed on KMS11 cell culture over a concentration range of BTZ versus BTZ–MIDA. Values are the mean ± SE for three replicates.

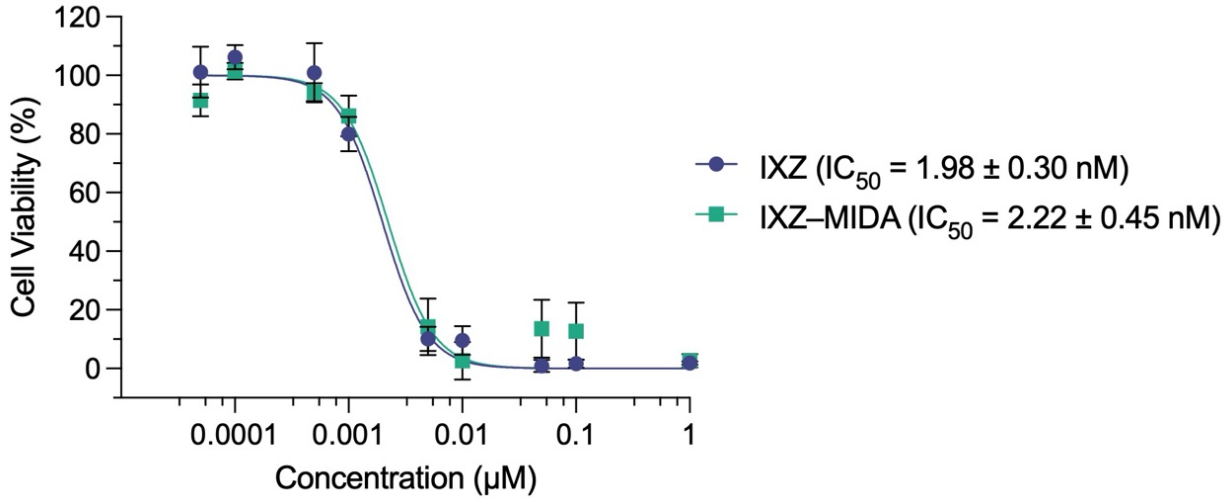


Fig. S30 48 h MTS cytotoxicity assay performed on KMS11 cell culture over a concentration range of IXZ versus IXZ–MIDA. Values are the mean ± SE for three replicates

HeLa Cell Culture (Cervical Cancer)

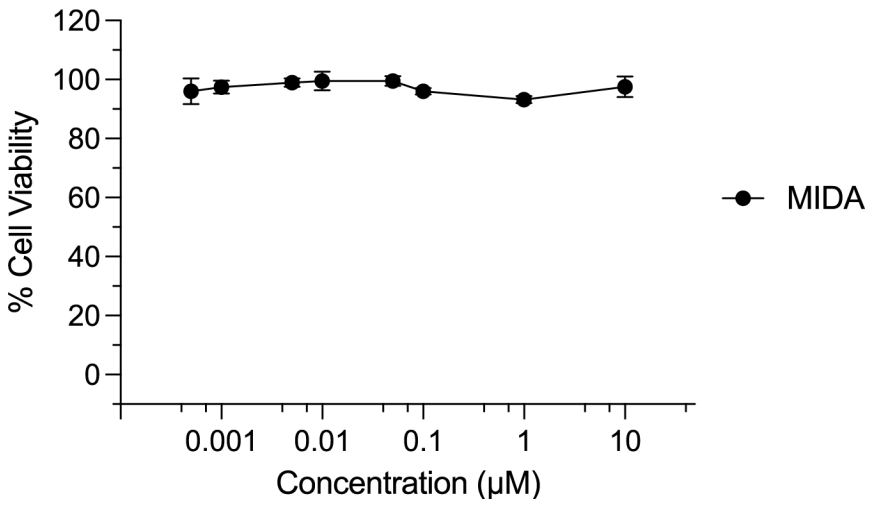


Fig. S31 48 h MTS cytotoxicity assay performed on HeLa cell culture over a concentration range of MIDA.

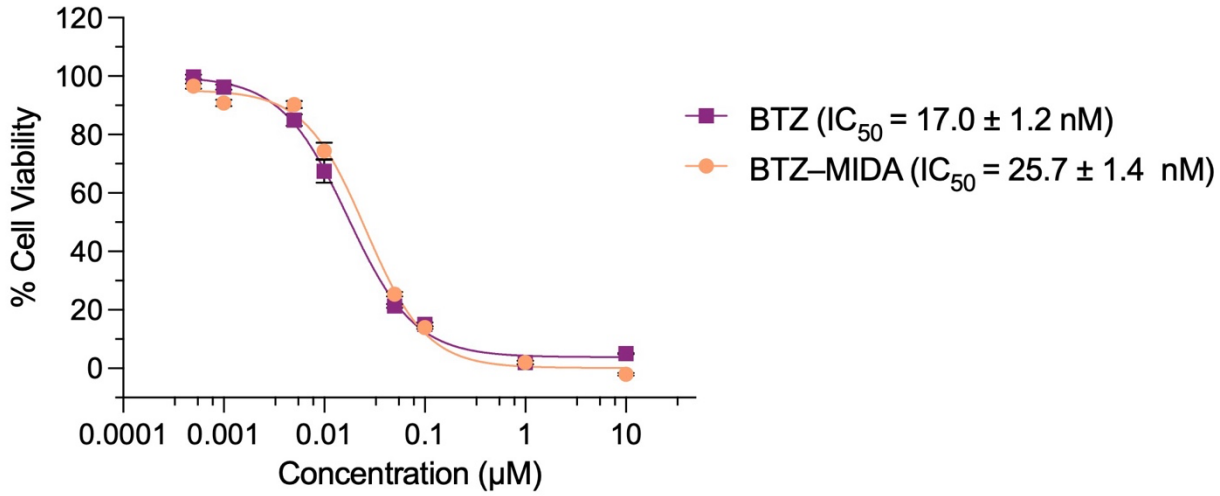


Fig. S32 48 h MTS cytotoxicity assay performed on HeLa cell culture over a concentration range of BTZ and BTZ–MIDA. Values are the mean ± SE for three replicates.

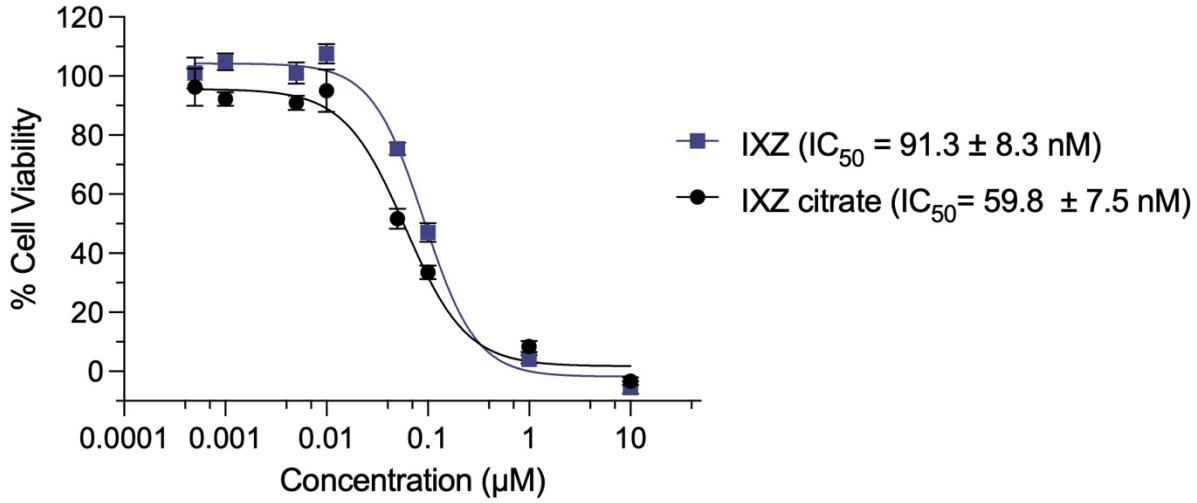


Fig. S33 48 h MTS cytotoxicity assay performed on HeLa cell culture over a concentration range of IXZ versus IXZ–citrate. Values are the mean ± SE for three replicates.

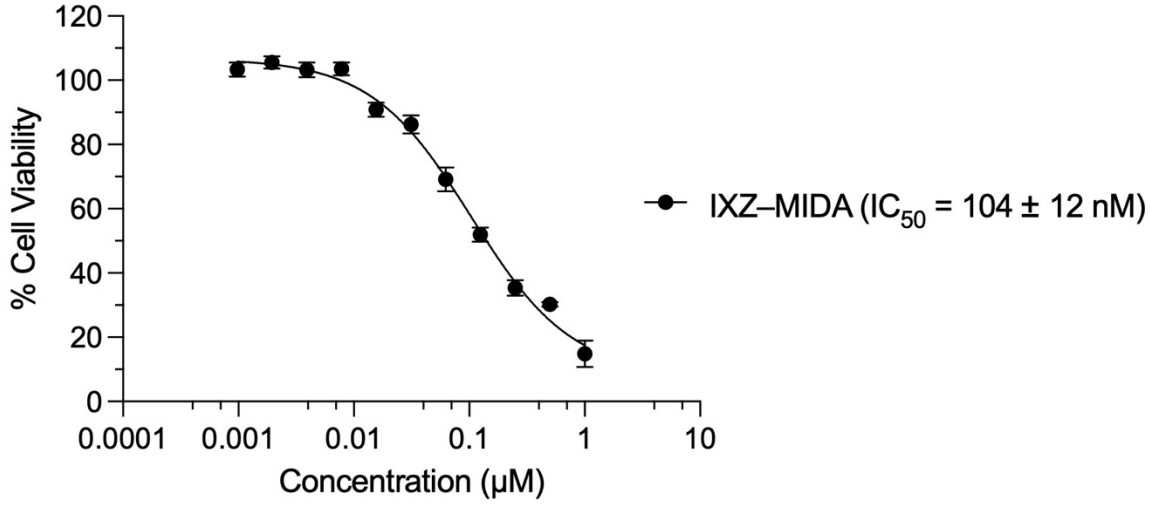


Fig. S34 48 h MTS cytotoxicity assay performed on HeLa cell culture over a concentration range of IXZ–MIDA. Values are the mean ± SE for three replicates.

M21 Cell Culture (Melanoma)

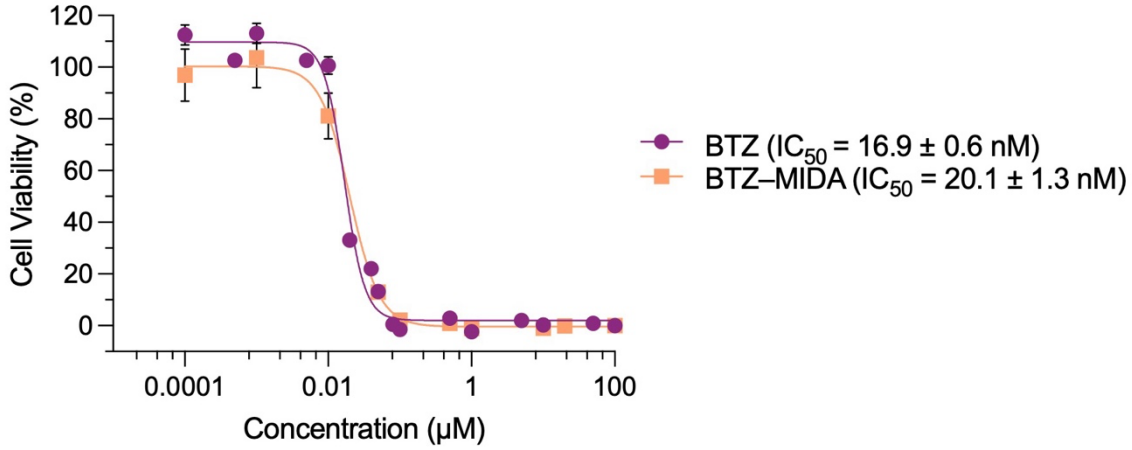


Fig. S35 48 h MTS cytotoxicity assay performed on M21 cell culture over a concentration range of BTZ versus BTZ–MIDA. Values are the mean ± SE for three replicates.

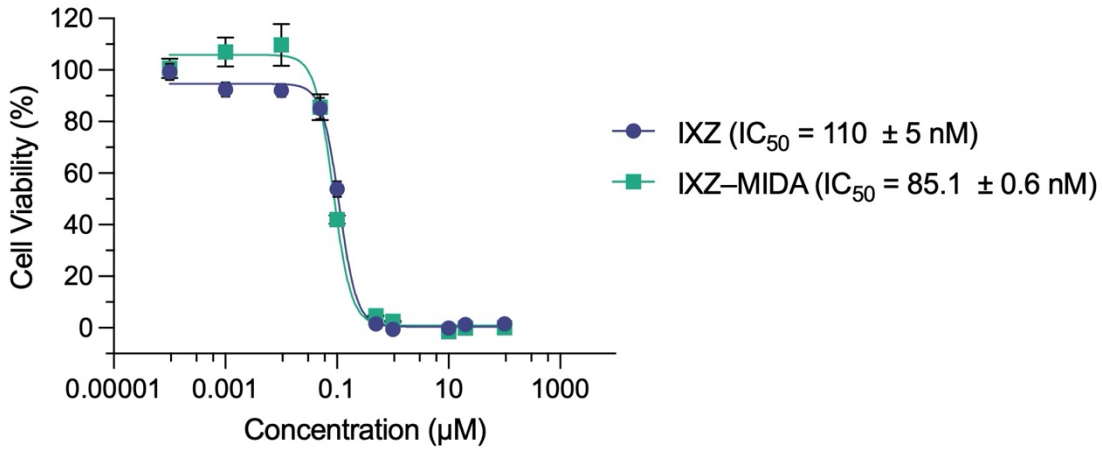


Fig. S36 48 h MTS cytotoxicity assay performed on M21 cell culture over a concentration range of IXZ versus IXZ–MIDA. Values are the mean ± SE for three replicates.

9. In Vitro Proteasome Activity Assay

The procedure is reported in the Materials and Methods section.

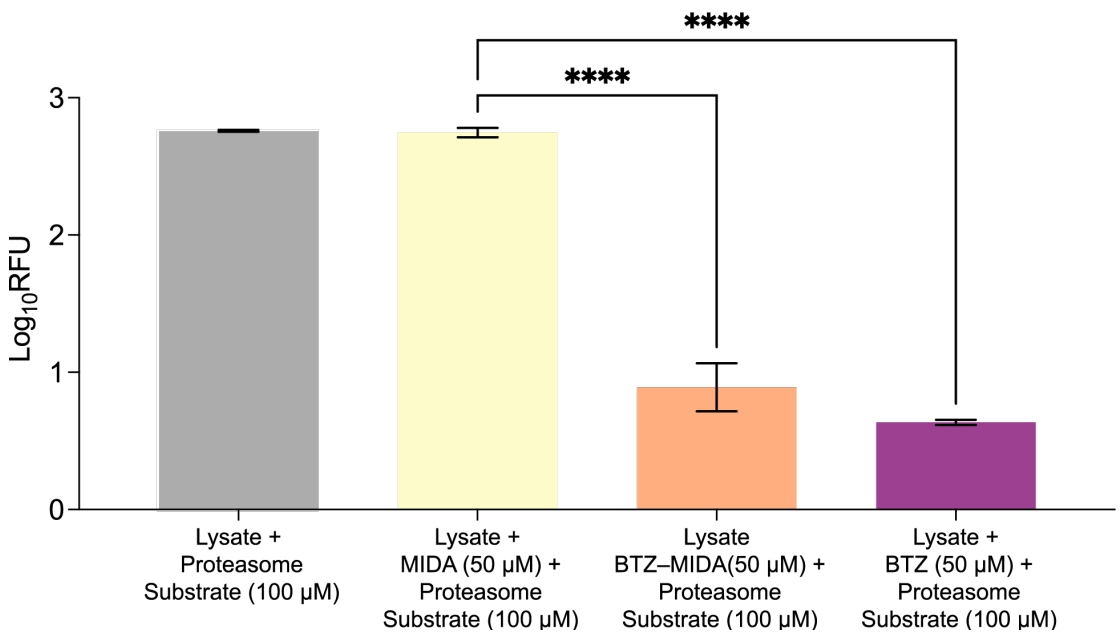


Fig. S37 Cell lysate proteasome activity assay using HAP1 cell lysate. Statistical significance was determined with an ordinary one-way ANOVA comparing BTZ and BTZ–MIDA to MIDA-only control, where **** refers to $P \leq 0.0001$. Statistics were calculated using GraphPad Prism software.

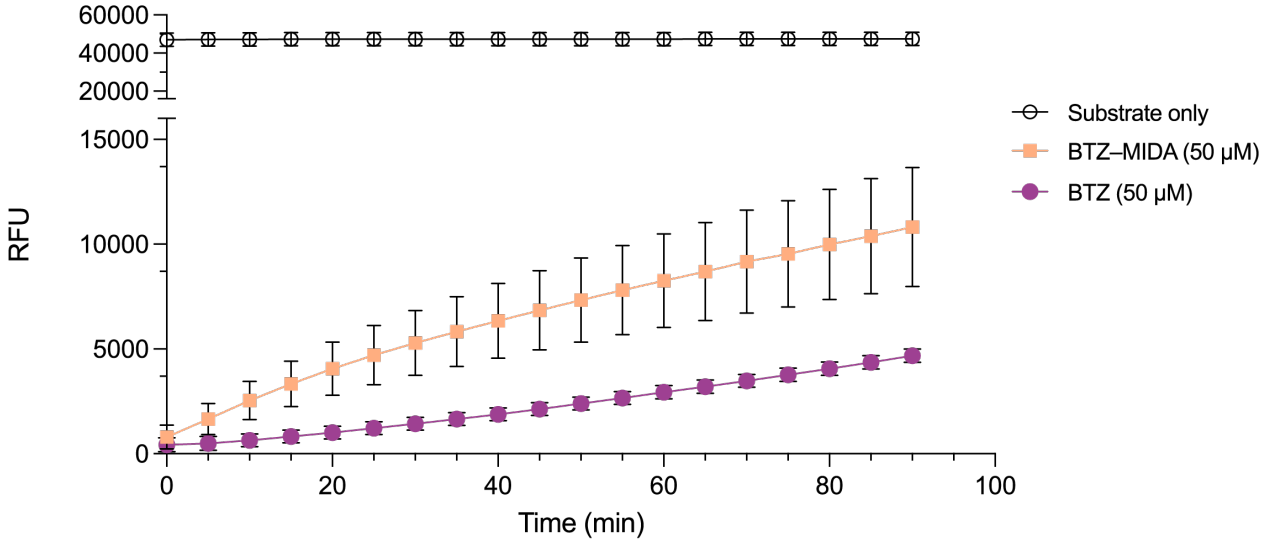


Fig. S38 Cell lysate proteasome activity assay using HAP1 cell lysate, shown here as a time course analysis of the first 90 min. Values are the mean ± SE for three replicates.

10. Esterase-mediated MIDA Ester Cleavage Studies

Pig Liver Esterase (PLE). Enzyme activity was confirmed by monitoring the absorbance of 4-nitrophenol at λ = 412 nm upon the enzymatic hydrolysis of 100 μM 4-nitrophenyl acetate in the presence of PLE (40 nM) in 50 mM sodium phosphate buffer, pH 8.0, at 25 °C. The MIDA ester hydrolysis assay was performed in 50 mM sodium phosphate buffer, pH 8.0. A 10 μL solution of BTZ–MIDA (5 mM) in anhydrous DMSO was diluted with 990 μL of buffer in an Eppendorf tube. A 10 μL solution of PLE (8 μM) in 50 mM sodium phosphate buffer, pH 8.0, was added to the respective tube. For the negative controls, 10 μL of buffer was added. The result was a final concentration of 80 nM PLE, 49.5 μM BTZ–MIDA, and 1% v/v DMSO. The samples were incubated at 37 °C on a shaker at 300 rpm. After incubation, the samples were filtered through an Amicon Ultra Centrifugal Filter (10 kDa MWCO) at 13,200 rpm for 2.5 min before injection into the LC-MS. For each sample, 20 μL was injected directly without dilution and separated using a 20–80% v/v MeCN gradient (Table S1). % hydrolysis of BTZ–MIDA was calculated with Eq S2.

Human Paraoxonase/Arylesterase 1 (PON1). Enzyme activity was confirmed by monitoring the absorbance of 4-nitrophenol at λ = 412 nm upon the enzymatic hydrolysis of 100 μM 4-nitrophenyl acetate in the presence of PON1 (71 nM) in 10 mM Tris–HCl buffer, 1 mM $CaCl_2$, pH 8.0, at 25 °C. The MIDA ester hydrolysis assay was performed in 10 mM Tris–HCl buffer, pH 8.0. A 10 μL solution of BTZ–MIDA (5 mM) in anhydrous DMSO was diluted with 990 μL of buffer in an Eppendorf tube. A 10 μL solution of PON1 (1.5 μM) in 10 mM Tris–HCl buffer, 1 mM $CaCl_2$, pH 8.0, was added to the respective tube. For the negative controls, 10 μL of buffer was added. The result was a final concentration of 15 nM PON1, 49.5 μM BTZ–MIDA, and 1% v/v DMSO. The samples were incubated at 37 °C on a shaker at 300 rpm. After the desired incubation times, the samples were filtered through an Amicon Ultra Centrifugal Filter, 30 kDa MWCO, 13,200 rpm for 2.5 min, before injection into the LC-MS. For each sample, 20 μL was injected directly without dilution and separated using a 20–80% v/v MeCN gradient (Table S1). % hydrolysis of BTZ–MIDA was calculated with Eq S2.

Human Carboxylesterase 1 (CES1). Enzyme activity was confirmed by monitoring the absorbance of 4-nitrophenol at λ = 412 nm upon the enzymatic hydrolysis of 100 μM 4-nitrophenyl acetate in the presence of CES1 (10 nM) in PBS, pH 7.4 at 25 °C. The MIDA ester hydrolysis assay was performed in PBS, pH 7.4. A 10 μL solution of BTZ–MIDA (5 mM) in anhydrous DMSO was diluted with 990 μL of PBS in an Eppendorf tube. 30 μL of a 1 μM solution of CES1 in PBS was added to the respective tube. For the negative controls, 30 μL of PBS was added. The result was a final concentration of 30 nM CES1, 48.5 μM BTZ–MIDA, and 1% v/v DMSO. The samples were incubated at 37 °C on a shaker at 300 rpm. After the desired incubation times, samples were filtered through Amicon Ultra Centrifugal Filter, 30 kDa MWCO, 13,200 rpm for 2.5 min, before injection into the LC-MS. For each sample, 10 μL was injected directly without dilution and separated using a 20–80% v/v MeCN gradient (Table S1). % hydrolysis of BTZ–MIDA was calculated with Eq S2.

Human Carboxylesterase 2 (CES2). Enzyme activity was confirmed by monitoring the absorbance of 4-nitrophenol at λ = 412 nm upon the enzymatic hydrolysis of 100 μM 4-nitrophenyl acetate in the presence of CES2 (10 nM) in 10 mM HEPES–NaOH buffer, pH 7.4, at 25 °C. The MIDA ester hydrolysis assay was performed in 10 mM HEPES–NaOH buffer, pH 7.4. A 10 μL

solution of BTZ–MIDA (5 mM) in anhydrous DMSO was diluted with 990 µL of buffer in an Eppendorf tube. A 50-µL aliquot of a 1 µM solution of CES2 in 10 mM HEPES–NaOH buffer, pH 7.4, was added to the respective tube. For the negative controls, 50 µL of buffer was added. The result was a final concentration of 48 nM CES2 and 48 µM BTZ–MIDA, with 1% v/v DMSO. The samples were incubated at 37 °C on a shaker at 300 rpm. After incubation, samples were filtered through an Amicon Ultra Centrifugal Filter, 30 kDa MWCO, 13,200 rpm for 2.5 min before injection into the LC-MS. For each sample, 20 µL was injected directly without dilution and separated using a 20–80% v/v MeCN gradient (Table S1). % hydrolysis of BTZ–MIDA was calculated with Eq S2.

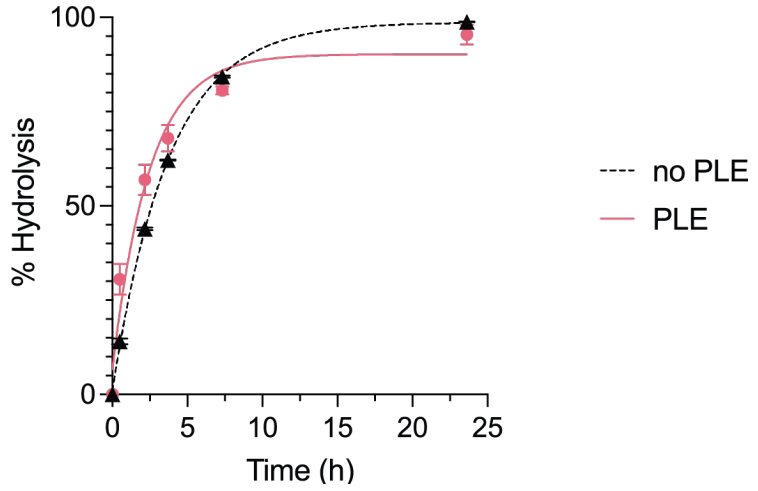


Fig. S39 Enzyme-mediated cleavage assay of BTZ–MIDA in the presence and absence of pig liver esterase (PLE). Values are the mean ± SE.

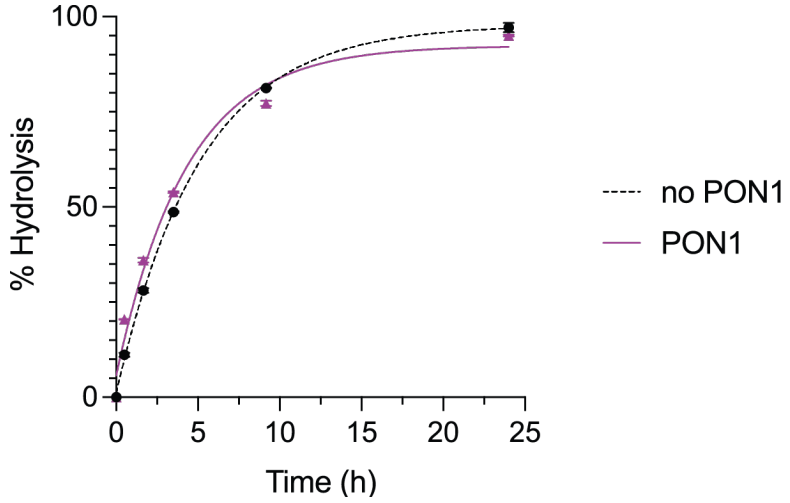


Fig. S40 Enzyme-mediated cleavage assay of BTZ–MIDA in the presence and absence of human paraoxonase 1 (PON1). Values are the mean ± SE.

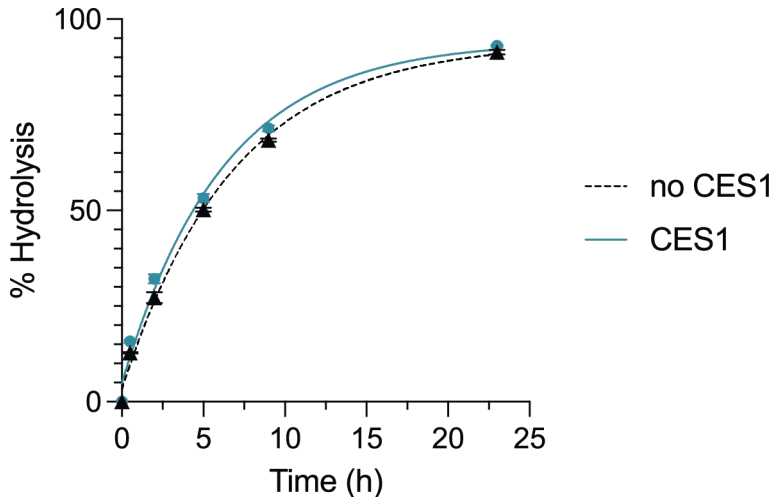


Fig. S41 Enzyme-mediated cleavage assay of BTZ–MIDA in the presence and absence of human carboxylesterase 1 (CES1). Values are the mean ± SE.

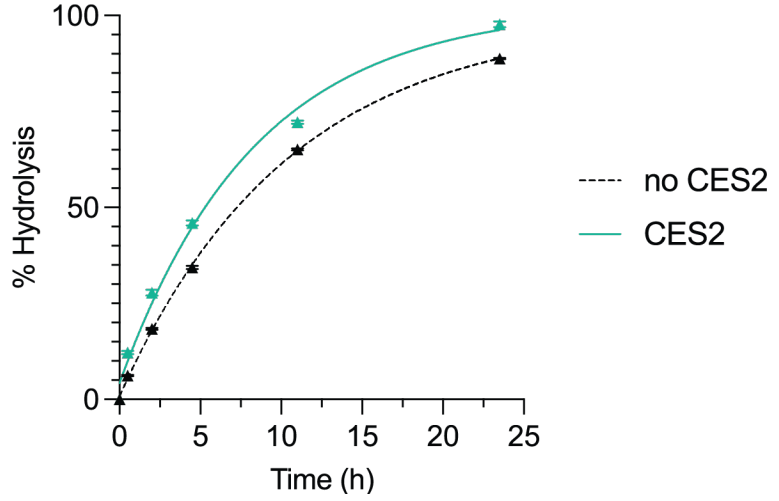


Fig. S42 Enzyme-mediated cleavage assay of BTZ–MIDA in the presence and absence of human carboxylesterase 2 (CES2). Values are the mean ± SE.

11. Computational Methods

The geometries of BTZ, BTZ–MIDA, IXZ, and IXZ–MIDA were optimized using density functional theory (DFT) at the M06-2X/6-31+G(d,p) level with the SMD solvation model for water (SMD-H_2O), as implemented in Gaussian 16.[5-8] Virtual models of BTZ, BTZ–MIDA, IXZ, and IXZ–MIDA are provided in the main text and in separate movie (mp4) files, prepared using UCSF ChimeraX or PyMOL v3.0. The figures below show energy-minimized molecular models that highlight the distances from the boron atom to the phenyl-ring centroid in BTZ and from the *N*-methyl carbon atom to the phenyl-ring centroid in BTZ–MIDA (Fig. S43 and S44, respectively).

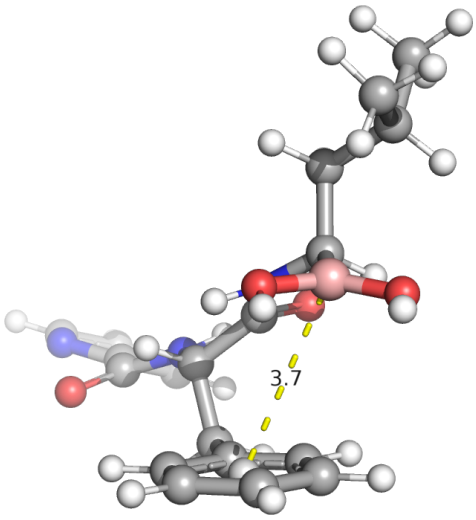


Fig. S43 DFT-optimized geometry of BTZ visualized using PyMOL v3.0. Distance (dashed line) is measured in angstroms from the boron atom to the center of the phenyl ring.

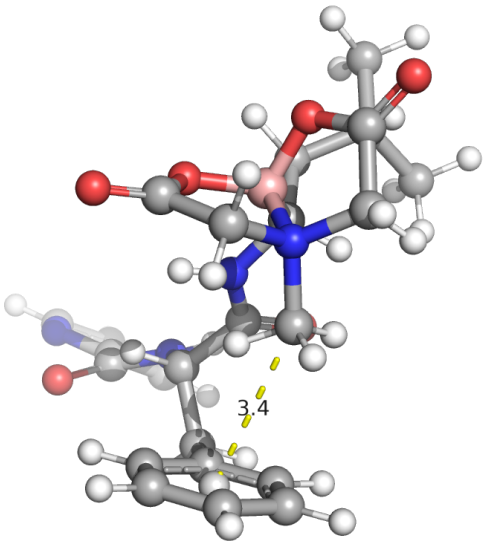


Fig. S44 DFT-optimized geometry of BTZ–MIDA visualized using PyMOL v3.0. Distance (dashed line) is measured in angstroms from the methyl carbon atom to the center of the phenyl ring.

Energy Decomposition Analysis of *N*-methyl–phenyl interaction in BTZ–MIDA

To quantify the contribution of the CH–π interaction, we performed an energy decomposition analysis using symmetry-adapted perturbation theory (SAPT)[9-12] at the SAPT0 level with the aug-cc-pVDZ basis set[13,14] in the Psi4 v.1.6.1 package.[15] We conducted parallel SAPT0 analyses of compounds with and without the *N*-methyl group on MIDA. Our results indicate that the *N*-methyl group plays a critical role in stabilizing the interaction between the MIDA *N*-methyl group and the

bortezomib phenyl ring. Though it creates a non-trivial steric clash in the process, the greater attractive interactions (electrostatics and dispersion) compensate for this effect, resulting in a net stabilization of 1.32 kcal/mol (ΔE_{int} = −1.32 kcal/mol) relative to the unmethylated system. This value is consistent with the view that CH–π interactions are predominantly driven by dispersion forces.

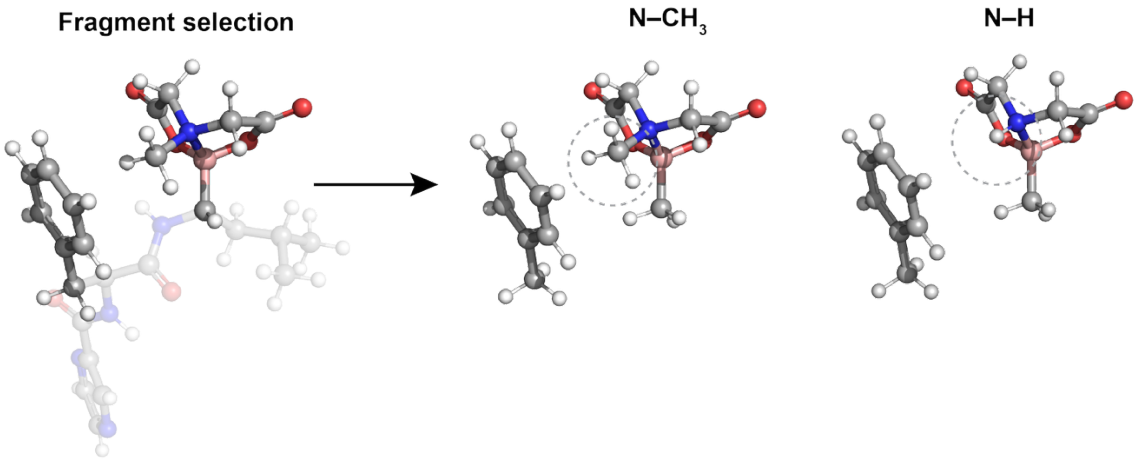


Fig. S45 Fragments of BTZ–MIDA selected for SAPT calculations. The fragment representing the removal of the *N*-methyl group of MIDA is N–H.

Table S4. Interaction energies between the phenyl group and the *N*-methyl-containing fragment and/or the fragment with the *N*-methyl group removed.

Component	N–CH₃ (kcal/mol)	N–H (kcal/mol)	Difference (kcal/mol)
E_{elst}	−4.457	−2.426	−2.032
E_{exch}	5.652	0.215	5.437
E_{ind}	−1.292	−0.633	−0.660
E_{disp}	−5.987	−1.916	−4.071
E_{int}	**−6.084**	**−4.760**	**−1.324**

E_{elst}: electrostatic interaction energy; E_{exch}: exchange (repulsive) interaction energy; E_{ind}: induction (polarization) interaction energy; E_{disp}: dispersion (London dispersion forces) interaction energy; E_{int}: sum of interaction energies

Parallel SAPT Analysis to Validate Null Impact of Fragment-based Approach

The optimized geometry of BTZ–MIDA was fragmented into two structures: (1) the phenyl ring of bortezomib, and (2) the methyl group from MIDA. Atoms not involved in the interaction were removed from the structure to reduce computational cost. To validate that the truncation did not artificially affect the interaction energy decomposition, we performed parallel SAPT0/aug-cc-pVDZ calculations on a "short" version retaining minimal structural information and a "long" version with additional context atoms (Fig. S46). Convergence of the interaction energies between

the two analyses demonstrates that the fragments accurately represent the CH–π interaction energetics and rely little on context atoms.

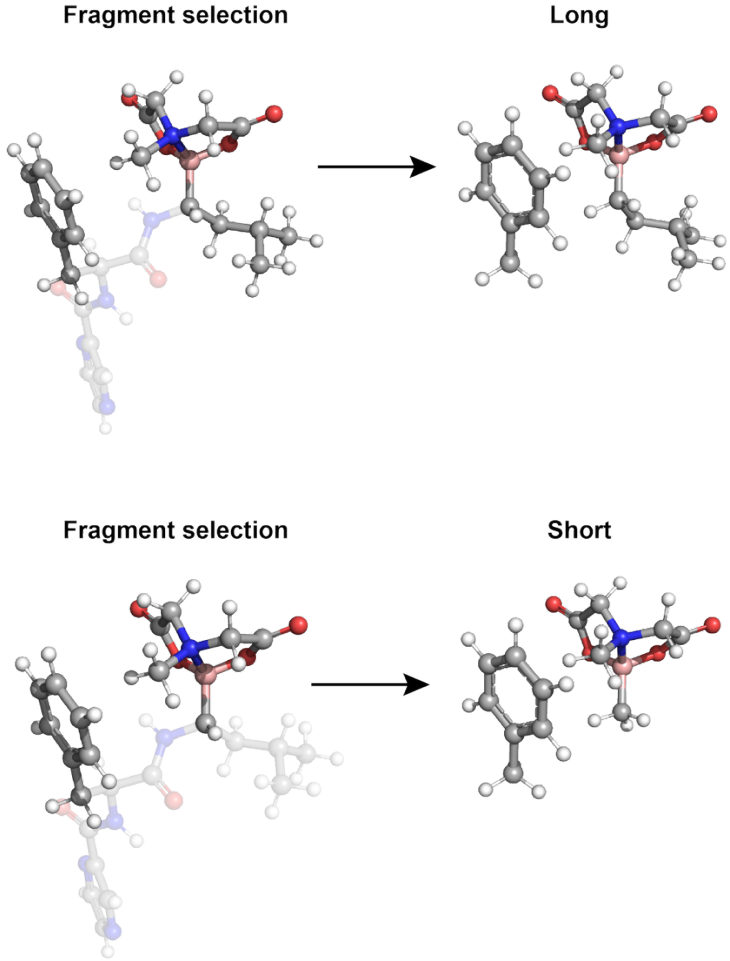


Fig. S46 Validation of the BTZ–MIDA fragments selected for SAPT calculations. "Short" and "long" represent the initial fragment of the MIDA–boronate and the extended fragment used to determine if the additional atoms of the BTZ backbone may influence our SAPT calculations.

Table S5. Interaction energies of the phenyl group with the "long" and "short" *N*-methyl-containing fragments.

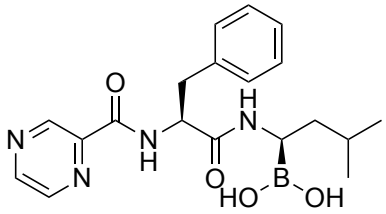
Component	Long (kcal/mol)	Short (kcal/mol)	Difference (kcal/mol)
E_{elst}	−4.370	−4.457	0.087
E_{exch}	5.621	5.652	−0.031
E_{ind}	−1.270	−1.292	0.022
E_{disp}	−6.144	−5.987	−0.157
E_{int}	**−6.163**	**−6.084**	**−0.079**

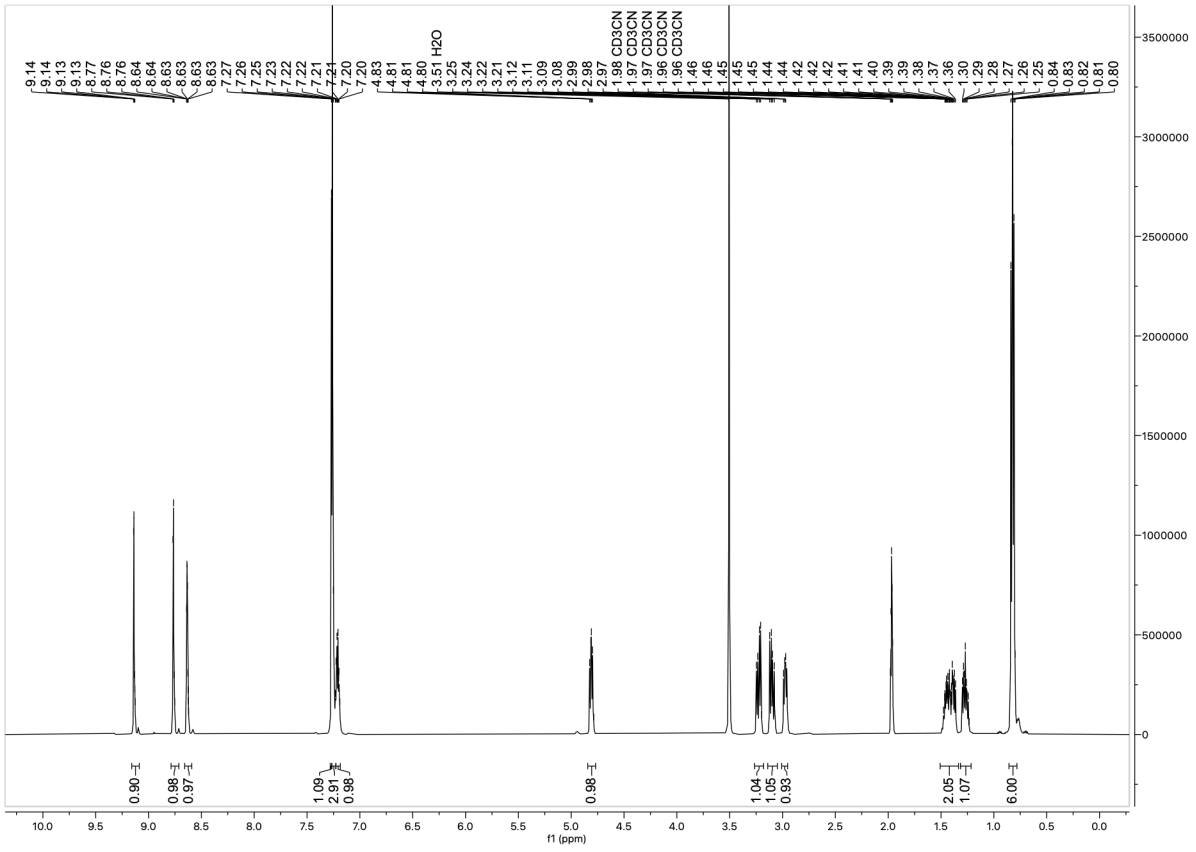
E_{elst}: electrostatic interaction energy; E_{exch}: exchange (repulsive) interaction energy; E_{ind}: induction (polarization) interaction energy; E_{disp}: dispersion (London dispersion forces) interaction energy; E_{int}: sum of interaction energies.

12. NMR Spectra

Bortezomib (BTZ)

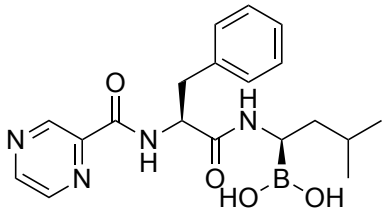
^{1}H NMR (500 MHz, CD_3CN/D_2O)

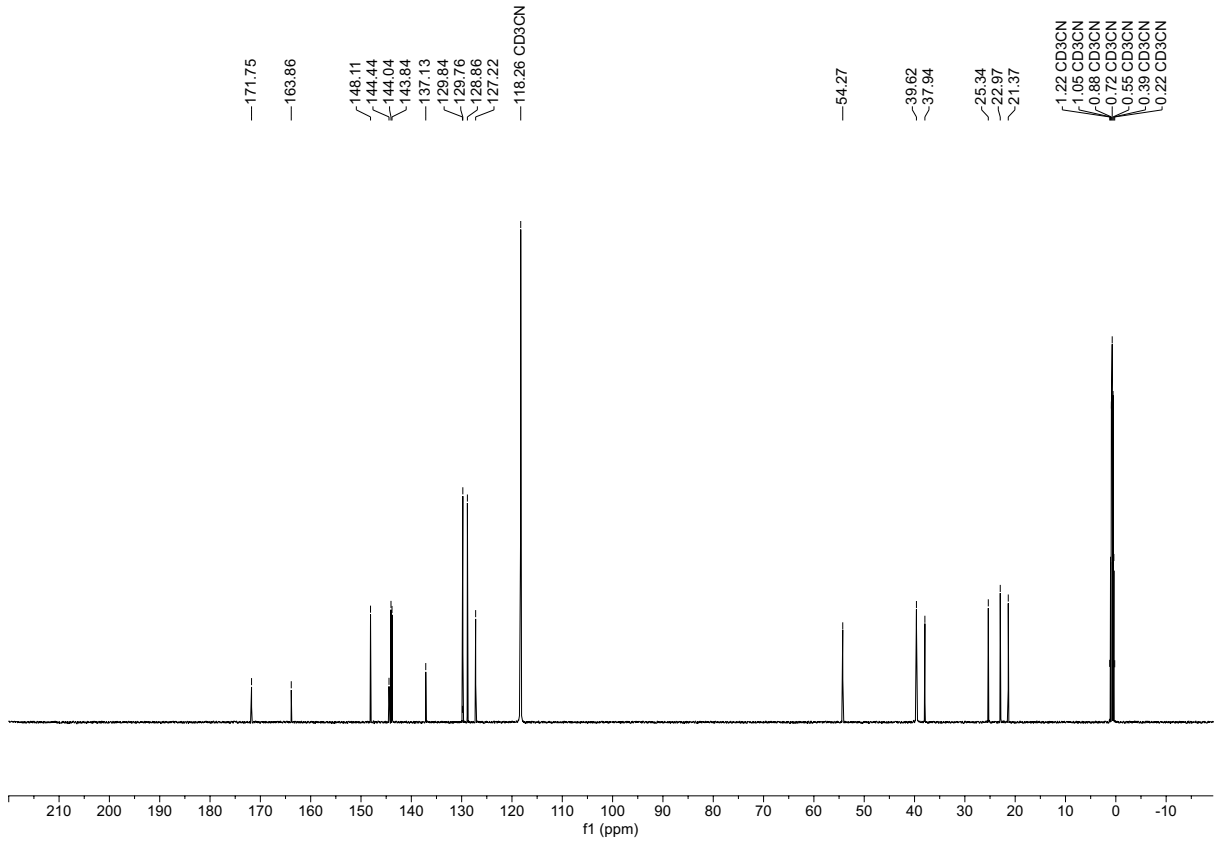




Bortezomib (BTZ)

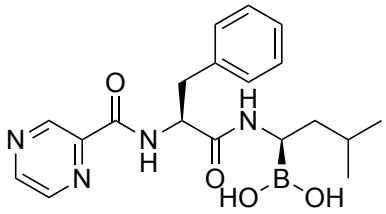
$^{13}C\{^{1}H\}$ NMR (126 MHz, CD_3CN/D_2O)

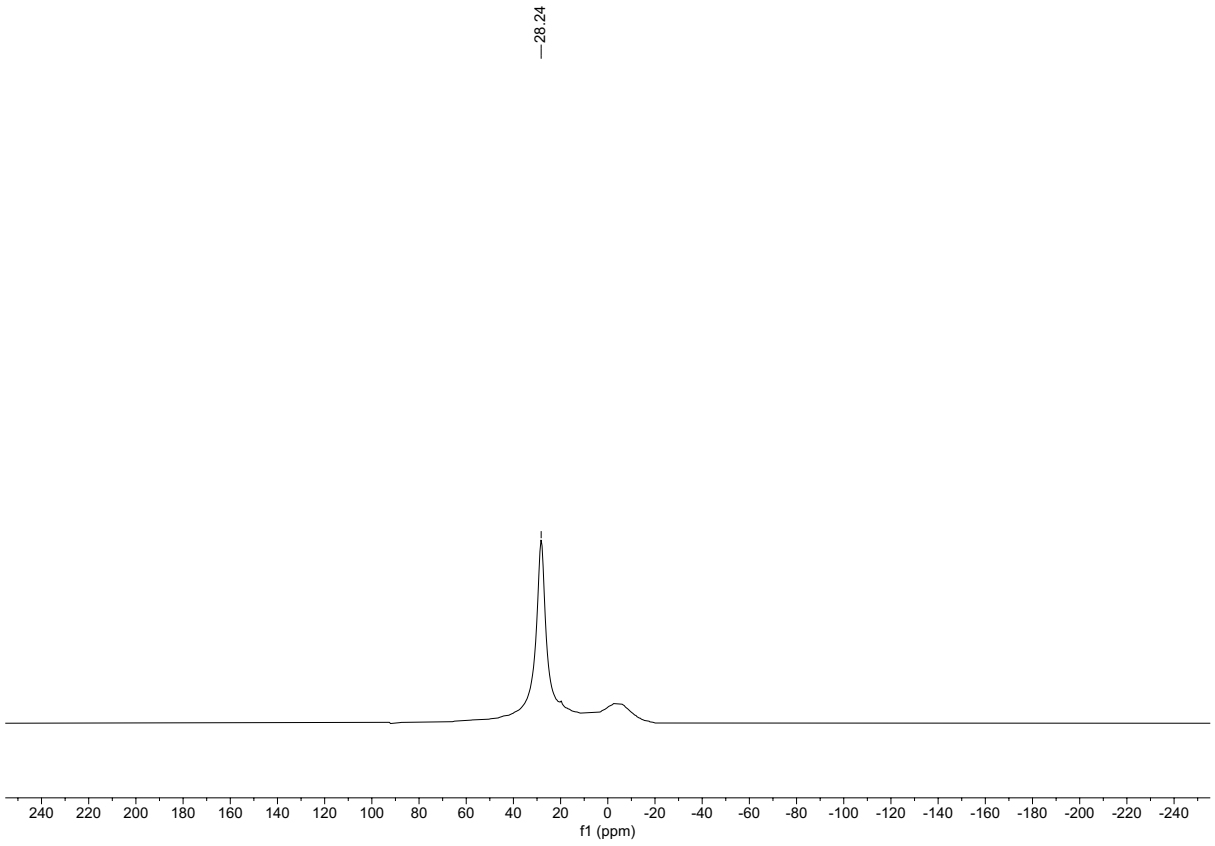




Bortezomib (BTZ)

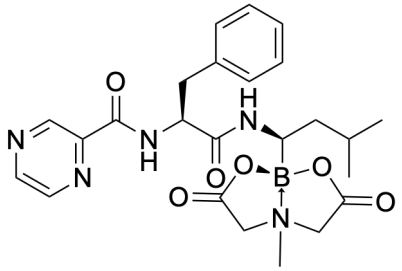
$^{11}B\{^{1}H\}$ NMR (160 MHz, CD_3CN/D_2O)

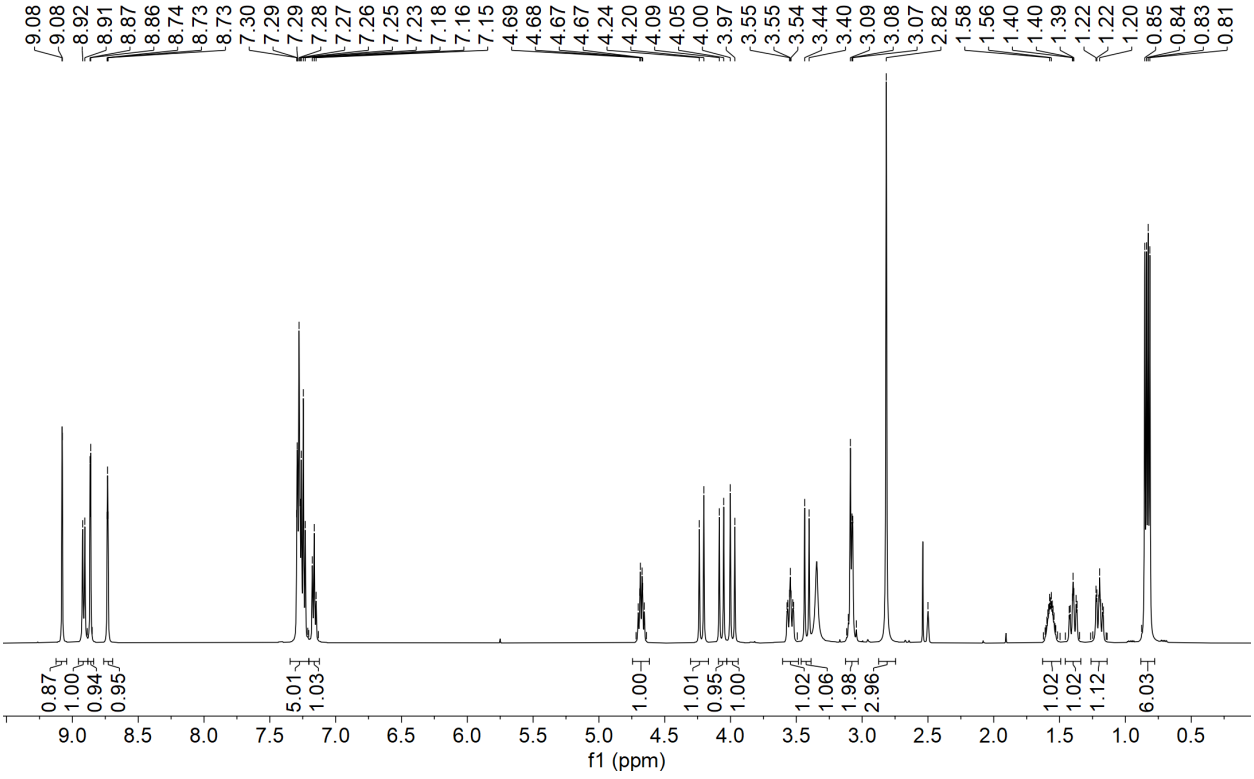




BTZ–MIDA

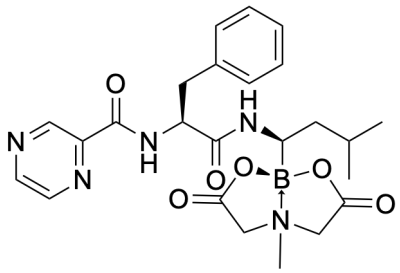
^{1}H NMR (500 MHz, DMSO-d_6)

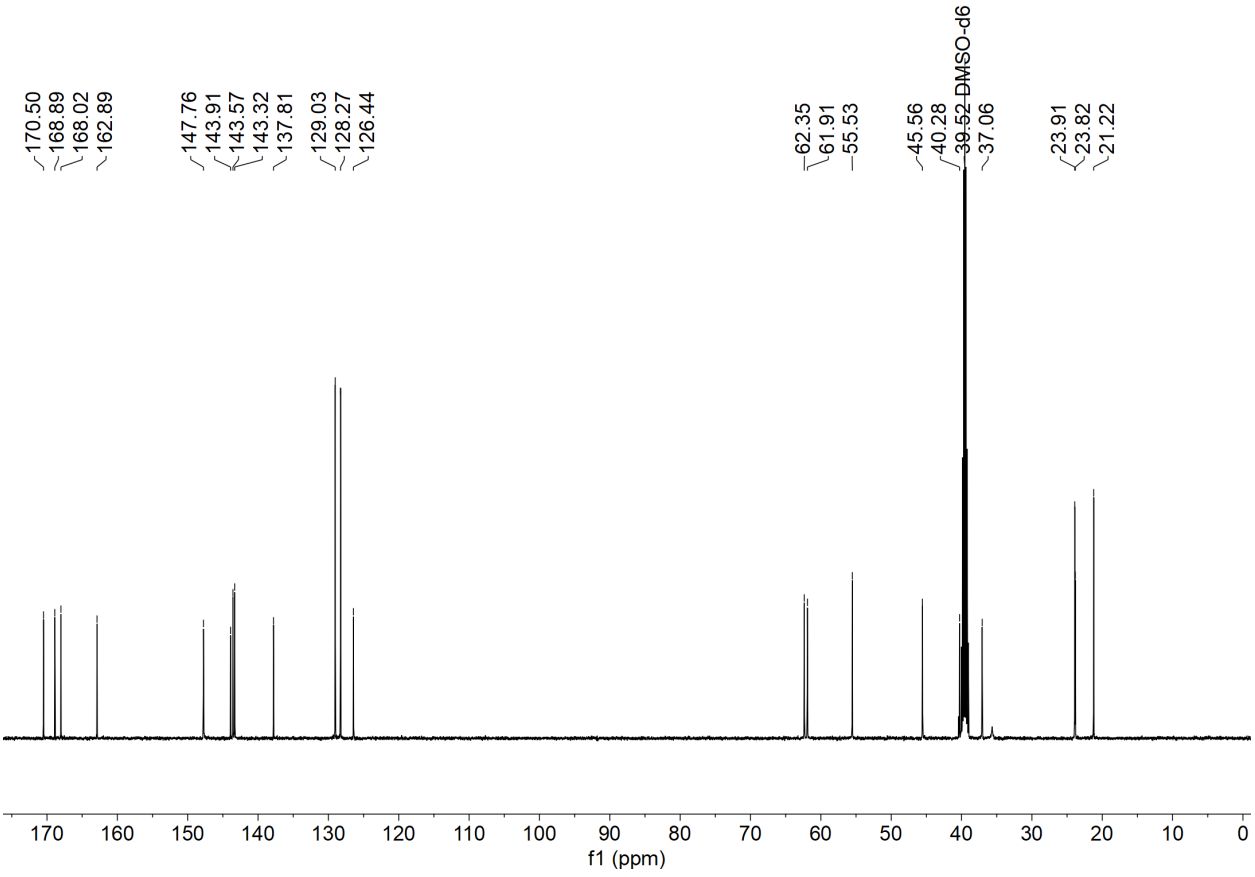




BTZ–MIDA

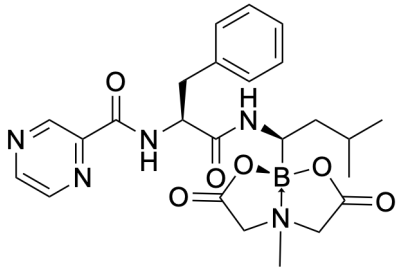
$^{13}C\{^{1}H\}$ NMR (126 MHz, DMSO-d_6)

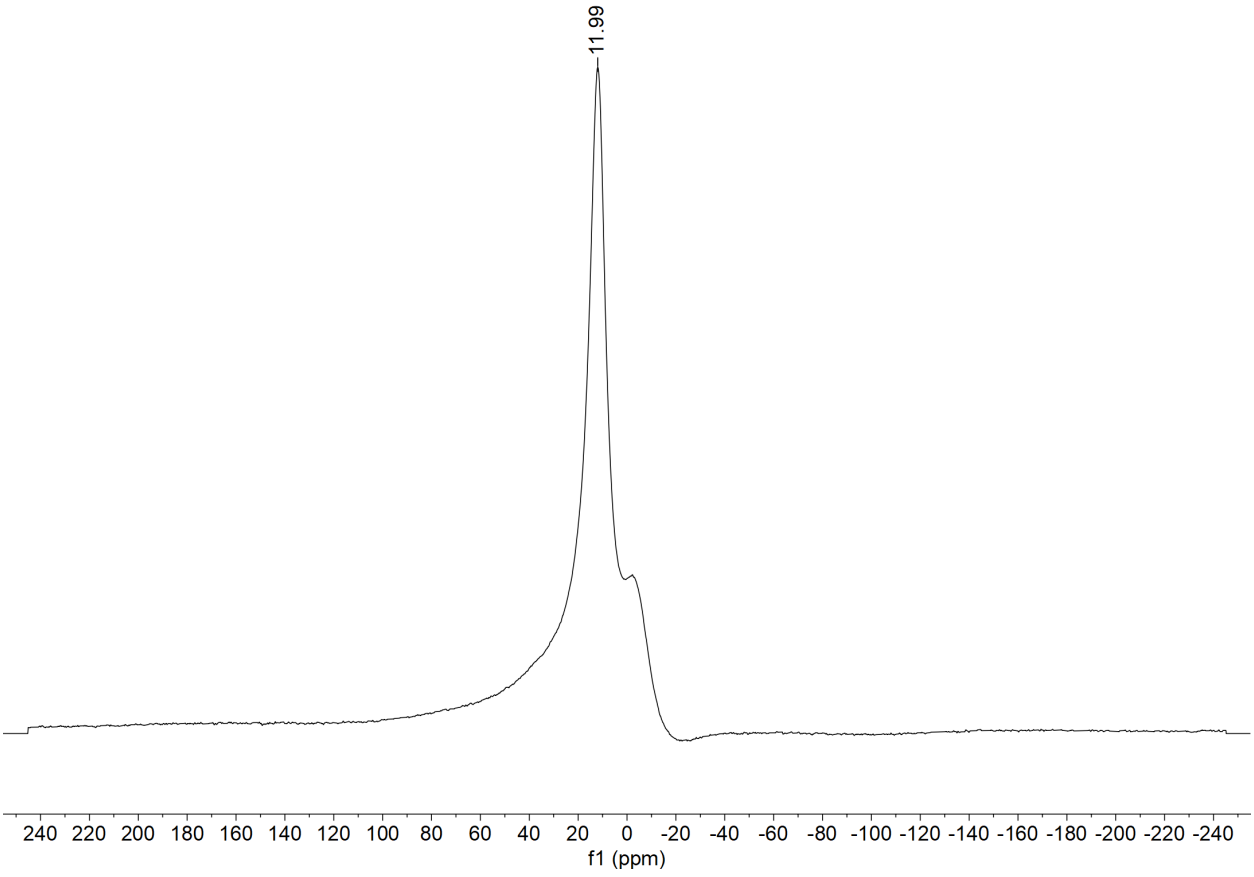




BTZ–MIDA

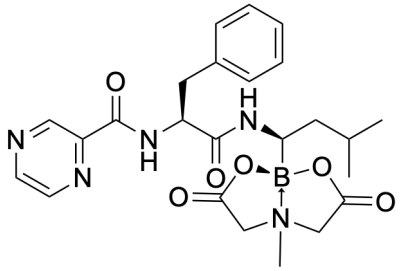
$^{11}B\{^{1}H\}$ NMR (160 MHz, DMSO-d_6)

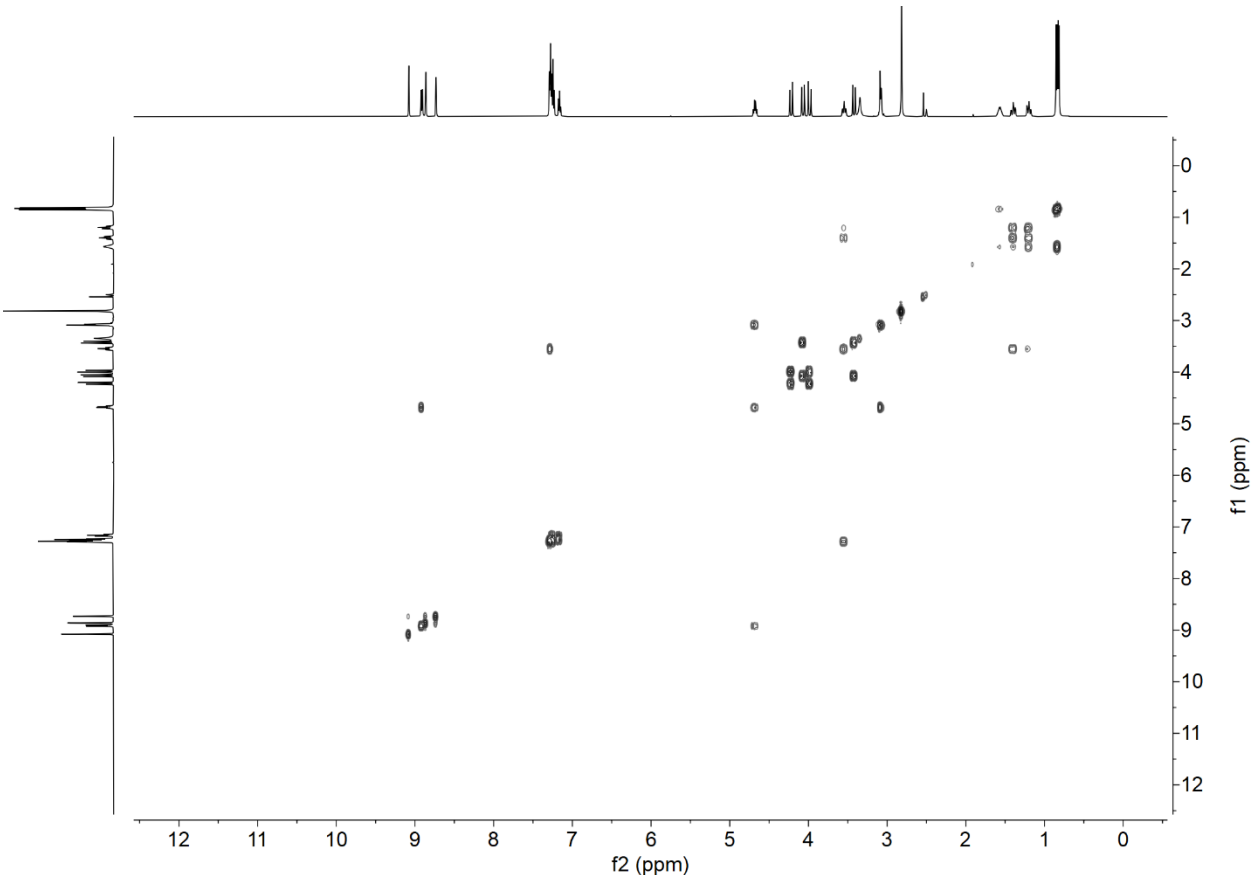




BTZ–MIDA

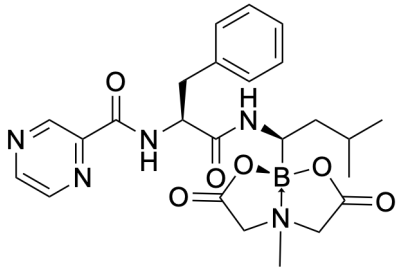
COSY (500 MHz, DMSO-d_6)

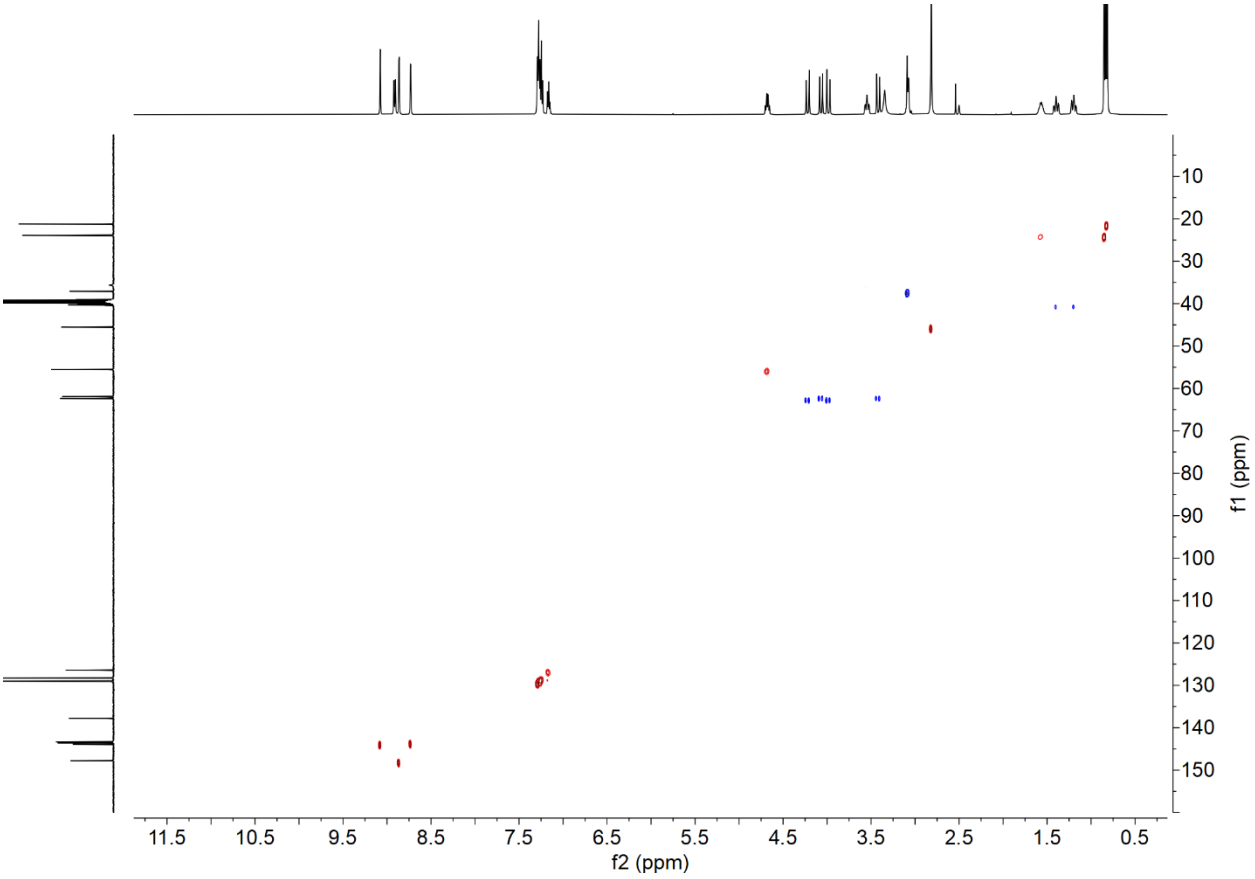




BTZ–MIDA

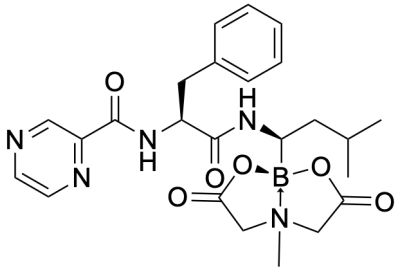
HSQC (500 MHz, DMSO-d_6)

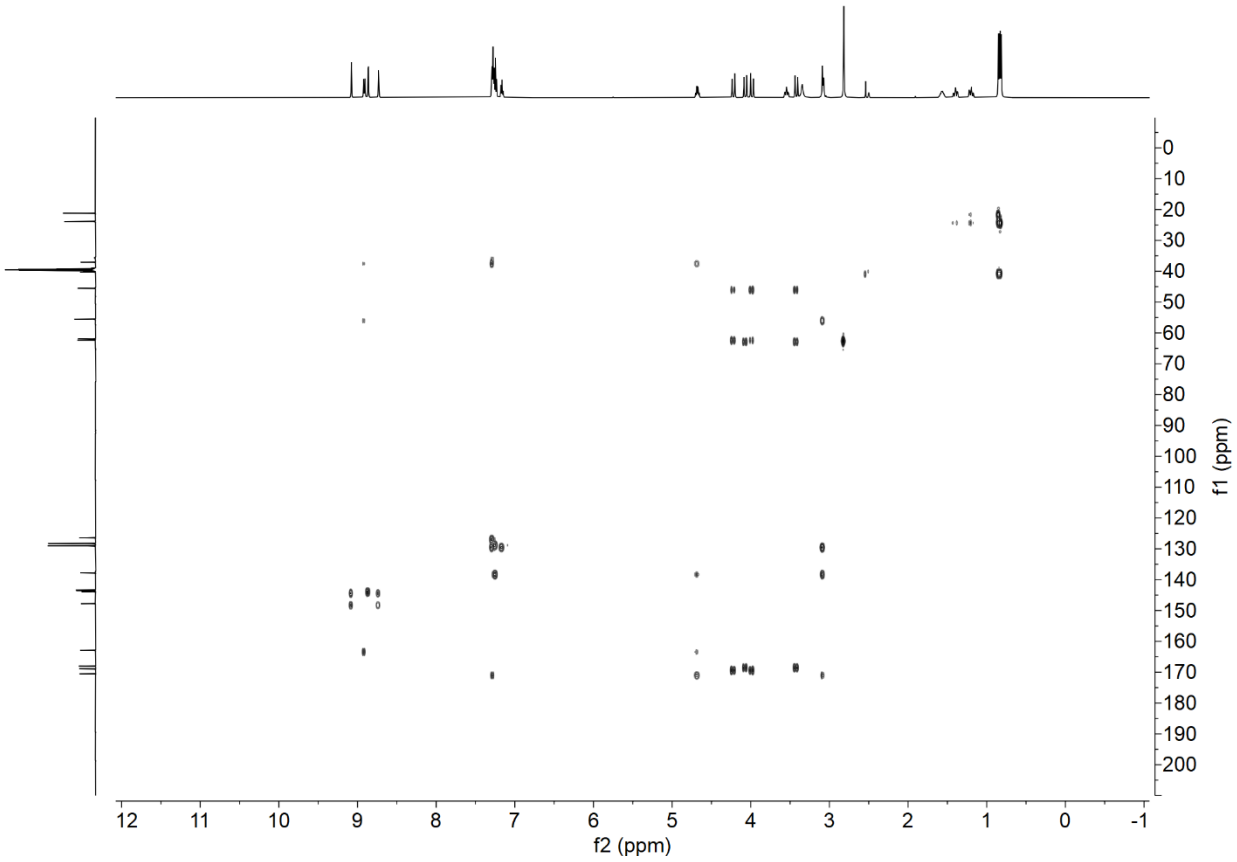




BTZ–MIDA

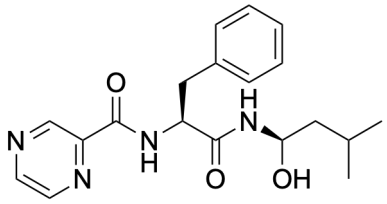
HMBC (500 MHz, DMSO-d_6)

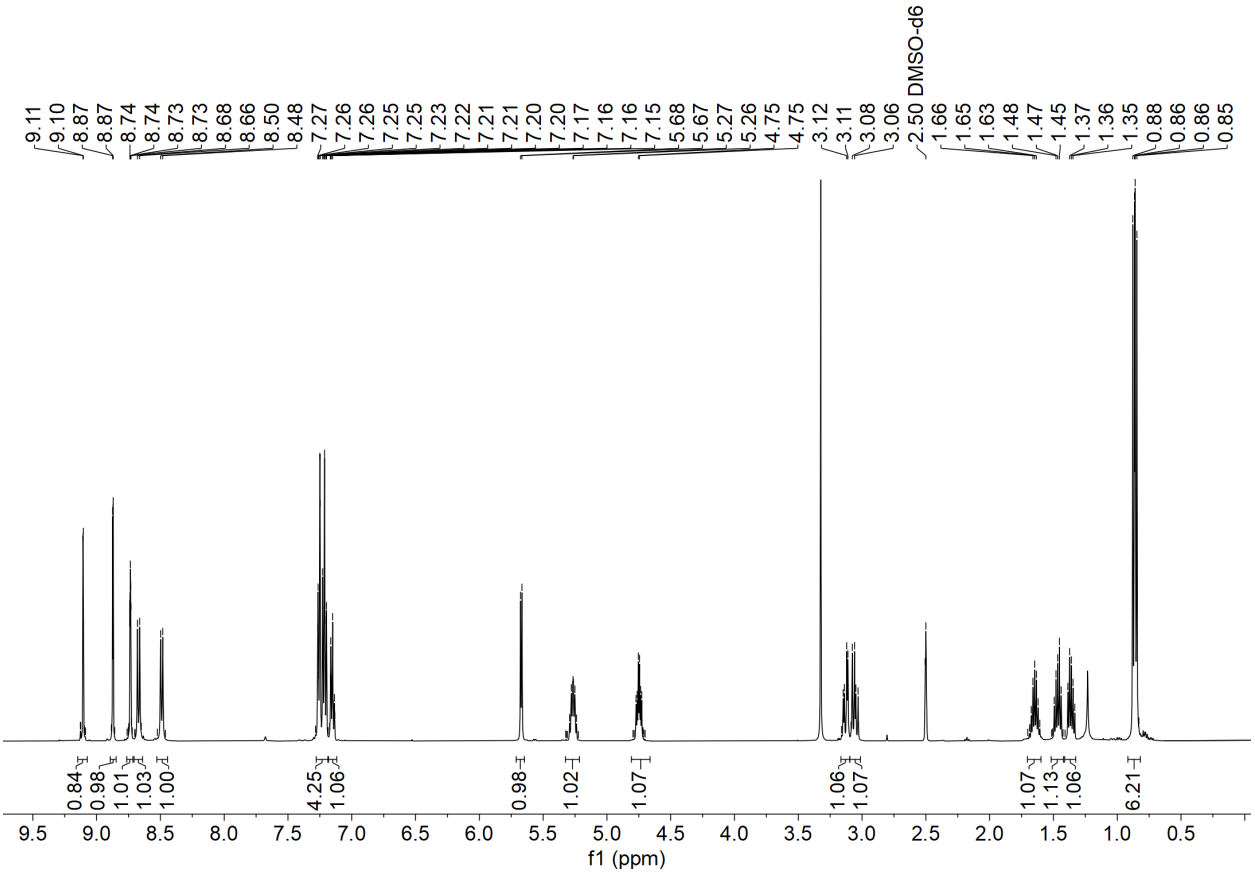




BTZ-ox-1

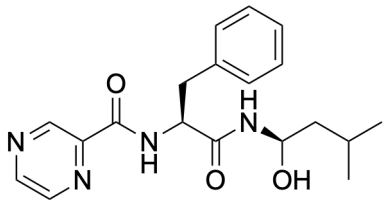
^{1}H NMR (500 MHz, DMSO-d_6)

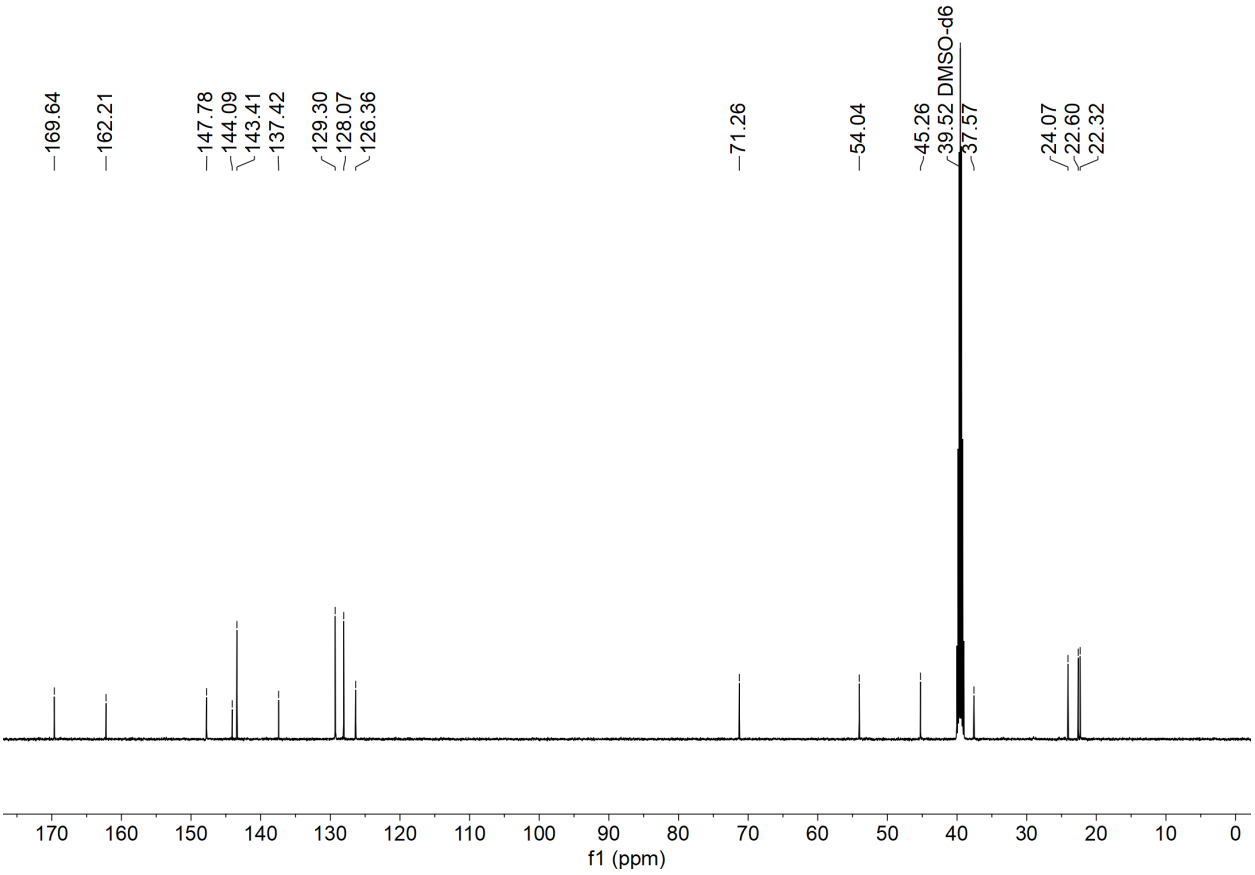




BTZ-ox-1

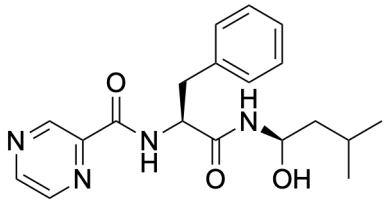
$^{13}C\{^{1}H\}$ NMR (126 MHz, DMSO-d_6)

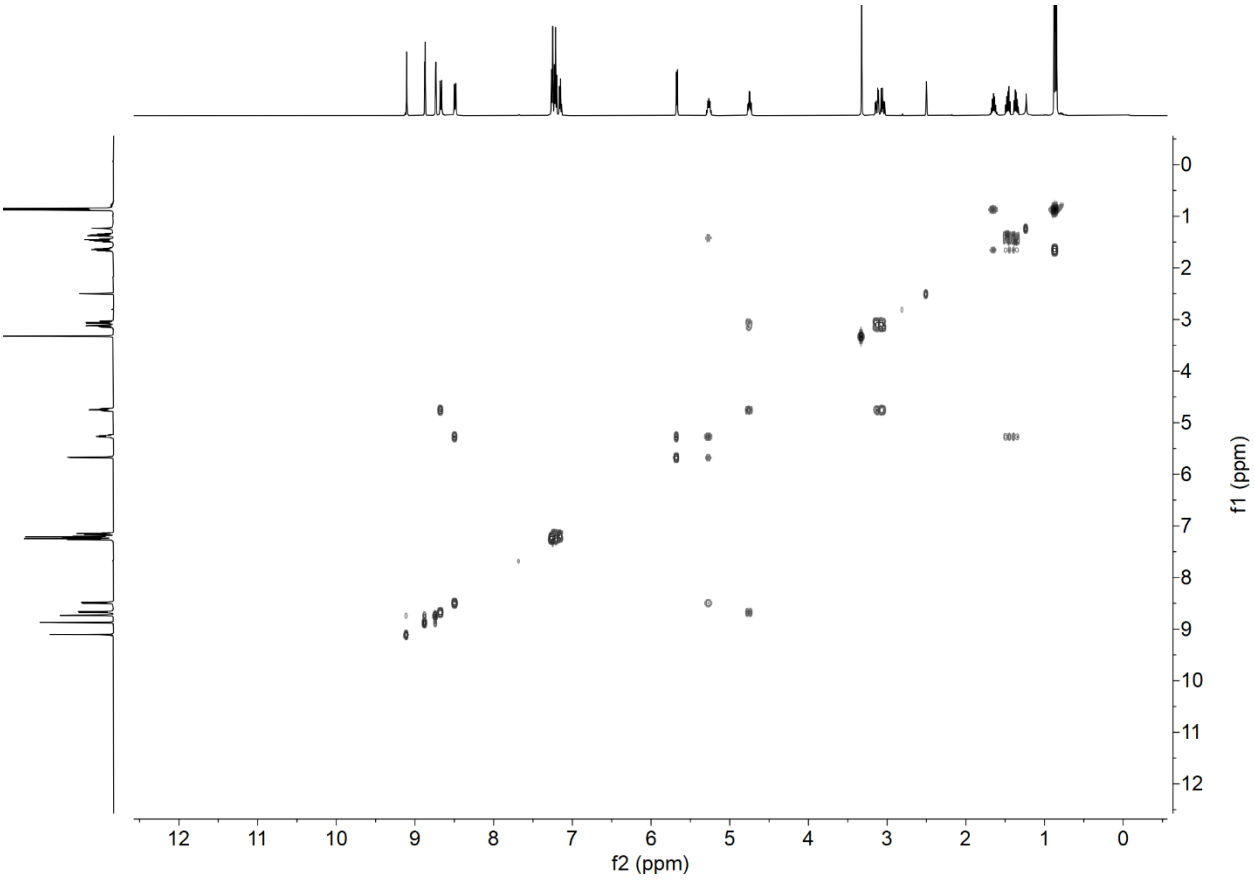




BTZ-ox-1

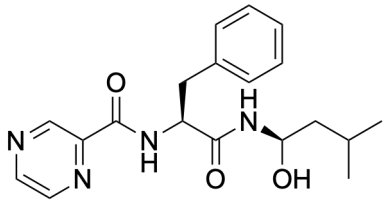
COSY (500 MHz, DMSO-d_6)

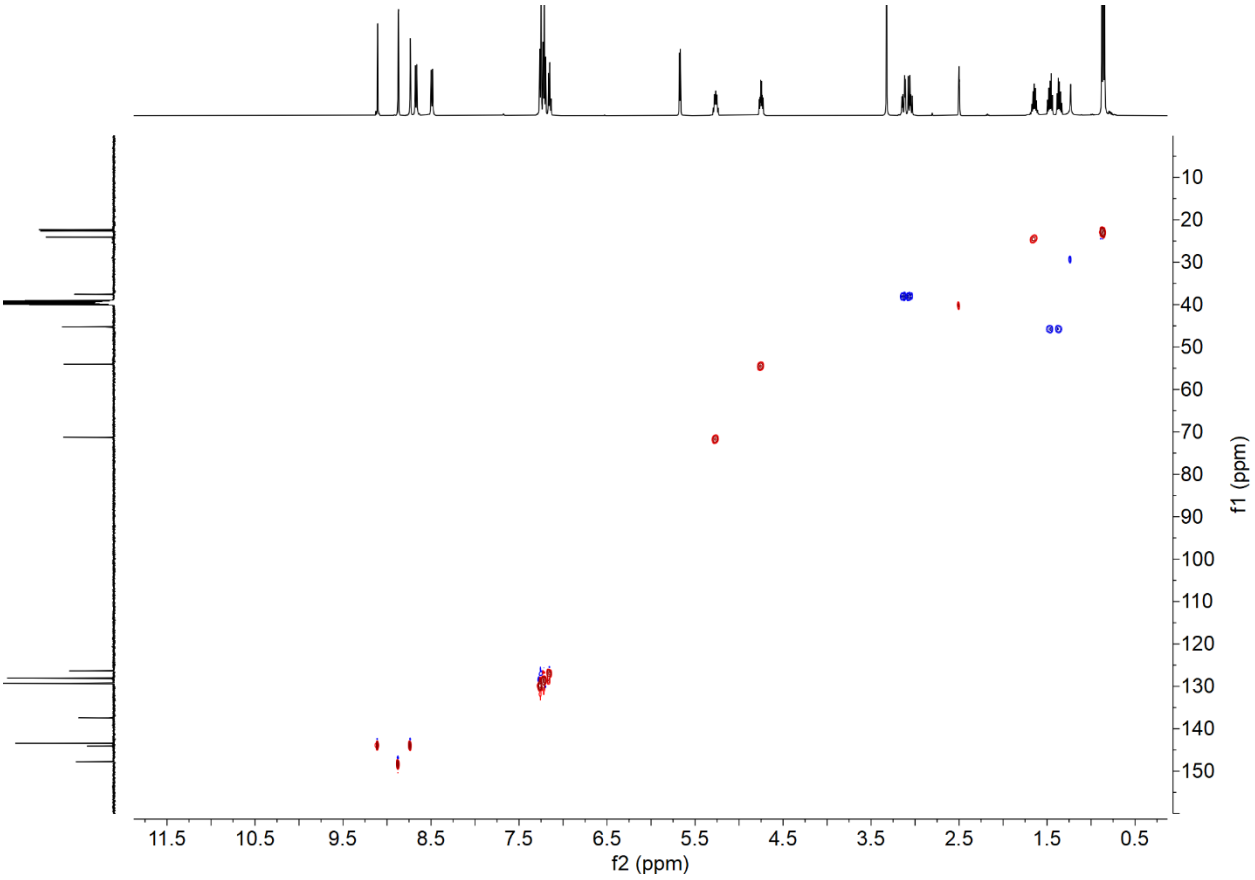




BTZ-ox-1

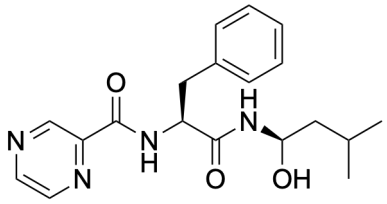
HSQC (500 MHz, DMSO-d_6)

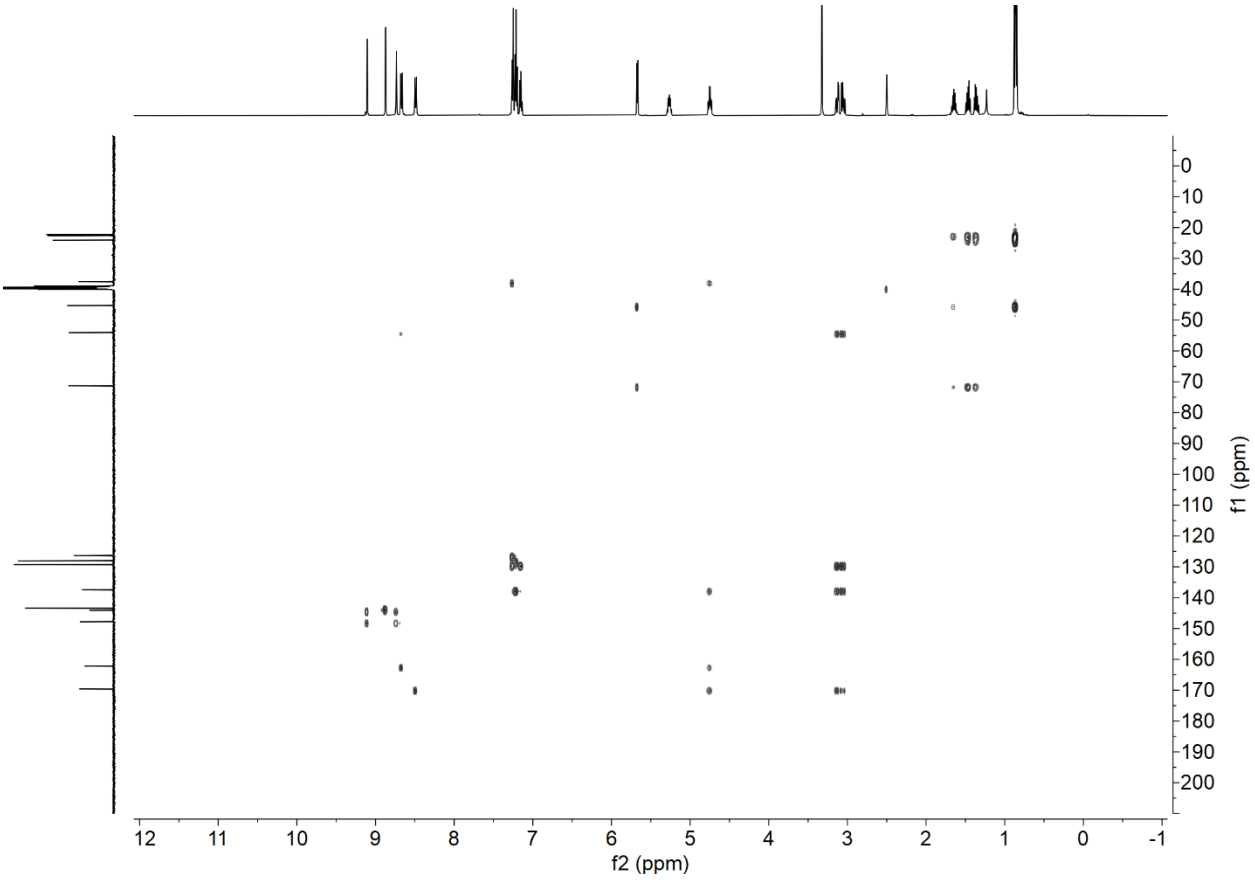




BTZ-ox-1

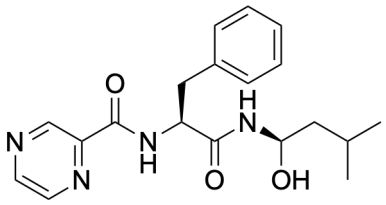
HMBC (500 MHz, DMSO-d_6)

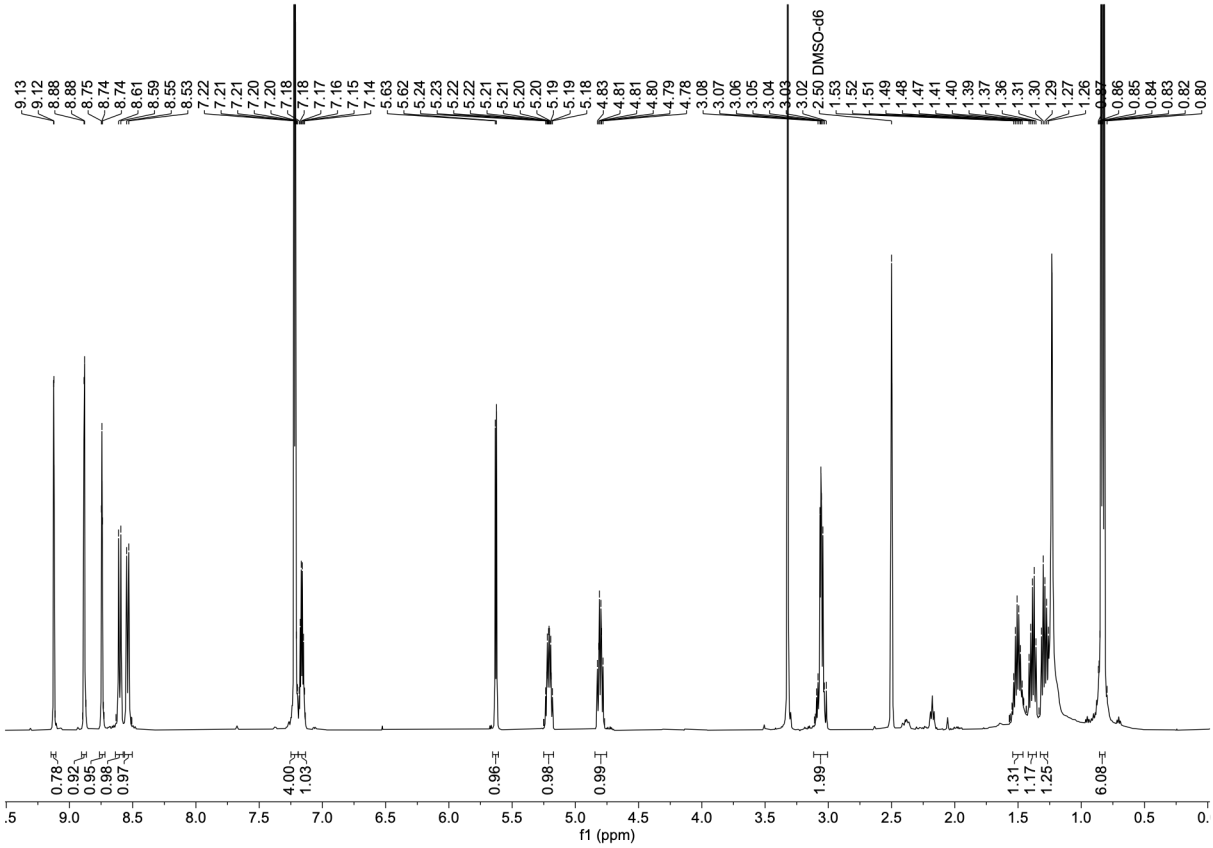




BTZ-ox-2

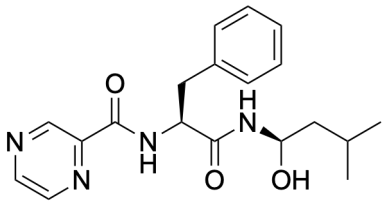
^{1}H NMR (500 MHz, DMSO-d_6)

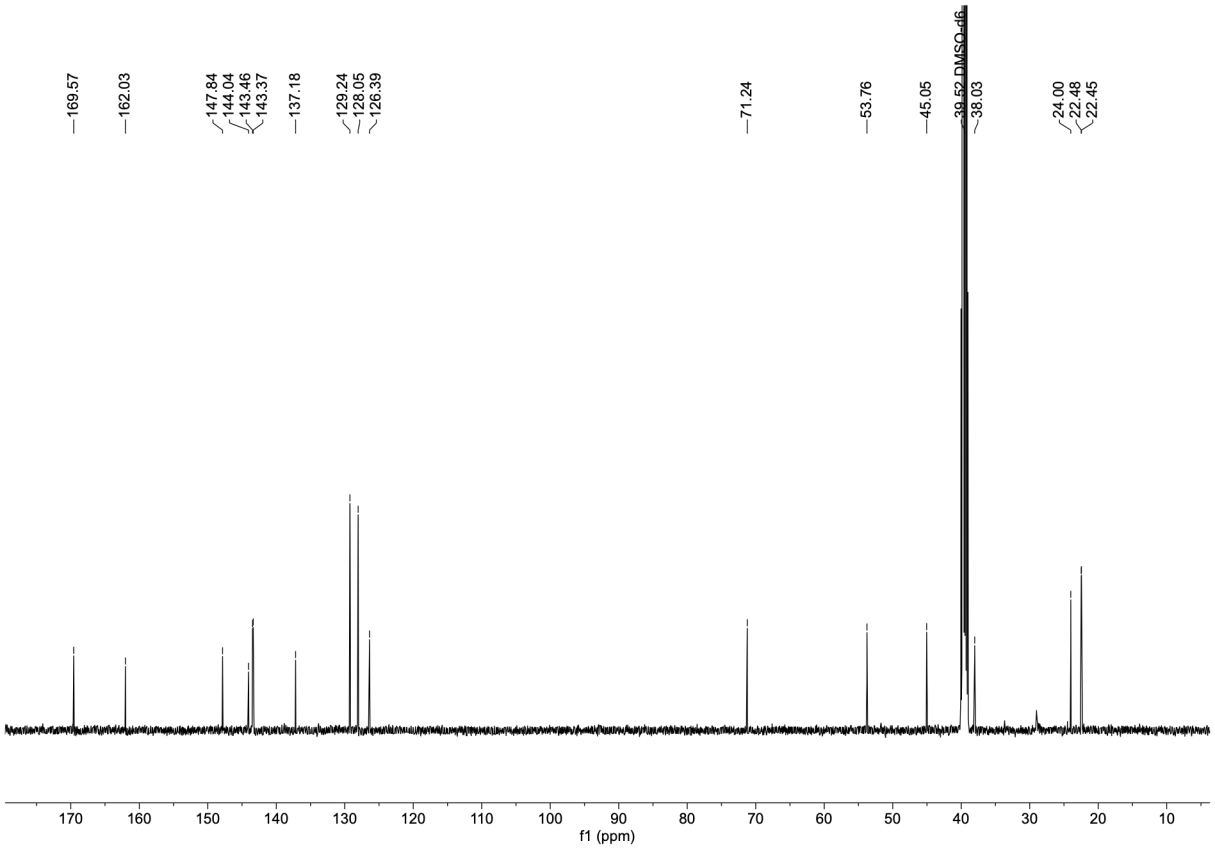




BTZ-ox-2

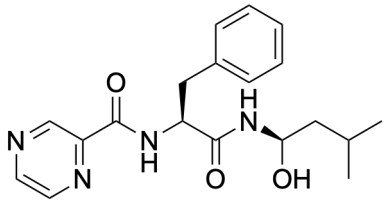
$^{13}C\{^{1}H\}$ NMR (126 MHz, DMSO-d_6)

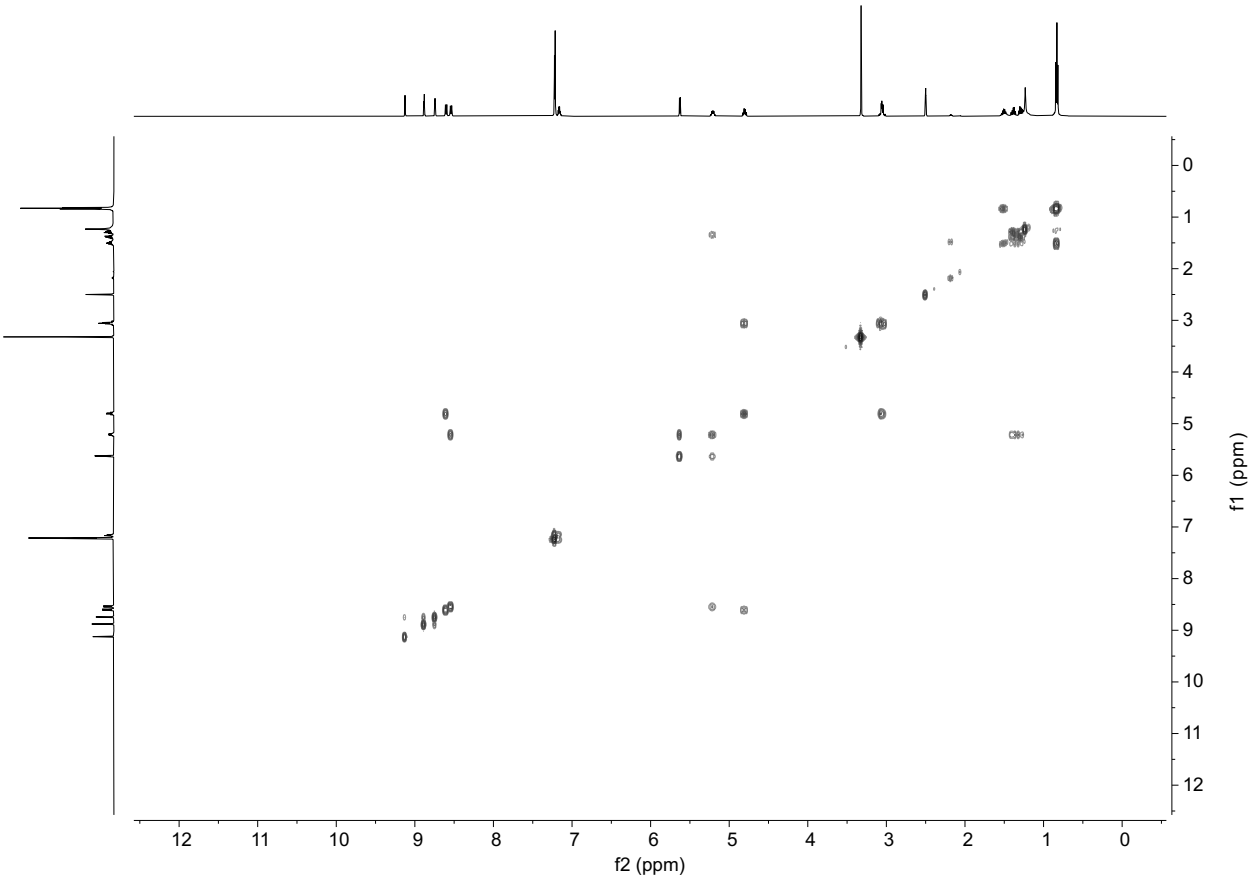




BTZ-ox-2

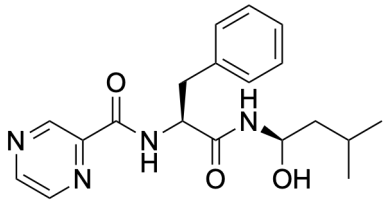
COSY (500 MHz, DMSO-d_6)

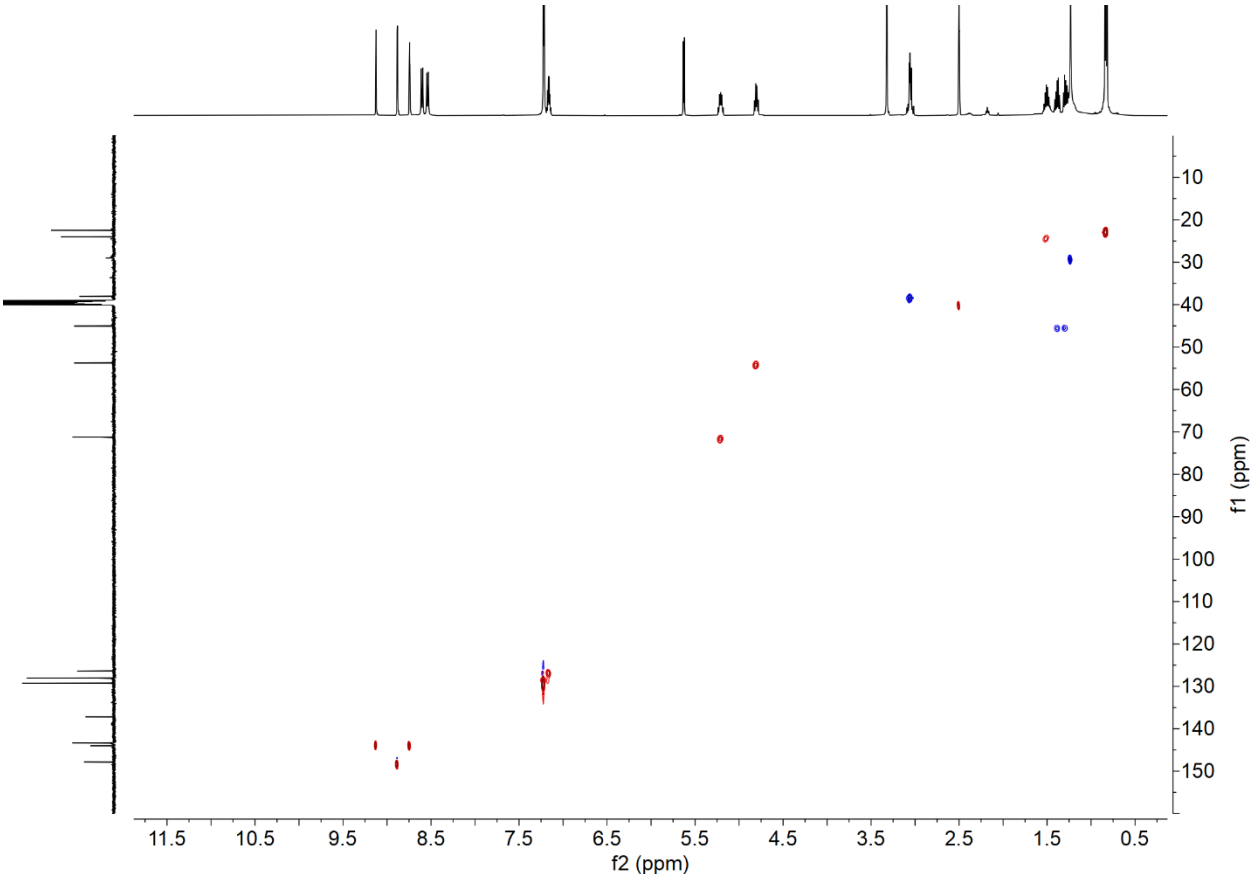




BTZ-ox-2

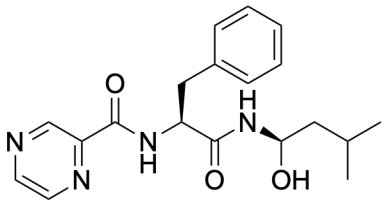
HSQC (500 MHz, DMSO-d_6)

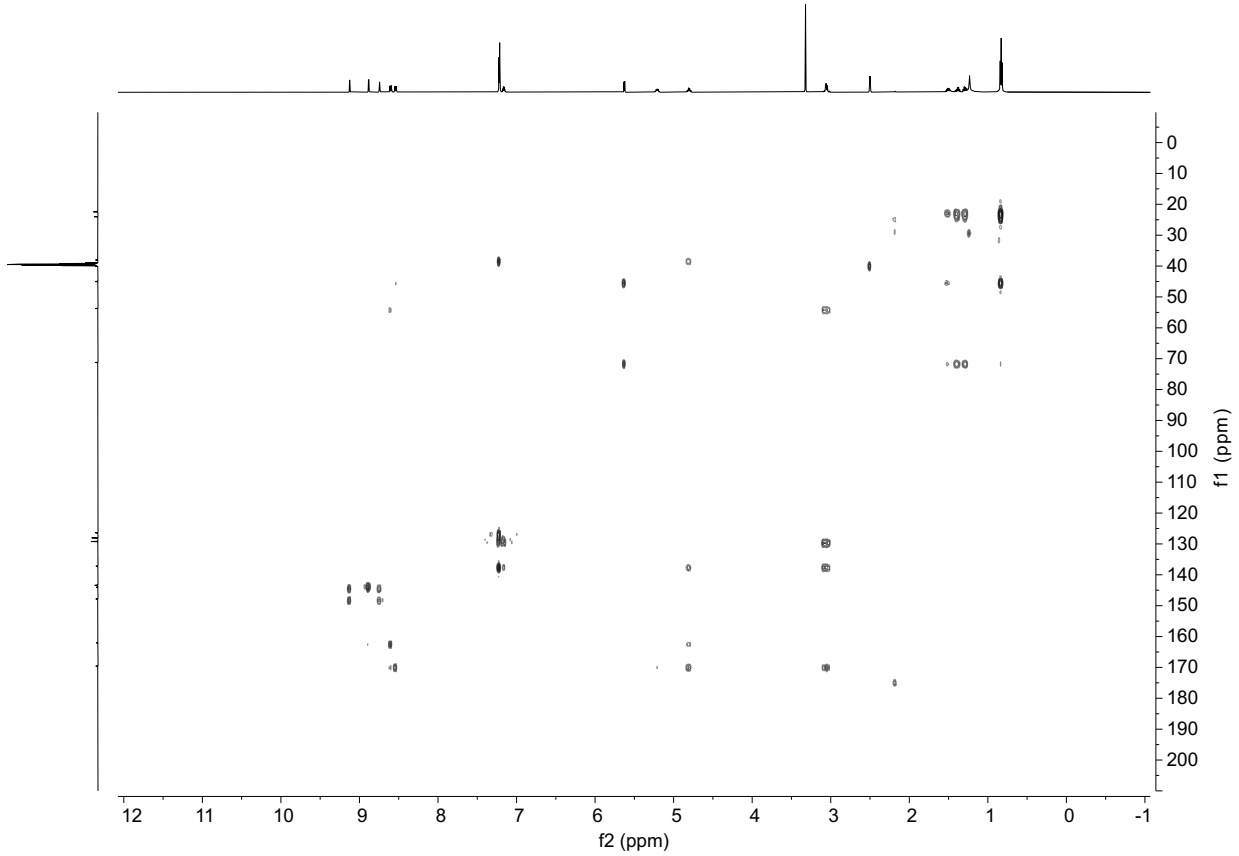




BTZ-ox-2

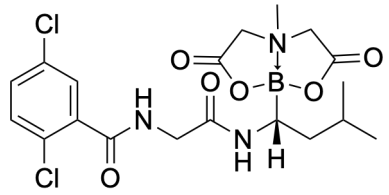
HMBC (500 MHz, DMSO-d_6)

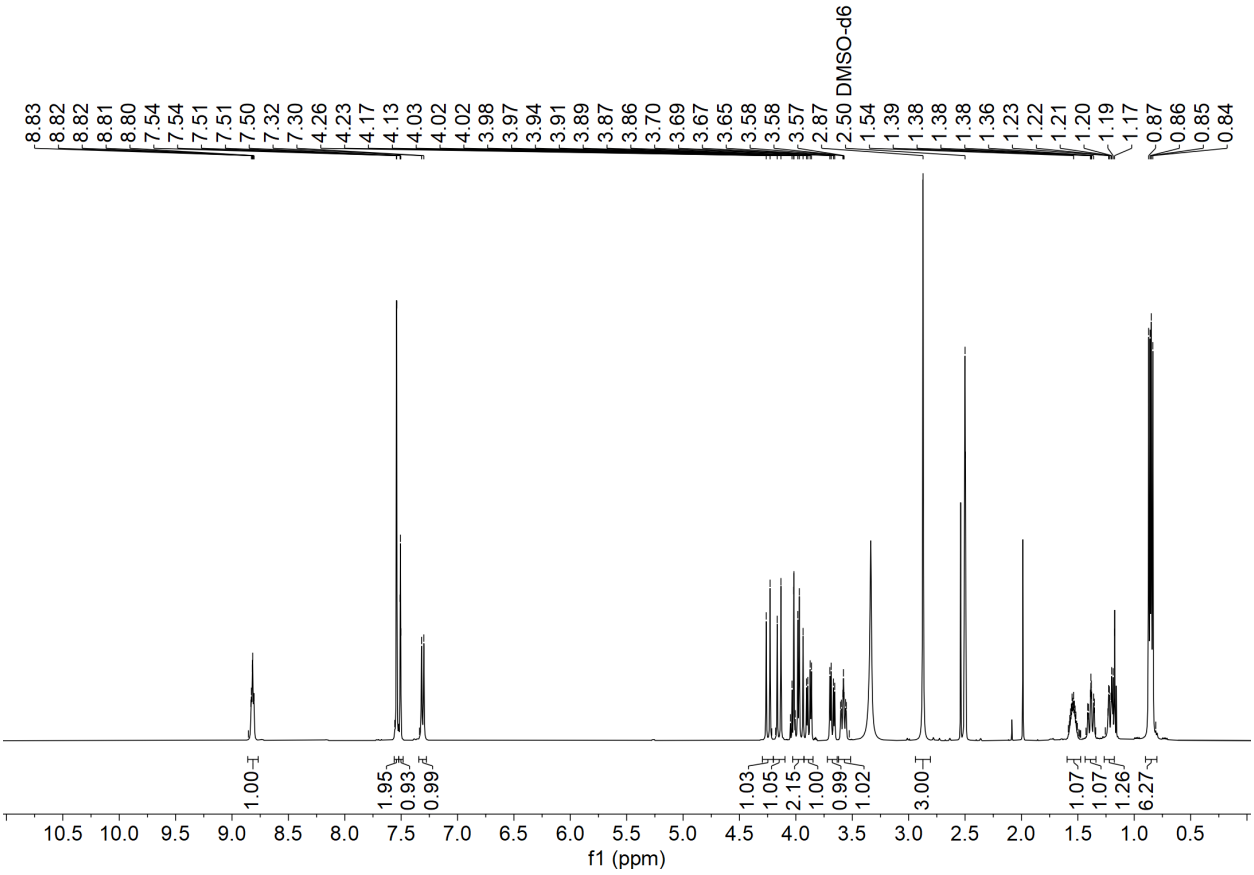




IXZ–MIDA

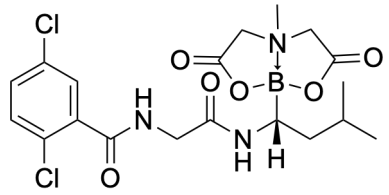
^{1}H NMR (500 MHz, DMSO-d_6)

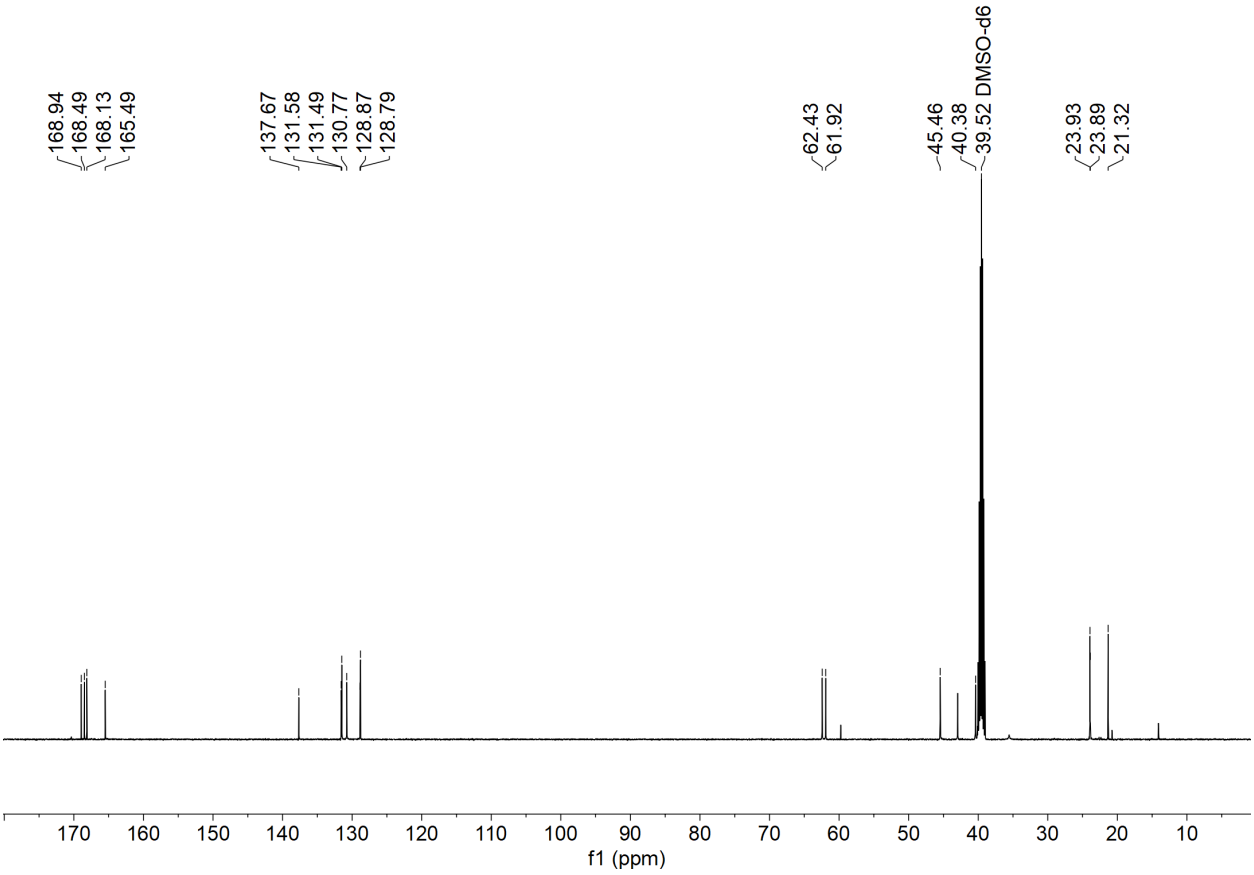




IXZ–MIDA

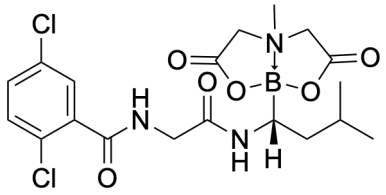
$^{13}C\{^{1}H\}$ NMR (126 MHz, DMSO-d_6)

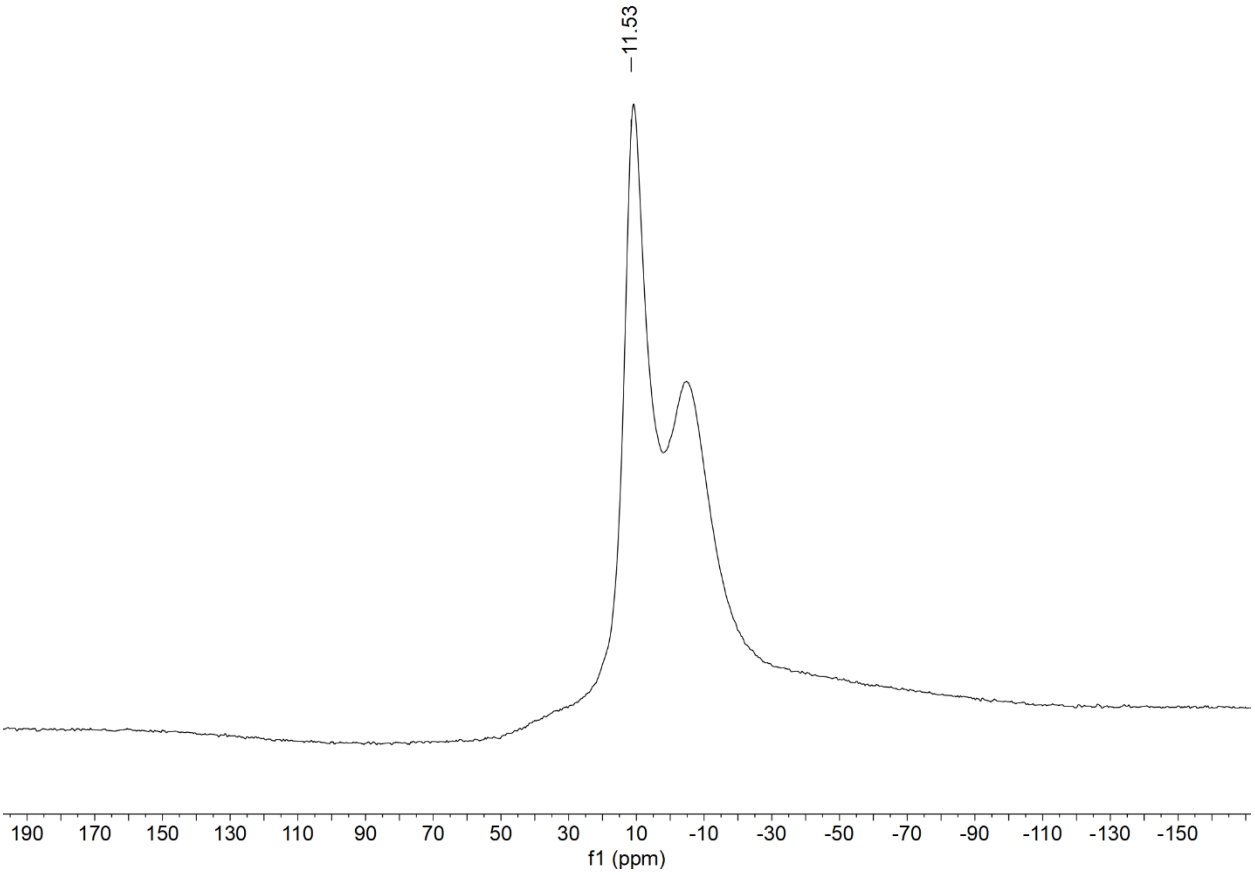




IXZ–MIDA

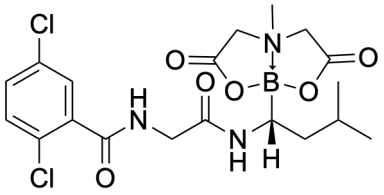
$^{11}B\{^{1}H\}$ NMR (160 MHz, DMSO-d_6)

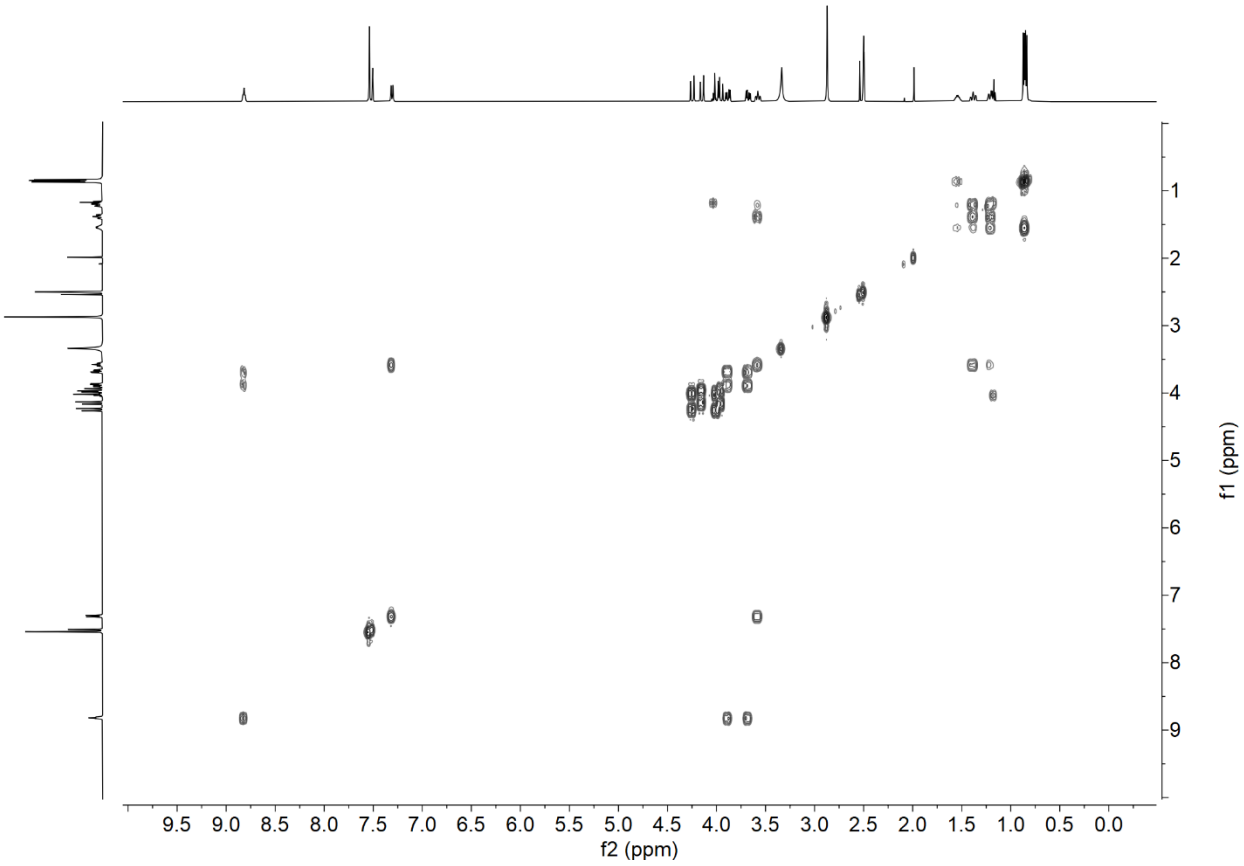




IXZ–MIDA

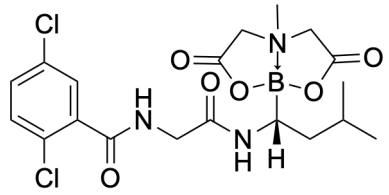
COSY (500 MHz, DMSO-d_6)

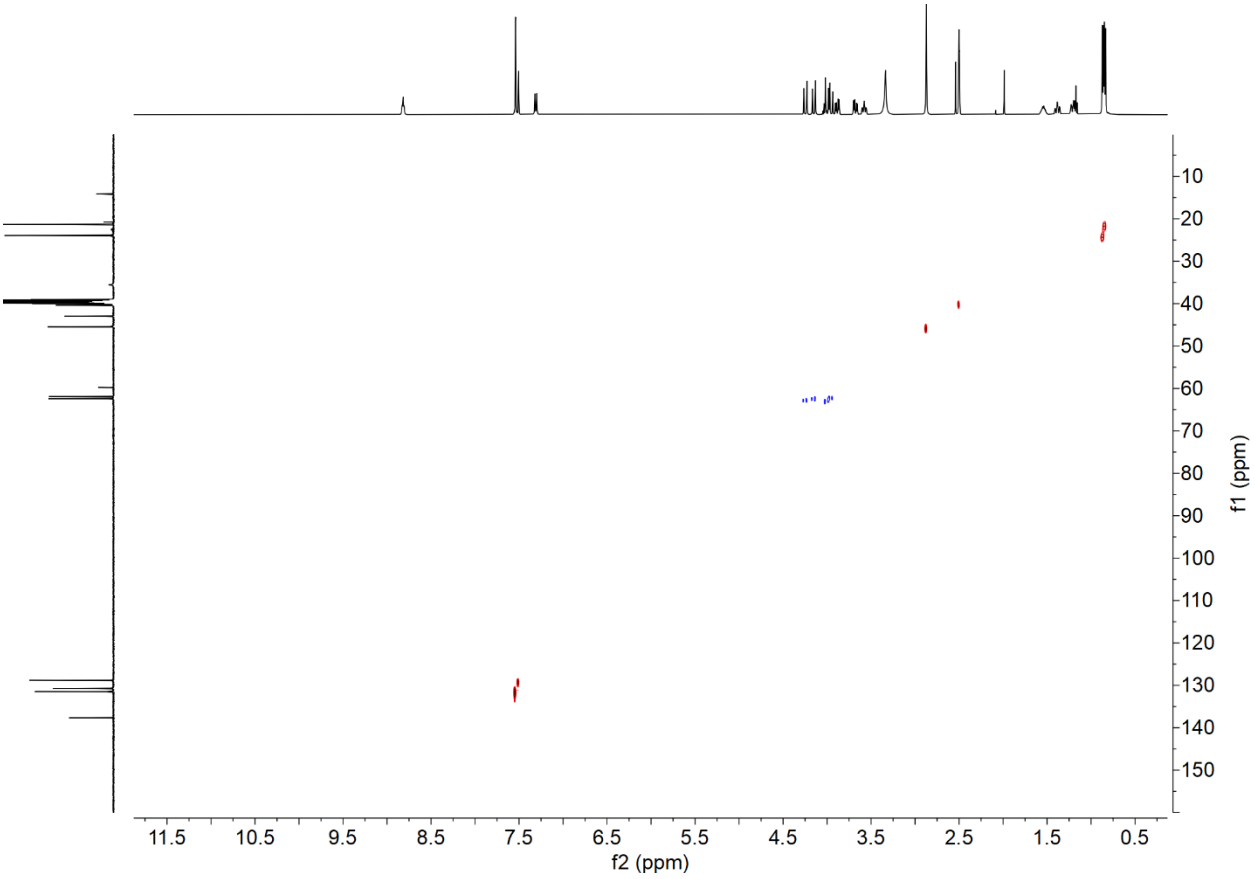




IXZ–MIDA

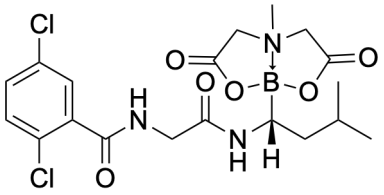
HSQC (500 MHz, DMSO-d_6)

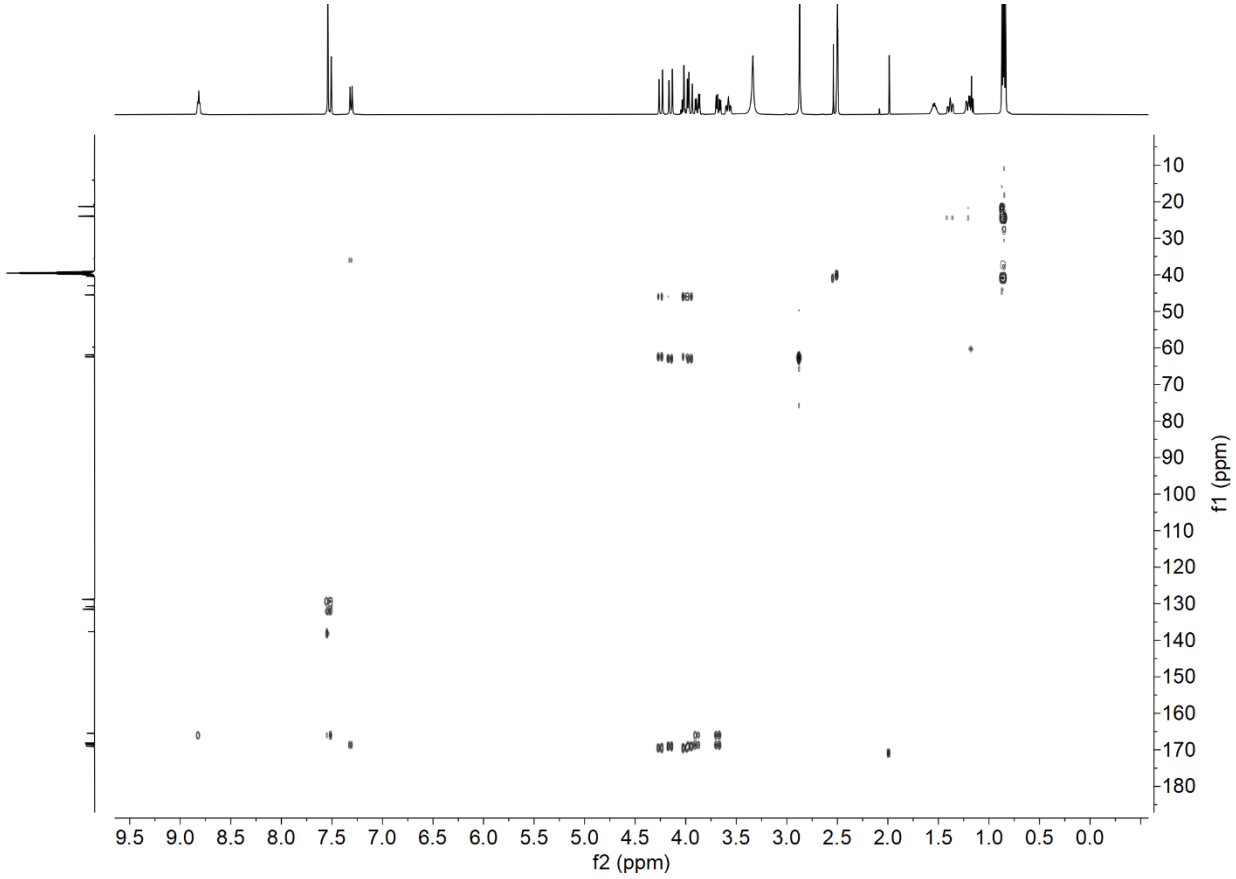




IXZ–MIDA

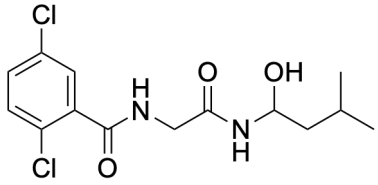
HMBC (500 MHz, DMSO-d_6)

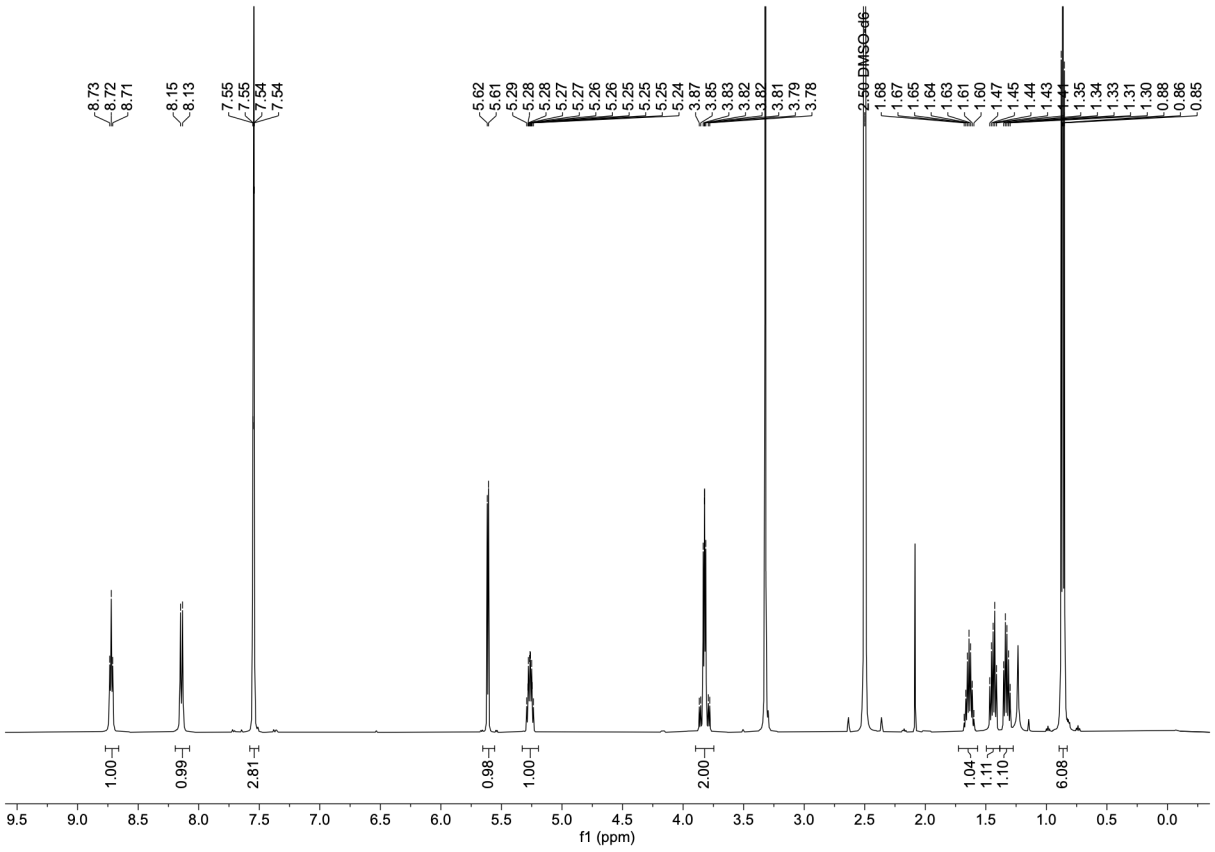




IXZ-ox

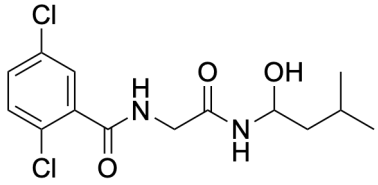
^{1}H NMR (500 MHz, DMSO-d_6)

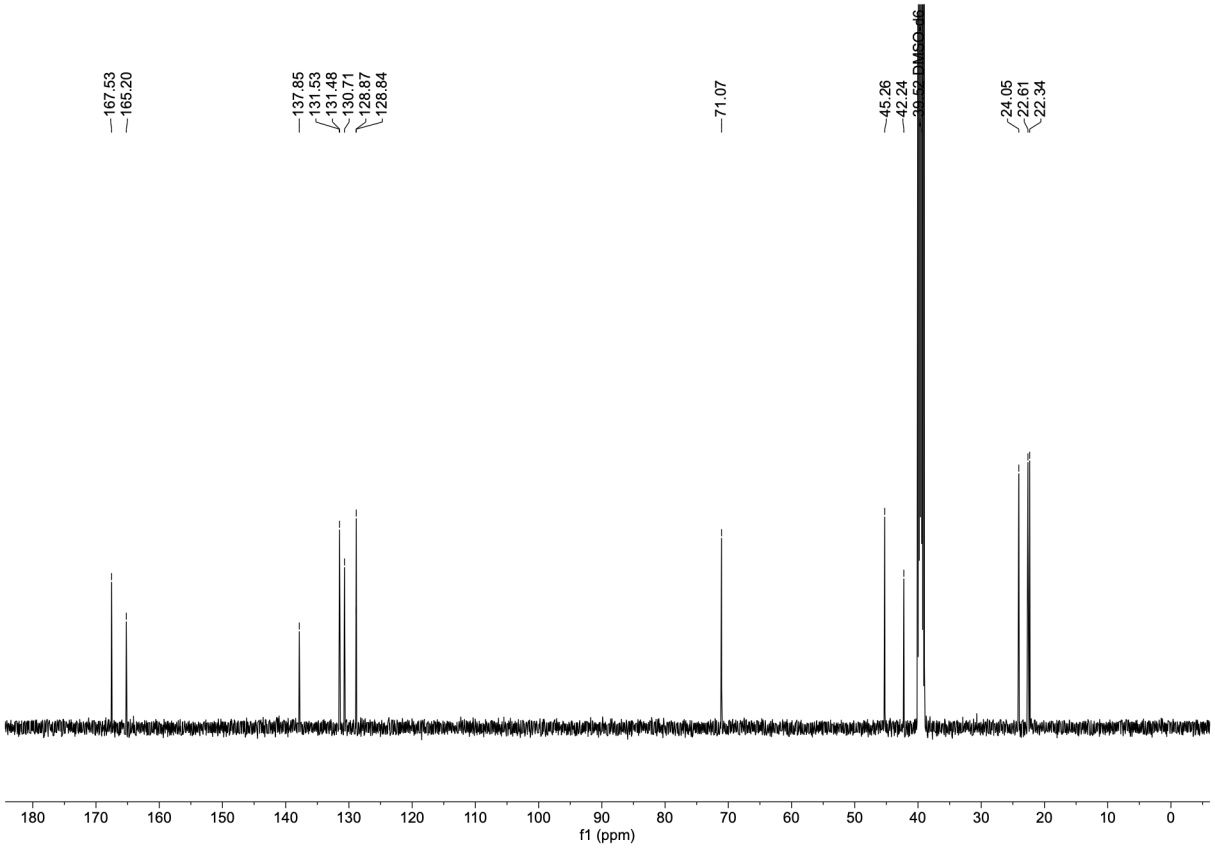




IXZ-ox

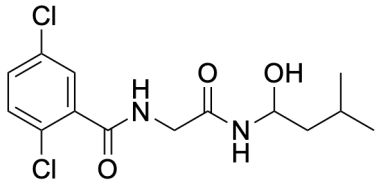
$^{13}C\{^{1}H\}$ NMR (126 MHz, DMSO-d_6)

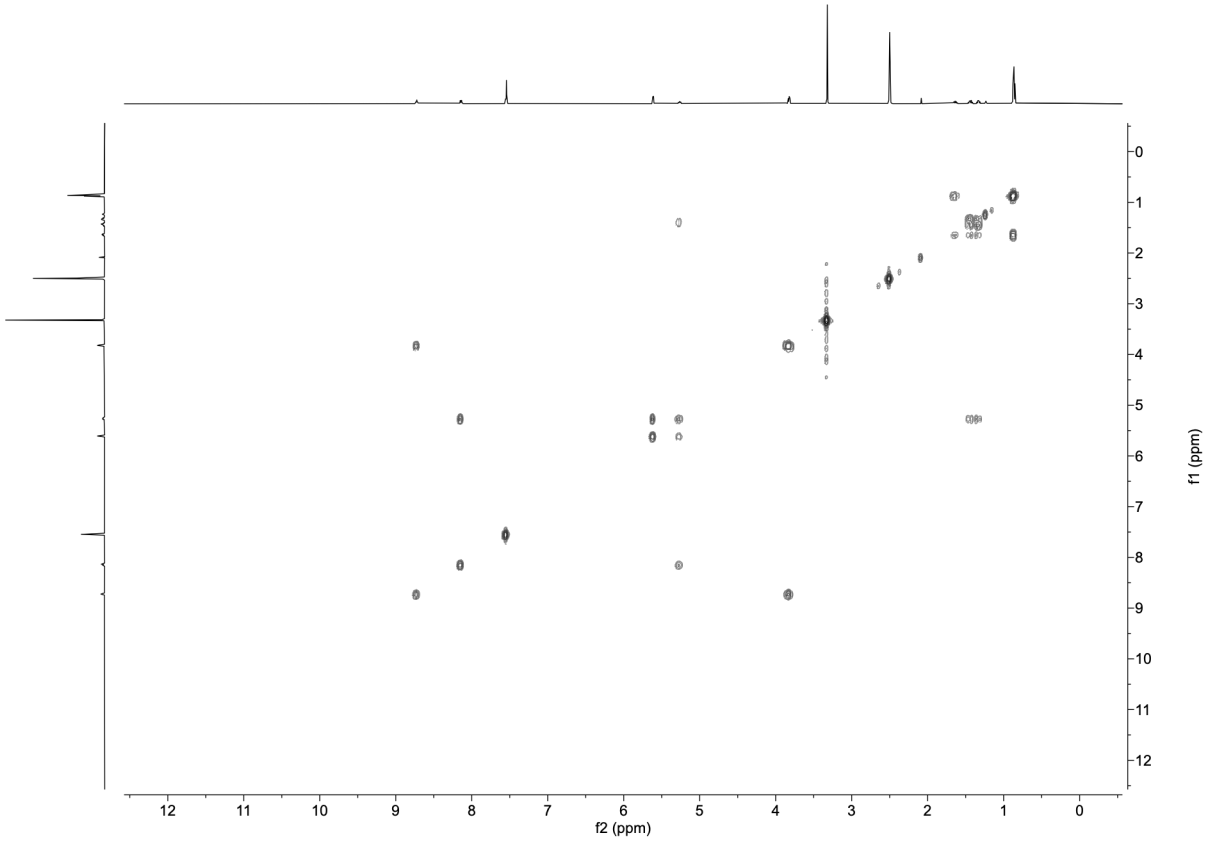




IXZ-ox

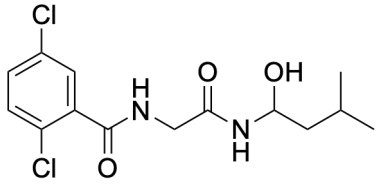
COSY (500 MHz, DMSO-d_6)

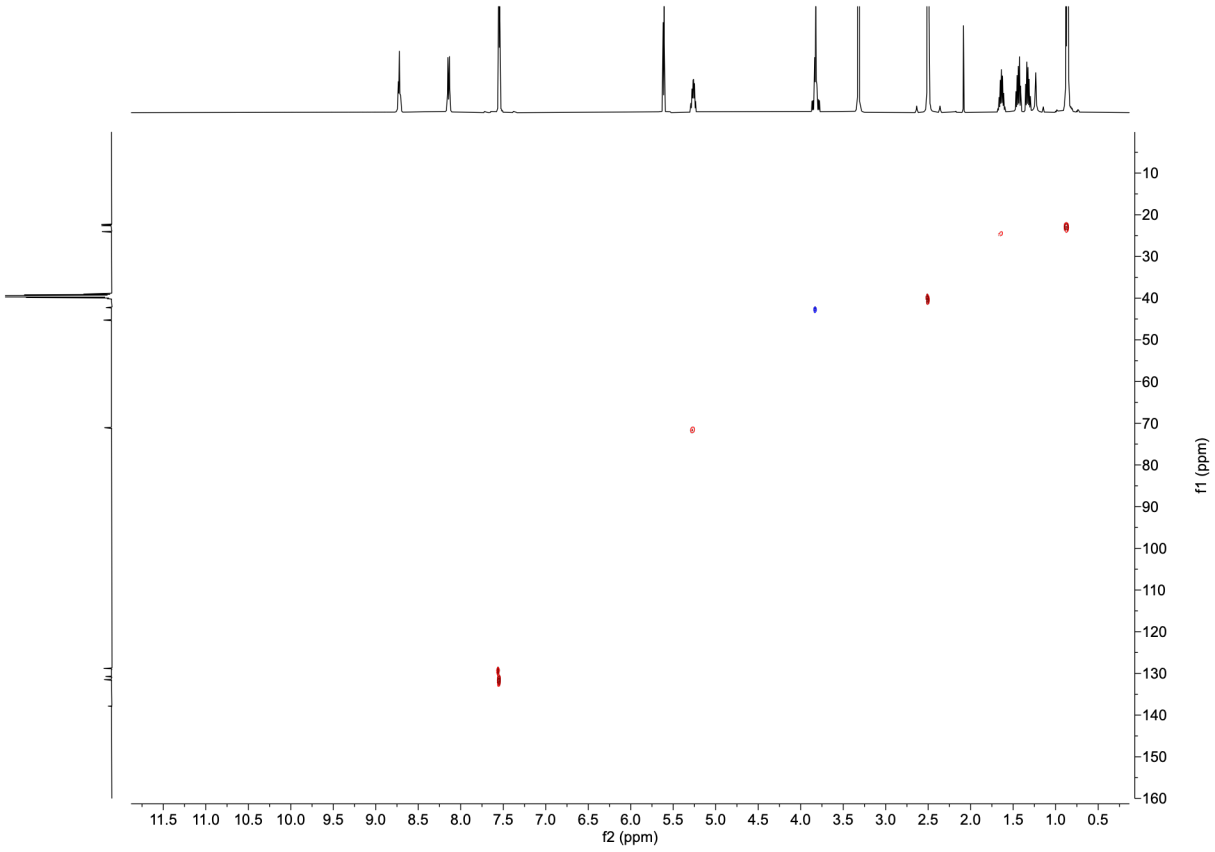




IXZ-ox

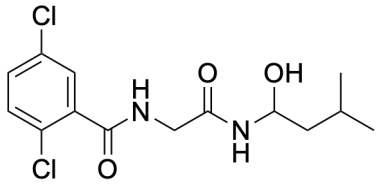
HSQC (500 MHz, DMSO-d_6)

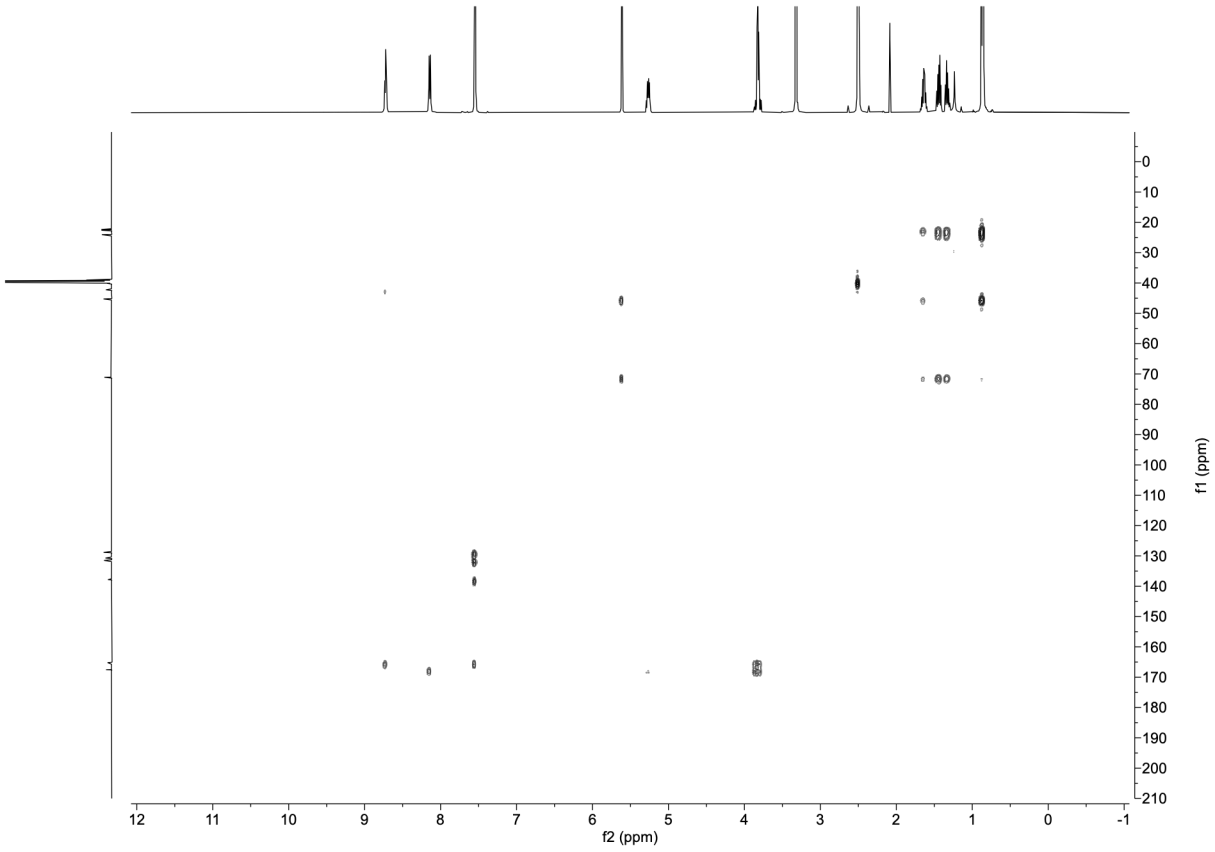




IXZ-ox

HMBC (500 MHz, DMSO-d_6)





13. Atomic Coordinates of DFT-Optimized Geometries

BTZ

C	6.718854	1.000581	-0.91636
C	4.677779	0.2853	-0.2397
C	4.961214	0.700334	1.061078
C	6.99811	1.428975	0.382391
H	7.449058	1.129433	-1.70844
H	4.252734	0.551757	1.870086
H	7.948206	1.899116	0.613601
N	5.56347	0.420783	-1.23184
N	6.126595	1.273289	1.378565
C	3.377283	-0.38311	-0.60362
O	3.340934	-1.26567	-1.46976
N	2.288385	0.044343	0.051182
H	2.348737	0.779836	0.748257
C	0.986423	-0.56209	-0.14936
H	0.85569	-0.77778	-1.21402
C	-0.06971	0.424885	0.326833
N	-1.23137	0.384215	-0.32618
H	-1.32003	-0.28493	-1.08446
C	-2.45641	1.010707	0.17834
H	-2.34531	1.100108	1.265505
C	-2.60876	2.432538	-0.39918
H	-1.72617	3.004736	-0.08677
H	-2.58331	2.380466	-1.49639
C	-3.88811	3.158211	0.046703
H	-4.14247	2.816501	1.060325
C	-3.65443	4.668479	0.096955
H	-3.34026	5.03609	-0.88771
H	-4.56916	5.200827	0.378208
H	-2.87255	4.925692	0.81851
C	-5.06414	2.851487	-0.88432
H	-5.23637	1.778506	-1.01516
H	-5.99155	3.289306	-0.5009
H	-4.8729	3.278428	-1.87617
B	-3.67225	0.027717	-0.12099
O	-3.62813	-0.67929	-1.29185
H	-4.34602	-1.31778	-1.41189
O	-4.67932	-0.06202	0.798977
H	-5.40054	-0.65676	0.546749
O	0.152706	1.153725	1.308632
C	0.855452	-1.87557	0.663336
H	1.659792	-2.53929	0.331567

H	1.019707	-1.63659	1.719231
C	-0.48667	-2.53899	0.479162
C	-0.74932	-3.30577	-0.66112
C	-1.50873	-2.35359	1.417547
C	-2.00364	-3.88609	-0.85476
H	0.037487	-3.45112	-1.39819
C	-2.76289	-2.93492	1.229118
H	-1.31694	-1.74761	2.3009
C	-3.01274	-3.70517	0.092264
H	-2.19121	-4.48233	-1.74279
H	-3.54357	-2.78634	1.969332
H	-3.98821	-4.15852	-0.05637

BTZ–MIDA

C	-7.13462	1.207574	1.480233
C	-5.29817	0.292274	0.519975
C	-5.75012	0.695094	-0.73566
C	-7.58337	1.620831	0.224591
H	-7.71344	1.425567	2.371656
H	-5.19544	0.461151	-1.63914
H	-8.51622	2.16603	0.126726
N	-5.99699	0.534502	1.63359
N	-6.8999	1.359948	-0.88935
C	-4.02155	-0.4867	0.698296
O	-3.93231	-1.36015	1.568449
N	-3.01112	-0.1629	-0.12438
H	-3.14035	0.544884	-0.84029
C	-1.76203	-0.91183	-0.12925
H	-1.54658	-1.21283	0.898717
C	-0.67995	0.031193	-0.64328
N	0.363595	0.23891	0.161306
H	0.373488	-0.22232	1.065037
C	1.43778	1.179202	-0.16505
H	1.661854	1.051137	-1.23214
C	0.986997	2.640863	0.060471
H	-0.1024	2.701305	-0.06784
H	1.197952	2.931068	1.098466
C	1.636853	3.645803	-0.90242
H	2.711972	3.429162	-0.96329
C	1.042529	3.532349	-2.30786
H	-0.03105	3.75714	-2.28349
H	1.521125	4.244047	-2.98865
H	1.16544	2.531394	-2.73333
C	1.463545	5.067904	-0.37055
H	1.940179	5.18678	0.608086

H	1.900495	5.80226	-1.05517
H	0.398133	5.304872	-0.25848
B	2.735538	0.81319	0.703086
O	2.407989	0.367757	2.068047
O	3.745855	1.902049	0.733438
O	-0.80536	0.566084	-1.75764
C	-1.87336	-2.1569	-1.02593
H	-2.7226	-2.7433	-0.65935
H	-2.10063	-1.8294	-2.04523
C	-0.61942	-2.99586	-1.01281
C	-0.27204	-3.72945	0.129206
C	0.213955	-3.05946	-2.1339
C	0.871866	-4.52632	0.141737
H	-0.91439	-3.68695	1.006421
C	1.357245	-3.86126	-2.1267
H	-0.04361	-2.48659	-3.02171
C	1.686682	-4.59905	-0.99034
H	1.123626	-5.09591	1.031378
H	1.990351	-3.90569	-3.0081
H	2.575316	-5.22308	-0.98328
C	3.207187	-0.60523	2.489038
C	4.788379	1.66083	-0.04375
O	5.674423	2.463356	-0.25592
O	3.154728	-1.08707	3.600108
C	4.195837	-1.00289	1.411474
H	4.303287	-2.08542	1.33584
H	5.165486	-0.5601	1.658013
C	4.704583	0.273199	-0.64992
H	4.35984	0.367928	-1.68412
H	5.659869	-0.25218	-0.62619
N	3.661147	-0.41644	0.147699
C	2.937433	-1.45465	-0.63755
H	3.657429	-2.20735	-0.96438
H	2.181657	-1.91341	0.00476
H	2.464359	-0.9857	-1.50047

IXZ

C	-5.50095	-0.33956	0.553075
C	-3.31002	-0.18212	-0.4253
C	-3.44993	1.206016	-0.45427
C	-5.63848	1.045142	0.534389
H	-6.54043	1.516877	0.908572
C	-2.10105	-0.90399	-0.95469
O	-2.2	-1.66533	-1.92723
N	-0.95558	-0.70461	-0.29899

H	-0.91154	-0.07363	0.495615
C	0.286915	-1.28489	-0.7583
H	0.284371	-2.3723	-0.62188
C	1.433327	-0.695	0.041233
N	2.659744	-0.97222	-0.39828
H	2.769104	-1.56316	-1.21596
O	1.227406	0.000177	1.051522
H	0.430976	-1.08232	-1.82412
C	-4.35615	-0.96103	0.073582
C	-4.60551	1.820824	0.01958
H	-4.70228	2.900374	-0.01871
H	-4.26086	-2.04235	0.087271
Cl	-2.1964	2.212394	-1.13758
Cl	-6.79812	-1.31875	1.189365
C	3.853512	-0.51392	0.320791
H	3.992141	-1.15862	1.198319
C	5.062627	-0.6537	-0.6134
H	5.177896	-1.70992	-0.89848
H	4.856696	-0.0918	-1.53388
C	6.383116	-0.15783	-0.01298
H	6.276998	0.912542	0.218936
C	6.741997	-0.8974	1.276657
H	7.727695	-0.58536	1.637085
H	6.020398	-0.7091	2.077062
H	6.775538	-1.97926	1.096429
C	7.502889	-0.30867	-1.04219
H	7.265682	0.222473	-1.96988
H	8.447826	0.085574	-0.65505
H	7.654391	-1.36704	-1.287
B	3.666958	0.99751	0.796298
O	3.276926	1.912052	-0.14601
H	3.198042	2.817872	0.183622
O	4.002109	1.319859	2.083771
H	3.914935	2.260071	2.295549

IXZ–MIDA

C	6.931748	0.58906	-0.3669
C	4.763564	-0.44082	-0.21504
C	5.015894	-0.71452	1.130041
C	7.180561	0.326825	0.976936
H	8.116026	0.627777	1.435641
C	3.500791	-0.84535	-0.92581
O	3.544456	-1.61989	-1.89228
N	2.368275	-0.2925	-0.48622
H	2.364175	0.314787	0.327921

C	1.084173	-0.65094	-1.04496
H	1.020106	-0.35139	-2.09597
C	-0.0122	0.039649	-0.24864
N	-1.25279	-0.15299	-0.70009
H	-1.3769	-0.74941	-1.51023
O	0.256637	0.719628	0.755416
H	0.934917	-1.7355	-0.99775
C	5.742372	0.207126	-0.97177
C	6.21589	-0.33725	1.726524
H	6.399738	-0.56607	2.770586
H	5.559568	0.411689	-2.02209
Cl	3.852674	-1.59019	2.095299
Cl	8.142714	1.41478	-1.31448
C	-2.4265	0.44127	-0.0447
H	-2.23659	0.34084	1.029973
C	-2.50776	1.940922	-0.38627
H	-1.48967	2.351564	-0.41853
H	-2.92918	2.054267	-1.3923
C	-3.31709	2.776157	0.612488
H	-4.26892	2.268022	0.817892
C	-2.56729	2.938326	1.936566
H	-3.16733	3.502465	2.658199
H	-2.31269	1.976262	2.393216
H	-1.63202	3.487526	1.771326
C	-3.63763	4.145365	0.014225
H	-4.23348	4.048668	-0.89946
H	-4.19557	4.766492	0.72262
H	-2.71093	4.67437	-0.24057
B	-3.74909	-0.41754	-0.44054
O	-3.38006	-1.75767	-0.93251
O	-4.63882	0.256696	-1.41681
C	-4.12307	-2.73625	-0.44784
C	-5.82996	0.57979	-0.94642
O	-6.66515	1.191439	-1.58226
O	-3.97836	-3.90449	-0.74412
C	-5.18315	-2.20963	0.488495
H	-6.14769	-2.29036	-0.01945
H	-5.21841	-2.78397	1.414986
C	-6.00343	0.119188	0.486072
H	-6.95688	-0.38821	0.635482
H	-5.96051	0.988858	1.145729
N	-4.84508	-0.77573	0.753328
C	-4.33896	-0.61552	2.14576
H	-5.12745	-0.9129	2.83947
H	-3.46317	-1.25333	2.27482

H -4.07346 0.429534 2.306153

14. References

1 M. R. Aronoff, B. VanVeller and R. T. Raines, *Org. Lett.*, 2013, **15**, 5382–5385.
2 A. H. Cory, T. C. Owen, J. A. Barltrop and J. G. Cory, *Cancer Commun.*, 1991, **3**, 207–212.
3 A. M. Kelly, P.-J. Chen, J. Klubnick, D. J. Blair and M. D. Burke, *Org. Lett.*, 2020, **22**, 9408–9414.
4 R. B. Wagh and J. M. Nagarkar, *Tetrahedron Lett.*, 2017, **58**, 4572–4575.
5 Y. Zhao and D. G. Truhlar, *Acc. Chem. Res.*, 2008, **41**, 157–167.
6 Y. Zhao and D. G. Truhlar, *Theoret. Chem. Acc.*, 2008, **120**, 215–241.
7 A. V. Marenich, C. J. Cramer and D. G. Truhlar, *J. Phys. Chem. B*, 2009, **113**, 6378–6396.
8 M. J. Frisch, G. W. Trucks, H. B. Schlegel, G. E. Scuseria, M. A. Robb, J. R. Cheeseman, G. Scalmani, V. Barone, G. A. Petersson, H. Nakatsuji, X. Li, M. Caricato, A. V. Marenich, J. Bloino, B. G. Janesko, R. Gomperts, B. Mennucci, H. P. Hratchian, J. V. Ortiz, A. F. Izmaylov, J. L. Sonnenberg, D. Williams-Young, F. Ding, F. Lipparini, F. Egidi, J. Goings, B. Peng, A. Petrone, T. Henderson, D. Ranasinghe, V. G. Zakrzewski, J. Gao, N. Rega, G. Zheng, W. Liang, M. Hada, M. Ehara, K. Toyota, R. Fukuda, J. Hasegawa, M. Ishida, T. Nakajima, Y. Honda, O. Kitao, H. Nakai, T. Vreven, K. Throssell, J. A. Montgomery Jr., J. E. Peralta, F. Ogliaro, M. J. Bearpark, J. J. Heyd, E. N. Brothers, K. N. Kudin, V. N. Staroverov, T. A. Keith, R. Kobayashi, J. Normand, K. Raghavachari, A. P. Rendell, J. C. Burant, S. S. Iyengar, J. Tomasi, M. Cossi, J. M. Millam, M. Klene, C. Adamo, R. Cammi, J. W. Ochterski, R. L. Martin, K. Morokuma, O. Farkas, J. B. Foresman and D. J. Fox, Gaussian 16 Rev. C.01, Wallingford, CT, 2016.
9 E. G. Hohenstein and C. D. Sherrill, *J. Chem. Phys.*, 2010, **132**, 184111.
10 E. G. Hohenstein, R. M. Parrish, C. D. Sherrill, J. M. Turney and H. F. Schaefer, III, *J. Chem. Phys.*, 2011, **135**, 174107.
11 T. M. Parker, L. A. Burns, R. M. Parrish, A. G. Ryno and C. D. Sherrill, *J. Chem. Phys.*, 2014, **140**, 094106.
12 A. M. Keys, D. W. Kastner, L. L. Kiessling and H. J. Kulik, *Chem. Sci.*, 2025, **16**, 1746–1761.
13 R. A. Kendall, T. H. Dunning, Jr. and R. J. Harrison, *J. Chem. Phys.*, 1992, **96**, 6796–6806.
14 R. C. Dey, P. Seal and S. Chakrabarti, *J. Phys. Chem. A*, 2009, **113**, 10113–10118.
15 D. G. A. Smith, L. A. Burns, A. C. Simmonett, R. M. Parrish, M. C. Schieber, R. Galvelis, P. Kraus, H. Kruse, R. Di Remigio, A. Alenaizan, A. M. James, S. Lehtola, J. P. Misiewicz, M. Scheurer, R. A. Shaw, J. B. Schriber, Y. Xie, Z. L. Glick, D. A. Sirianni, J. S. O'Brien, J. M. Waldrop, A. Kumar, E. G. Hohenstein, B. P. Pritchard, B. R. Brooks, H. F. Schaefer, III, A. Y. Sokolov, K. Patkowski, A. E. DePrince, III, U. Bozkaya, R. A. King, F. A. Evangelista, J. M. Turney, T. D. Crawford and C. D. Sherrill, *J. Chem. Phys.*, 2020, **152**, 184108.